ON THE MACHINING DYNAMICS OF TURNING AND MICRO-MILLING PROCESSES

A Thesis

by

ERIC BEN HALFMANN

Submitted to the Office of Graduate Studies of
Texas A&M University
in partial fulfillment of the requirements for the degree of

MASTER OF SCIENCE

August 2012

Major Subject: Mechanical Engineering

On The Machining Dynamics of Turning

and Micro-milling Processes

ON THE MACHINING DYNAMICS OF TURNING AND MICRO-MILLING PROCESSES

A Thesis

by

ERIC BEN HALFMANN

Submitted to the Office of Graduate Studies of
Texas A&M University
in partial fulfillment of the requirements for the degree of

MASTER OF SCIENCE

Approved by:

Chair of Committee,	C. Steve Suh
Committee Members,	Alan Palazzolo
	Jyhwen Wang
	Wayne Hung
Head of Department,	Jerald A. Caton

August 2012

Major Subject: Mechanical Engineering

ABSTRACT

On The Machining Dynamics of Turning
and Micro-milling Processes. (August 2012)
Eric Ben Halfmann, B.S., Lamar University
Chair of Advisory Committee: Dr. C. Steve Suh

Excessive vibrations continue to be a major hurdle in improving machining efficiency and achieving stable high speed cutting. To overcome detrimental vibrations, an enhanced understanding of the underlying nonlinear dynamics is required. Cutting instability is commonly studied through modeling and analysis which incorporates linearization that obscures the true nonlinear characteristics of the system which are prominent at high speeds. Thus to enhance cutting dynamics knowledge, a comprehensive nonlinear turning model that includes tool-workpiece interaction is experimentally validated using a commercial laser vibrometer to capture tool and workpiece vibrations. A procedure is developed to use instantaneous frequency for experimental time-frequency analysis and is shown to thoroughly characterize the underlying dynamics and identify chatter.

For the tests performed, chatter is associated with changing spectral components and bifurcations which provides a view of the underlying dynamics not experimentally observed before. Validation of the turning model revealed that the underlying dynamics observed experimentally are accurately captured, and the coupled tool-workpiece chatter

vibrations are simulated. The stability diagram shows an increase in the chatter-free limit as the spindle speed increases until 1500rpm where it begins to level out. At high speeds the workpiece dominates the dynamics, and excessive workpiece vibrations create another stability limit to consider. Thus, workpiece dynamics should not be neglected in analyses for the design of machine tools and robust control laws.

The chip formation mechanisms and high speeds make micro-milling highly non-linear and capable of producing broadband frequencies that negatively affect the tool. A nonlinear dynamic micro-milling model is developed to study the effect of parameters on tool performance through spectral analysis using instantaneous frequency. A lumped mass-spring-damper system is assumed for modeling the tool, and a slip-line force mechanism is adopted. The effective rake angle, helical angle, and instantaneous chip thickness are accounted for. The model produced the high frequency force components seen experimentally in literature. It is found that increasing the helical angle decreased the forces, and an increase in system stiffness improved the dynamic response. Also, dynamic instability had the largest effect on tool performance with the spindle speed being the most critical parameter.

ACKNOWLEDGEMENTS

I would like to thank God for my many blessings and for the opportunity to attend Texas A&M. I am very appreciative of my fiancé for the never-ending love and support she provides me. I would like to thank my family, especially my parents, for the enduring love, support, guidance, and prayers throughout my life providing me with the foundation needed to be successful.

I would also like to express my sincere gratitude to my academic advisor, Dr. C. Steve Suh, for dedicating the time to mentor me and help me develop the professional and critical thinking skills needed to effectively approach and solve a problem. His continuous guidance and support provided me with a fulfilling research experience and an enthusiasm for the pursuit of knowledge. I would like to thank Dr. Wayne Hung for the knowledge shared about machining experiments and for allowing me access to the lathe machine and laser sensor utilized for my experimental work. My thanks also go to doctoral student Meng-Kun Liu for his companionship and professionalism in lab, and for taking the time to help me learn concepts important to my research.

Finally, I would like to thank Dr. Alan Palazzolo and Dr. Jywhen Wang for serving on my advisory committee and for contributing to my positive educational experience which benefited me in reaching my goals and developing career goals.

TABLE OF CONTENTS

Page

Page

LIST OF FIGURES

FIGURE Page

FIGURE Page

FIGURE Page

FIGURE Page

FIGURE Page

FIGURE Page

LIST OF TABLES

1. INTRODUCTION

1.1 Turning Overview and Literature Review

Metal cutting technologies are important manufacturing processes for the production of quality products from a wide range of materials. Metal cutting consists of removing material from the workpiece with a cutting tool in order to sculpt a desired design. The inputs for the cutting process are the cutting tool design and constituent, workpiece configuration and material, cutting fluid, spindle speed, feed rate, depth-of-cut (DOC), and machine tool assembly [1]. The configuration of these parameters will have a major impact on the dynamics of the system which affects the overall vibrations. System vibrations have a direct impact on the tool wear, workpiece tolerance, surface roughness, and cutting forces which are main outputs for measuring cutting performance [1]. The advancement of technology and the need to improve efficiency requires improved tolerances and the use of higher cutting speeds. Higher cutting speeds increase the forcing frequency of the process greatly affecting the dynamic response. Enhanced knowledge of cutting dynamics will directly benefit the improvement of metal cutting. The turning process consists of a rotating workpiece secured by the chuck and tailstock, and a tool with only translational motion removing material to produce parts with a circular cross-section (Fig. 1.1). The amount of material removed during the

---

This thesis follows the style of the Journal of Manufacturing Science and Engineering.

turning process is determined through the selection of the chip thickness (feedrate) and DOC as illustrated in Fig. 1.2. The cutting tool inclination, rake, and lead angles are dominant tool parameters which affect the distribution of the cutting forces in the global coordinates at the cutting edge (Fig. 1.3).

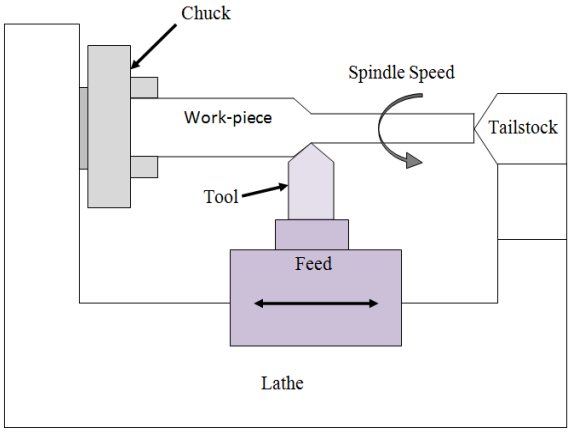

Fig. 1.1 Basic lathe cutting configuration

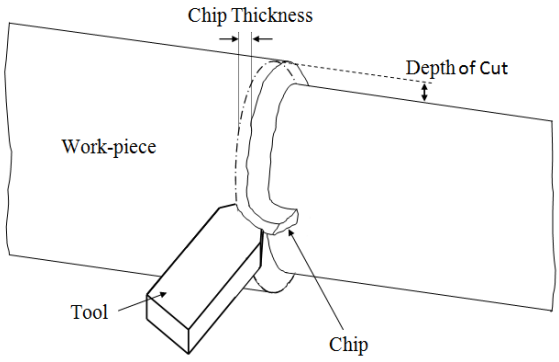

Fig. 1.2 Material removal process for turning

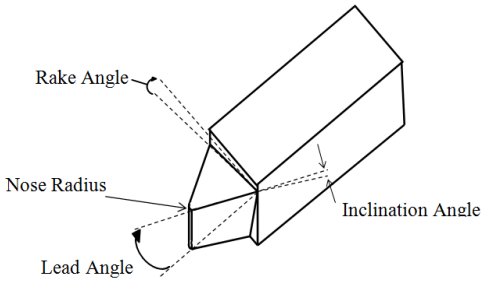

Fig. 1.3 Illustration of main lathe cutting tool angles

Excessive machining vibrations such as chatter are detrimental to tool integrity and product quality, thus considered a main culprit in compromising manufacturing efficiency. Chatter is observed by the operator as excessive noise and poor workpiece surface finish and was investigated in the 1940s for its adverse effect on chip formation, surface roughness, and tool vibrations [2]. One mechanism which causes chatter is the regenerative effect. The regenerative chatter is due to the relative motion between the tool and workpiece as well as the phase difference between the current tool position and the tool position the previous revolution in time. As the tool and workpiece vibrate, a wavy finish is left on the surface of the workpiece, and when these motions become out of phase the instantaneous chip width will become increasingly large causing the vibration magnitude to continuously grow to an unstable limit. Mathematical modeling of the metal cutting process is effective for studying machining instability. General chatter vibrations of the machine tool were studied in [3] and the theory of nonlinear regenerative chatter was analyzed in [4] in which nonlinear stiffness was applied to the structure and a nonlinear force coefficient was used. In [5] nonlinearity was introduced

by the tool leaving the cut under excessive vibration amplitudes and through nonlinear force characteristics. These studies investigated the effect that nonlinearities have on traditional stability lobes resulting in stable, conditionally stable, and unstable regions. Analytical studies of 2 degree-of-freedom (DOF) cutting systems were analyzed in [6-8] to further investigate the effect of wave generation on instability and how frictional force affects the stability lobes. In [9] a milling stability diagram is developed by first linearizing a 2 DOF milling model, followed by selecting a chatter frequency, solving the eigenvalue, calculating the critical DOC, and determining the spindle speed. These early analytical models are expanded to a multidimensional model that includes tool nose radius [10, 11], process damping [12], and tool wear [13]. While analytical methods are effective at producing stability lobes, linearization necessarily obscures the true nonlinear characteristics, thus rendering the use of stability lobes for chatter suppression both inaccurate and ineffective. Also, the stability lobes are developed without regard to resulting vibrations [14], so stable cutting conditions that may have unacceptable vibration amplitude are not accounted for. Chatter therefore remains a major issue in today's machine shops [15].

The methods reviewed provide limited insight into the nonlinear underlying dynamics of chatter vibrations because they do not allow for nonlinearities. To fully understand machining instability, nonlinear characteristics must be retained as machining is by nature nonlinear and non-stationary [16]. The advancement of computing power and nonlinear dynamic analysis techniques allows for further analysis of the machining process through the simulation of advanced models. Reference [17]

investigated the dynamics involved in the cutting process by analyzing a 3D model that includes friction and uses the systems boundary theorem to study the interactions between the tool jumping out-of-the-cut, tool rubbing but not cutting, and the tool cutting phases. In [16] phase portraits were used to provide insight into the state of the system but they failed to reveal detail information about the dynamics, and [18] analyzed the classic 1 DOF delay-differential equation with the previous workpiece motion assumed to be sinusoidal. Along with the study reported in [19] where subcritical Hopf bifurcation emerged in a 2 DOF nonlinear model, these studies concluded that bifurcated and possibly chaotic motion could be present in machining. It is suggested in [20] and [21] that 1 DOF models cannot resolve the complex nonlinear motions and thus models with more degrees of freedom are needed and should be judged on their ability to resolve nonlinear dynamics. The model in [22] used Simulink to configure different blocks together to incorporate nonlinear effects and predict surface generation. In [23] a comprehensive three-dimensional force model considering the tool nose radius and different tool angles was developed. However, these three-dimensional (3D) models fail to incorporate workpiece motion limiting the ability to fully investigate the dynamics. Turning is inherently a 3D process that includes the tool and workpiece vibrations which are necessarily coupled [24-25] due to nonlinear characteristics such as the tool jumping out of the cut and workpiece motions exceeding that of the tool [26]. Thus, to successfully model the turning process, the tool and workpiece motions have to be simultaneously considered. Of the handful of models that incorporate workpiece motions and three-dimensional force equations, only the comprehensive three-

dimensional model presented in [24-25] considers the simultaneous, coupled tool and workpiece vibrations without employing linearization techniques.

The analytical and numerical analysis of mathematical models is important for studying the cutting process and providing guidance for experimental research which would aid in achieving improved solutions for avoiding harmful vibrations. Analytical models develop stability lobes which benefit the machine operators by providing a guideline for chatter-free cutting parameters. However, to fully resolve the issue of chatter, the underlying dynamics must be fully understood. This can only be realized through complete nonlinear modeling and analysis of the coupled tool and workpiece interactions. Thus, it is important to investigate the ability of a mathematical model to capture the underlying dynamics so that the model can be confidently used to study the process. The thesis research presented will study the ability of the model in [24] to effectively capture the underlying dynamics of the turning process. In Section 3 the model will be briefly introduced and the experimental design used to capture tool and workpiece vibrations for model validation will be presented.

Adequate modeling or experimental analysis would not provide the desired insight if the analysis techniques used are not effective at handling nonlinear systems. Traditionally chatter is defined as the appearance of a chatter frequency close to a dominant frequency of the machine tool system, increasing vibration amplitude, poor surface finish, and increased noise [15]. The visual inspection of workpiece surface finish and the audible recognition of chatter by the operator are subjective methods for defining and identifying chatter, and resulted in delayed chatter detection in [26]. Thus,

it is important to monitor the system with a tool capable of quantitatively identifying and defining cutting instability. Analyzing the system in the frequency domain has been found to be effective for quantitative chatter recognition, and the analysis of numerical and experimental data overwhelmingly utilizes Fast Fourier Transform (FFT) for spectral analysis [11-13, 23]. Although commonly used, FFT has serious drawbacks in the processing of nonlinear and non-stationary signals because it is the integration of the signal over all time which is an averaging of the frequency spectrum with a fixed resolution [27]. Local properties and nonlinear interactions can be averaged out making FFT poor in resolving nonlinear features. In [28] the instability of a milling process is analyzed using discrete wavelet transform and the concept of energy variation. It is illustrated that instability, depending on the state of deterioration, could be multi-periodic, aperiodic, or chaotic. This demonstrates the need for analyzing machining in the time-frequency domain since dynamic instability is characterized by a change in the period and frequency that are coupled. Of the many time-frequency analysis tools available, instantaneous frequencies (IFs) determined by the Hilbert-Huang Transform (HHT) provides the best resolution needed in resolving the transition from stability to instability [29, 30]. The HHT applies a sifting process called Empirical Model Decomposition (EMD) to decompose a multi-component signal into a set of mono-component units called Intrinsic Mode Functions (IMFs). Once IMFs are obtained, Hilbert Transform is then performed to determine the IFs of the signal. Both IF and EMD have been successfully applied to the detection of damaged gears [31], the showing of different responses of a nonlinear rotor model [32], and the resolving of the

transition from stability to instability in a machining research [33]. Application of IF to experimental machining vibrations, however, is not available in the literature. Thus, in this research IF will be the main tool used to characterize the machining vibrations and FFT, phase portrait, and Poincare section will be applied to further validate the dynamic state of motion identified with IF. In Section 2 these analysis tools will be introduced and applied to example signals, and in Section 4 a method is developed and employed to effectively characterize experimental turning dynamics using IF. This will be followed by Section 5 where the model in [24] is validated and instability is investigated.

1.2 Micro-milling Overview and Literature Review

Micro-technologies are widely used in the area of medicine, life sciences, communications, and mobility [34], and as micro-technologies continue to be developed they will need increased functionality and to withstand harsher environments. This requires a wide range of materials and complex 3D features which increases the importance of micro-manufacturing research to meet and enhance these demands. Defined as cutting at values less than 1 mm [35], micro-milling is able to produce complex 3D miniature components out of a wide range of materials. Micro-milling is subject to sudden and excessive vibrations and forces that negatively impact the longevity of the tool and the ability to control component quality [36]. To address these challenges, modeling is important for gaining a better understanding of the effect different mechanisms and cutting parameters have on the dynamics. Also, modeling provides guidance for empirical research that assists in further understanding the process [35-36]. Modeling of the macro-milling process has been widely researched with many

analytical and time domain simulation methods developed. The analytical milling model in [9] that takes the Fourier series expansion of time-varying milling force coefficients is expanded to develop a three-dimensional chatter stability model for ball end, bull nose, and inclined cutting edges in [37]. The solution for these dynamic models is purely analytical and in the frequency domain, and requires the selection of a chatter frequency which is commonly chosen around a dominant mode of the system. A semi-discrete time domain solution is proposed in [38] that considers time-varying coefficients and is compared to the frequency domain solution which shows the two methods produce similar stability lobes. The analytical method is compared to a time domain technique which uses constant cutting force coefficients in [39] and it is shown that instability at higher speeds which is observed experimentally is not predicted. An improved three-dimensional cutting force model that accounts for tool helical angle is presented in [40] along with a new method for estimating the cutting force coefficients and run-out parameters. Cutting force coefficient models accurately predict the magnitude of forces but fail to resolve the higher frequency components seen experimentally unless the chip thickness is correctly developed and the constantly changing tool angles are accounted for. The model in [41] utilizes a nonlinear cutting force coefficient relationship to accurately predict the cutting forces as well as produce a nonlinear milling model.

Micro-milling is a highly nonlinear process so a time domain simulation method is preferred for studying the dynamics of the system since it allows for nonlinear characteristics and changing variables to be accounted for [14]. Micro-milling cannot directly adopt the methods used for modeling macro-milling due to different cutting

force mechanisms at work and the increased tool radius-to-feed rate ratio. Tool run-out affects the micro-milling process more due to the small size of the tool. Tool run-out was investigated experimentally in [42] using a laser displacement sensor, its effect on micro-milling was discussed in [35, 36], and simulated in [43] which demonstrated how run-out increases the cutting forces on the tool. Tool run-out is due to spindle-tool misalignment and imperfections in the micro-tool. These parameters are controlled through increasing the precision of the micro-cutting center and the uniformity of the micro-tool. The focus of this research is to investigate the effect that cutting parameters have on the instability of micro-milling and to ultimately determine the parameters critical to the process, so tool run-out is neglected in the model development. Another difference between macro and micro-milling is that as the tool approaches the workpiece, the material is compressed and is either plowed under or formed into a chip [44], and the minimum chip thickness determines whether a chip is formed. When the uncut chip thickness is less than the minimum chip thickness, all of the material is plowed under the tool and results in only plowing forces being present and the plowed material elastically recovering by some amount. To simulate the dynamics of the system, all of these nonlinear mechanisms acting on the micro-milling process need to be addressed.

An analytical model is developed in [45] that uses experimentally determined coefficients which help to accurately predict the magnitude of the forces and to quickly monitor cutting forces. A mechanistic force model that utilizes material properties as well as an experimental constant to calibrate the forces is developed in [46]. The model

in [43] utilizes cutting force coefficients and studies the effect that run-out and elastic recovery of the workpiece has on the cutting forces, however, this model does not always predict the high frequency components seen experimentally. Due to the micro-nature of the cutting process, the cutting forces are affected by the microstructure of the materials. A model was developed in [47, 48] that can handle multiple phases in the workpiece, and the cutting parameters for ferrite and pearlite are studied in depth. The force mechanism in [49] is based off of experimentally observed material flow angles and the chip formation is modeled as a process of shear where the shear zone is determined by the coefficient of friction between the chip and tool. This paper developed equations for contact friction, contact stress, and material spring back but was validated for low speeds only. The method in [50] developed cutting force coefficients that are independent of cutting process parameters and incorporates an effective rake angle. Here equations were developed for the cutting force coefficients and experimental data was used to determine these coefficients which proved effective in predicting the cutting forces under multiple cutting parameters. Another proven effective method for developing the cutting forces is the slip-line method. A very detailed and elaborate slip-line model is developed in [51] that accounts for many of the features that occur near the tool edge during cutting. Earlier slip-line models were developed in [52, 53] to predict the shearing and plowing forces. The slip-line model developed in [54] built upon and improved the model in [53] by accounting for the dead metal cap and the frictional forces associated with it.

The research in [43, 45-53] focuses on the development of a forcing mechanism that accurately simulates the forces in micro-milling. Validation is performed by comparing a few rotations of the cutter under stable cutting conditions with experimental data. Further analysis into the effect of process variables on dynamic stability is limited. Thus, little research has been done investigating the dynamics of micro-milling with the goal of better understanding how the cutting parameters including feed rate, DOC, and spindle speed, among others affect the stability of the system. This is important in determining the cutting parameters critical to the process. This research will investigate micro-milling through the development of a nonlinear dynamic model in Section 6 capable of resolving the nonlinear dynamic signature of the micro-milling process. The force mechanism will account for shearing and plowing forces, and the dynamic effective rake angle. A novel approach for determining the chip thickness by considering the elastic recovery of the material and the tool disengaging the workpiece is developed, and the tool helical angle is accounted for by assuming that the tool can be split into axial elements. This model is then validated in Section 7 by comparing the simulations with experimental data in literature as well as investigating the stability of these simulations using IF and FFT. Finally, the model is used to study the effect that the tool angles and system stiffness have on the resulting cutting forces and dynamic response in Section 8.

1.3 Research Objectives

The dynamic response of the tool in turning and micro-milling greatly affects the tool wear rate and cutting forces which increase the probability of tool failure. Excessive vibrations also impact workpiece tolerance and surface roughness which contributes to decreased process efficiency and is still a prominent issue in machining. This hinders the advancement of high speed machining because process nonlinearities are more prominent at high spindle speeds due to the increased forcing frequency. To fully address the issue of excessive machining vibrations, the underlying dynamics of the process need to be fully understood. Comprehensive mathematical models provide an effective means for studying the process and obtaining an enhanced understanding of the underlying dynamics as well as developing solutions and control algorithms for handling instability. However, mathematical models must be experimentally validated in order to be established as a competent tool for dynamic analysis. In addition, appropriate nonlinear analysis techniques need to be applied in order to unveil the true dynamics of the system. Thus, the overall objective of the research is to provide further insight into the underlying dynamics of the machining process through the analysis and experimental validation of the turning model in [24] using IF, and the analysis of micro-milling dynamics by developing a nonlinear dynamic model. The research objectives will be accomplished through the following tasks:

- Develop an experimental test set-up to acquire tool and workpiece vibrations
- Generate a procedure for analyzing experimental vibrations using IF
- Investigate the transition to unstable experimental cutting using IF

- Compare experimental and numerical dynamics using the model in [24]
- Use the model in [24] to produce a thorough stability diagram considering the dynamics of both the tool and workpiece
- Confirm tool – workpiece interaction is prominent and non-negligible
- Investigate high speed turning dynamics using the model in [24]
- Develop a nonlinear micro-milling model which correctly calculates the instantaneous chip thickness, accounts for tool geometry, workpiece properties, and nonlinear forcing mechanisms
- Compare model simulations to experimental data in literature
- Investigate the effect that process parameters have on the resulting cutting forces and dynamic stability

The realization of the tasks presented will provide further insight into machining instability as well as provide tools and knowledge needed to accurately characterize the dynamics of machine cutting technologies and develop solutions to mitigate excessive vibrations.

2. INTRODUCTION AND FUNDAMENTALS OF ANALYSIS TOOLS

2.1 Fundamentals of Fourier Transform

The analysis method developed by John Fourier has been used in all areas of engineering and is a common method for converting an analog signal, $x(t)$, into frequency-domain information [55, 56]. This analysis is commonly termed as the Fourier transform and is used to reveal the spectral characteristics of a signal. Engineers usually associate the Fourier transform as an extension of the Fourier series by allowing the period, T, of the signal to approach infinity. Fourier series is used in vibrations to develop an analytical representation in time of a periodic time signal [55]. Hence, it is an orthogonal projection of the signal with respect to the basis set which are typically the sine and cosine functions. The Fourier series of the time function, $F(t)$, is commonly expressed in vibrations courses using the following equations [55],

$$F(t) = a_0/2 + \sum_{n=1}^{\infty}(a_n \cos(n\omega_T t) + b_n \sin(n\omega_T t)) \tag{2.1}$$

where:

$$\omega_T = 2\pi/T \tag{2.2}$$

$$a_0 = (2\pi/T)\int_0^T F(t)dt \tag{2.3}$$

$$a_n = (2/T)\int_0^T F(t)\cos(n\,\omega_T)dt \tag{2.4}$$

$$b_n = (2/T)\int_0^T F(t)\sin(n\,\omega_T)dt \tag{2.5}$$

To extend the Fourier series to Fourier transform, the period T is extended to infinity and the Fourier series is expressed as:

$$F(t) = (1/2\pi)\int_{-\infty}^{\infty}\left[\int_{-\infty}^{\infty} x(t')e^{-j\omega t'}dt'\right]e^{j\omega t}d\omega \quad (2.6)$$

The integral inside the brackets is the Fourier transform and for a finite energy function of real-variable, t, the Fourier transform is expressed as:

$$\hat{x}(\omega) = (1/2\pi)\int_{-\infty}^{\infty} x(t)e^{-j\omega t}dt \quad (2.7)$$

The computation of Fourier series and Fourier transform requires integration and analytically describes the signal through elementary functions such as sine and cosine. The signals encountered in real life are usually not represented by these elementary functions, so to apply these techniques to real-world signals, the discrete Fourier series and discrete Fourier transform are directly computed using numerical algorithms, thus producing an approximate spectrum of the original analog signal. The Fourier transform integral in (2.7) can be approximated using the following discrete form,

$$\hat{x}(\omega) = (1/2\pi)\sum_{i=0}^{N-1} x(t_i)e^{-i\omega t_i}\Delta t \quad (2.8)$$

This series sum can be applied to discretely sampled data where Δt is the sampling rate. The Fourier transform is incorporated in the analysis conducted throughout this research due to its extensive use in industry and research for spectral analysis of vibration signals. This will allow for a comparison to the effectiveness of IF and to confirm observations made in the time-frequency domain.

2.2 Fundamentals of Instantaneous Frequency

Machining is a nonlinear and non-stationary system which can have a time-varying amplitude and frequency. The commonly used FFT analysis is not able to resolve time-varying frequencies in the signal and the objective of the research to observe the transition of system dynamics requires the ability to resolve individual spectral components in time. Instantaneous Frequency (IF) as presented in [30] is briefly reviewed in the followings. The idea of instantaneous frequency is different from the traditional definition of Fourier frequency which requires a complete revolution of a sine or cosine wave. Also, IF encountered an early difficulty due to the non-unique way of defining the instantaneous frequency [30]. A general signal with both time-varying amplitude and frequency can be written as:

$$x(t) = a(t)\cos(\varphi(t)) \tag{2.9}$$

where $a(t)$ is the instantaneous amplitude and $\varphi(t)$ is the instantaneous phase. There are an infinite number of ways to express a signal in the form shown in Eq. (2.9) and hence the difficulty of not having a unique definition of instantaneous frequency [32]. This was overcome by using the Hilbert Transform, defined in Eq. (2.10) to make the data analytical.

$$y(t) = H\big(x(t)\big) = (P/\pi)\int_{-\infty}^{\infty}(x(\tau)/(t-\tau))d\tau \tag{2.10}$$

where P is the Cauchy principle value. From Eq. (2.10), $x(t)$ and $y(t)$ form the complex pair for the analytical signal, $z(t)$.

$$z(t) = x(t) + iy(t) = a(t)e^{i\varphi(t)} \tag{2.11}$$

This provides a uniquely defined instantaneous amplitude and instantaneous phase which are expressed as:

$$a(t) = \sqrt{x(t)^2 + y(t)^2} \tag{2.12}$$

$$\varphi(t) = arctan(x(t)/y(t)) \tag{2.13}$$

Then the instantaneous frequency is defined as the time derivative of the instantaneous phase and is provided in Eq. (2.14) where it is also converted to hertz.

$$IF = (1/2\pi)\,(d\varphi(t)/dt)\ \text{Hz} \tag{2.14}$$

This definition for instantaneous frequency works well for mono-frequency signals but does not work well for multi-component signals [30, 32]. This prompted the development of a process that decomposed the original signal into its multiple mono-frequency components so that the definition of IF above could be applied to each individual component. The Empirical Mode Decomposition (EMD) method is described in [30]. This method is based on the assumption that the original signal is composed of several intrinsic mode functions (IMFs). An IMF is defined as a function with the two following characteristics: (1) the number of extrema, zeros, and zero crossings must either equal or differ at most by one and (2) at any point in time the mean value of the envelope defined by the local maxima and the envelope defined by the local minima equals zero. The EMD process is adaptive with the basis of the decomposition based on the data itself making it suitable for resolving data that are both nonlinear and non-stationary. The basis of the method is to decompose the signal based off of the characteristics of the IMFs in the data empirically. The EMD process can be implemented using the following procedure:

1. Identify the extrema and then connect the local maxima with a cubic spline to make the upper envelope and connect the local minima with a cubic spline to make the lower envelope.
2. Subtract the mathematical mean of the two envelops from the original signal to obtain the first component, h_1.
3. Continue the sifting process given in Eq. (2.15) until the first IMF of the signal is obtained. The stop criterion in [30] is used to determine when adequate sifting has been done and an IMF has been identified.
4. Once this is done, the first IMF is obtained. This would be the mode with the highest frequency and is denoted as c_1 in Eq. (2.16). Next the first IMF is extracted from the original data has shown in Eq. (2.17).

$$h_{1(k-1)} - m_{1k} = h_{1k} \tag{2.15}$$

$$c_1 = h_{1k} \tag{2.16}$$

$$z(t) - c_1 = r_1 \tag{2.17}$$

5. The residue, r_1, still containing information of the lower frequency modes is then treated as new data, and the sifting process is performed on it.
6. This procedure is repeated until all of the IMFs of the system have been identified and extracted from the original signal leaving only the final residue which is a monotonic function in which no other IMFs can be extracted.

The original signal can be restored by simply summing all the IMFs and the residue as shown in Eq. (2.18).

$$z(t) = \sum_{i=1}^{n} c_i + r_n \tag{2.18}$$

Once all of the IMFs have been extracted from the original signal, a complete set of mono-component signals which make up the original signal are obtained. The Hilbert transform is then applied to each IMF to determine the instantaneous frequency.

2.3 Introduction to Phase Portrait and Poincare Section

Phase portraits and Poincare sections are useful tools for classifying the state of motion of a nonlinear system [57]. The state space in nonlinear dynamics as defined in [58] is a generalization of the traditional phase space of the Hamiltonian dynamics. The phase diagrams contain important information about the behavior of a nonlinear dynamic system. By plotting the displacement vs. velocity of a system, a qualitative description of the state of motion of the system is obtained. The phase diagram of a linear system will typically have one loop indicating that the phase space and thus the dynamics of the system repeat in time, suggesting a state of periodic motion. A nonlinear system may have changing dynamics in time and thus the phase diagram will demonstrate this change of dynamics. Information about the attractors of the system such as a single point, limit cycle, and torus can be obtained using phase diagrams [58]. A Poincare section can be obtained by sampling the phase diagram at a particular frequency. If a data point of the displacement and velocity response of a perfect sine wave is pulled out once every period, then this will result in a single point in the velocity vs. displacement plane because history will repeat itself. If there are two modes in the signal composed of two perfect sine waves, then there will be two points in the Poincare section. For a chaotic response when history doesn't repeat itself there will be an infinite number of points in the Poincare section. Thus, the phase and Poincare plots can be used to obtain

a qualitative overview of the dynamics of a nonlinear system, but are not able to provide detailed information about the frequencies of the system.

2.4 Summary and Examples

This subsection will utilize various signals to visualize differences in the ability of the analysis tools described to investigate the dynamics of a frequency- and amplitude-modulated signal. As described in Section 2.1, Fourier transform is a linear transformation which attempts to describe the signal as the elementary functions sine and cosine. The Fourier transform is also globally inclusive as it integrates the signal over the full length of time and thus cannot identify local properties of the signal. Signals in the real-world are usually not represented by these elementary functions and have time-varying frequency characteristics. Instantaneous Frequency utilizes the signal itself to decompose it into its mono-frequency components and doesn't try to describe the signal as elementary functions as this is unrealistic for nonlinear and real-world signals. In addition, IF identifies the exact frequency values at that moment in time so it provides the best time frequency resolution possible. Figure 2.1 is the analysis of a basic low frequency signal with a higher frequency wave riding on it. The discrete Fourier transform (DFT) plot shows that the higher frequency component of 55 Hz, which is lower in energy, is not as dominant as the 10 Hz component. The IF plot clearly shows both the 55 and 10 Hz modes throughout the duration of the signal. The phase portrait reveals a stable system which is repeating its motion in time and the Poincare section contains two points indicating there are two frequencies in the signal. Figure 2.2 is a signal with a time-varying frequency and amplitude. At the 4 second mark, the

frequency of the signal changes from 10 to 30 Hz and the amplitude increases from 1 to 1.25. The DFT plot is unable to provide any information about the changing frequency spectrum and shows both modes as if they were in the signal throughout all time. The IF plot captures the change of frequency in the signal right at the 4 second mark and decidedly identifies both frequencies. This demonstrates the ability of IF to locate the time moment when the dynamics of the signal changed. The phase portrait clearly shows that two frequencies are present and the Poincare section has two points corresponding to the two frequencies of the signal. The previous two examples illustrated the accuracy of IF to identify the frequency components in the signal and the advantage that IF provides when analyzing a frequency-modulated signal. The following example demonstrates a case when Fourier transform is not able to provide any useful information, but IF is able to show the exact frequency spectrum of the signal. Figure 2.3 is a signal where the amplitude and frequency are linearly modulated in time. The Fourier transform suggests that there are a wide range of frequencies throughout the signal. The IF plot correctly shows a linearly changing frequency spectrum. The phase diagram has a spiral due to the linearly increasing frequency and the Poincare section has multiple points which are not repeating in time because the dynamics are changing from one moment in time to the next.

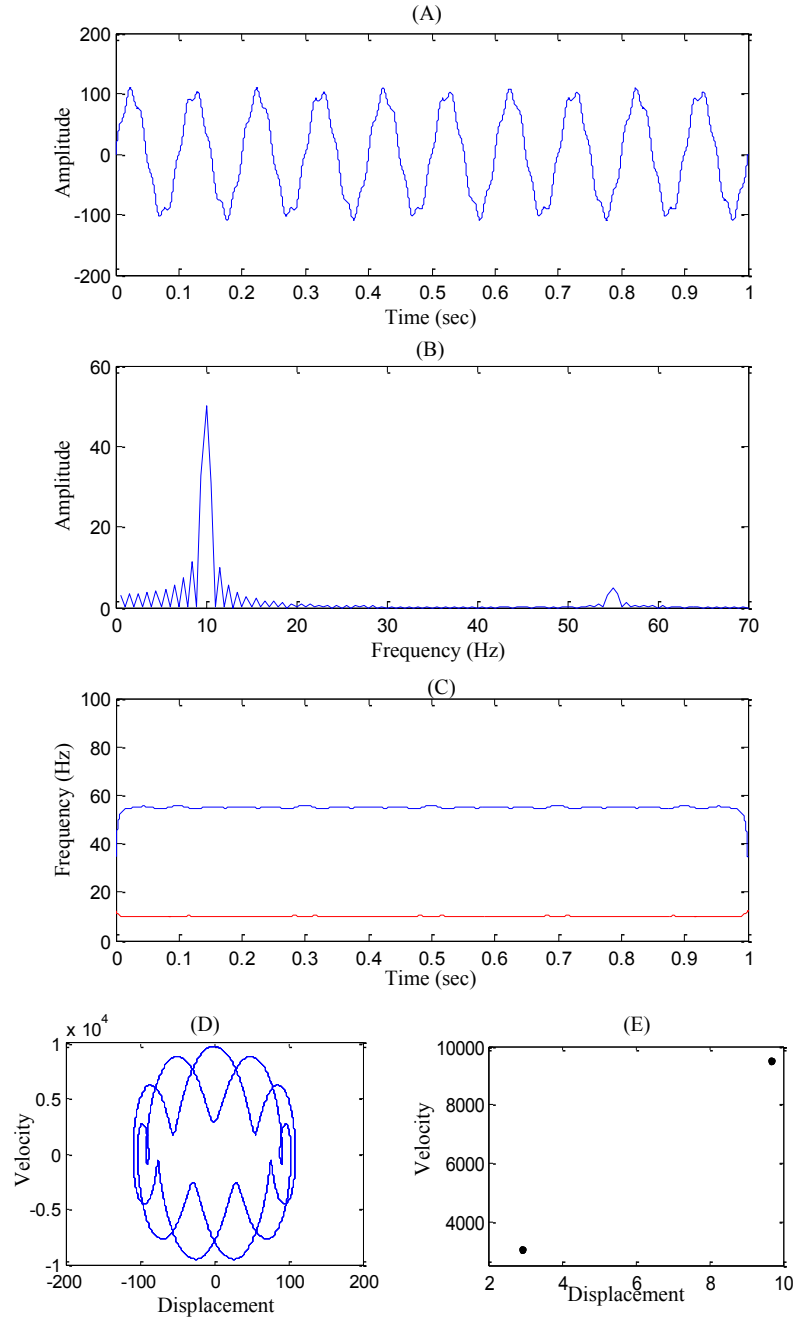

Fig. 2.1 Time response (A), DFT (B), IF (C), Phase portrait (D), and Poincare section (E) of the following signal. $f(t) = 100sin(2\pi 10t) + 7sin(2\pi 55t)$

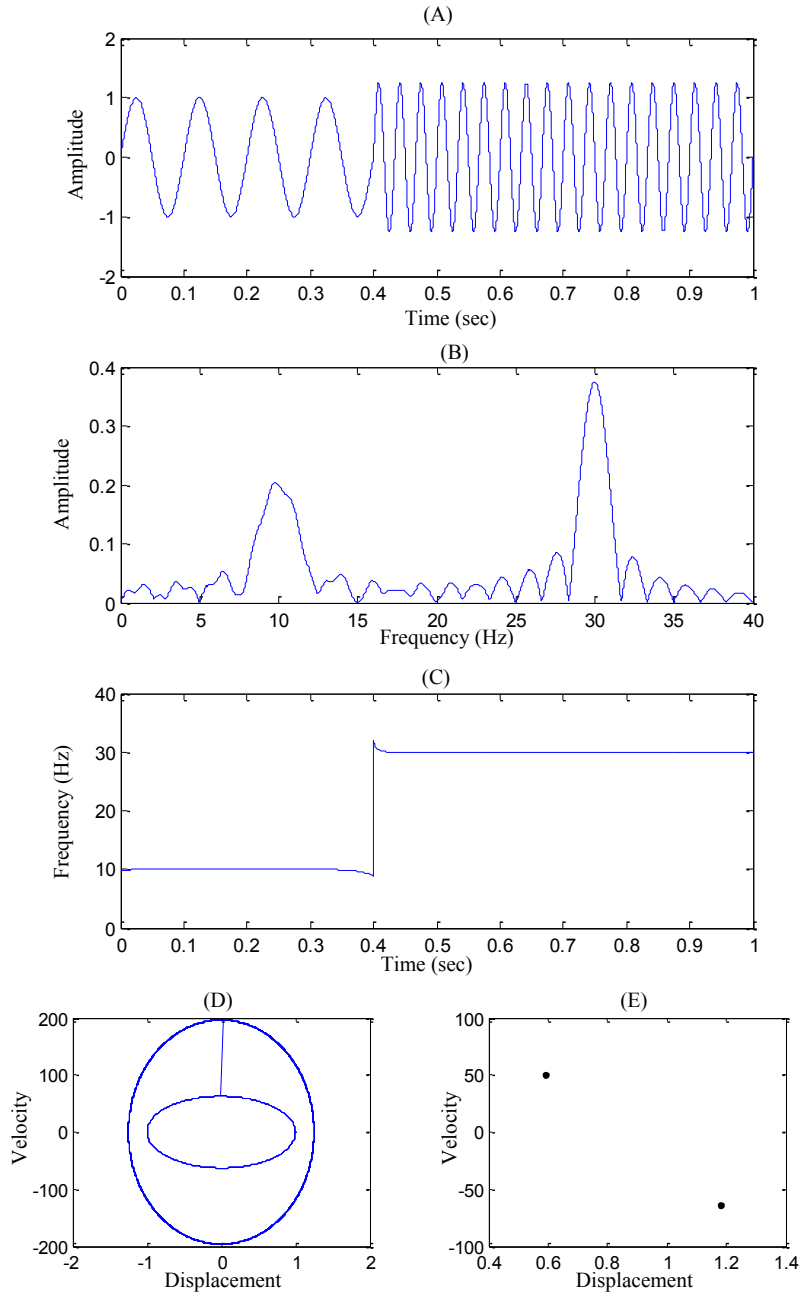

Fig. 2.2 Time response (A), DFT (B), IF (C), Phase portrait (D), and Poincare section (E) sampled at 10 Hz of a mono-frequency signal. $f(t) = \begin{cases} sin(2\pi 10t), & t < 0.4 \\ 1.25sin(2\pi 30t), & t \geq 0.4 \end{cases}$

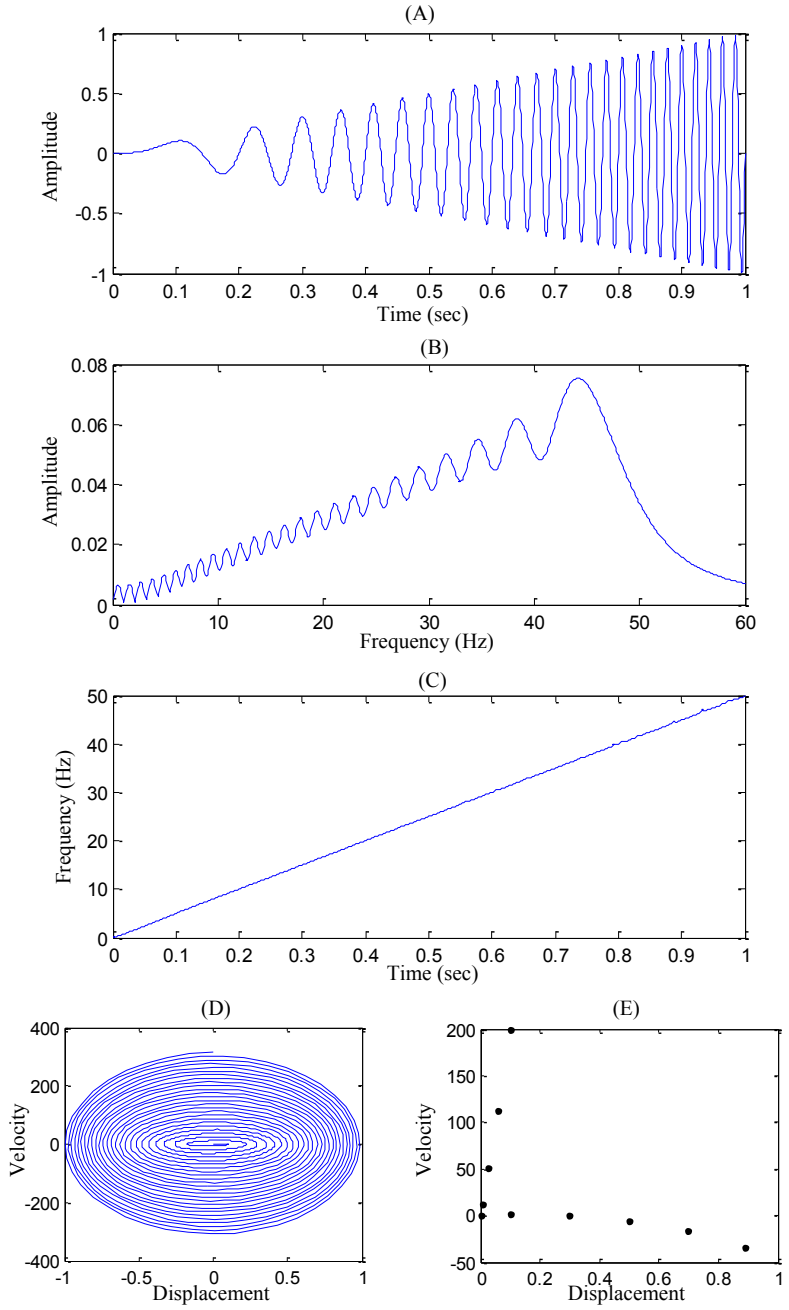

Fig. 2.3 Time response (A), DFT (B), IF (C), Phase portrait (D), and Poincare section (E) sampled at 10 Hz of the following chirp signal. $f(t) = tsin((\pi 50t)t)$

The final example in this section is a signal which more accurately represents vibrations in the machining process. In machining there are typically at least two frequencies in the signal which are the tool natural frequency and the spindle speed. Figure 2.4 demonstrates a signal that has a higher frequency component in 200 Hz which would correspond to the tool natural frequency and a lower frequency component in 25 Hz which relates to the spindle speed. This signal also demonstrates period-doubling bifurcation of the higher frequency component at the 0.5 second mark. The DFT shows all three frequencies and the amplitude of each frequency corresponds to the amplitude of that component of the signal. The IF plot captures the moment in time that period-doubling bifurcation occurs as well as identifies the frequency value for each mode. As the signal shifts there are discontinuities that occur which result in sharp fluctuations seen in the IF plot until the signal settles out. The phase diagram demonstrates multiple circles and the Poincare section has only two points suggesting there are two frequencies in the signal because the Poincare sampling rate is a multiple of both higher frequencies. This example was performed to illustrate the ability of IF to accurately characterize the transition to instability of a nonlinear signal. The route-to-chaos of a dynamic system involves bifurcations of the signal which are identified in the frequency domain [28]. Fourier transform is not able to observe this transition and thus IF is the analysis tool of choice employed throughout this research to identify the state of motion of a system.

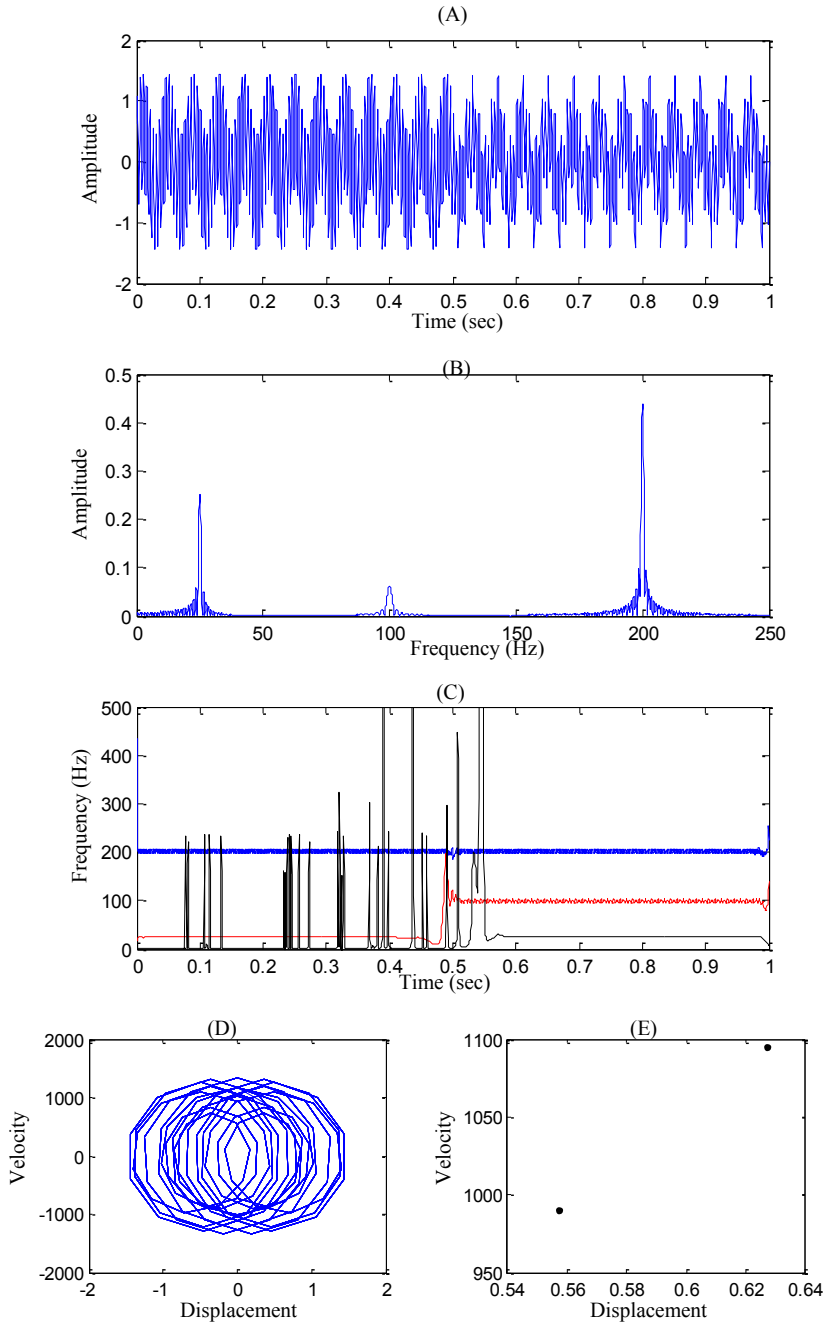

Fig. 2.4 Time response (A), DFT (B), IF (C), Phase portrait (D), and Poincare section (E) sampled at 25 Hz of the following signal that experiences a bifurcation.

$$f(t) = \begin{cases} 0.5sin(2\pi 25t) + sin(2\pi 200t), & t < 0.5 \\ 0.5sin(2\pi 25t) + sin(2\pi 200t) + 0.25sin(2\pi 100t), & t \geq 0.5 \end{cases}$$

3. TURNING EXPERIMENT

3.1 Description of 3D Turning Model

The turning experiment is designed utilizing the observations made by the research in [24]. The basis of the model in [24] is that the workpiece consists of three distinct sections: un-machined, being machined, and machined. The un-machined section is fixed to the spindle with the machined section supported by the tailstock. The workpiece in Fig. 3.1 is modeled as three rotors connected to each other via a shaft of negligible mass. The rotors are assumed to be rigid and remain vertical at all times. Eccentricity is assumed to be proportional for each section, and static deflection of the workpiece is assumed for a uniform bar since the DOC is small compared to the overall diameter. The mass of each section is assumed to act on its own center of mass and the thickness of each rotor is kept the same as the length of that respected section. This makes the thickness of the being machined section, t_o, very small. However, this is where the cutting force acts and thus the response of Rotor 2 is important to the dynamics of the 3-rotor system. The workpiece considers the changing stiffness and mass due to material continuously being removed during cutting. This makes the stiffness and mass of the workpiece nonlinear, and the tool is modeled with a linear and nonlinear stiffness term.

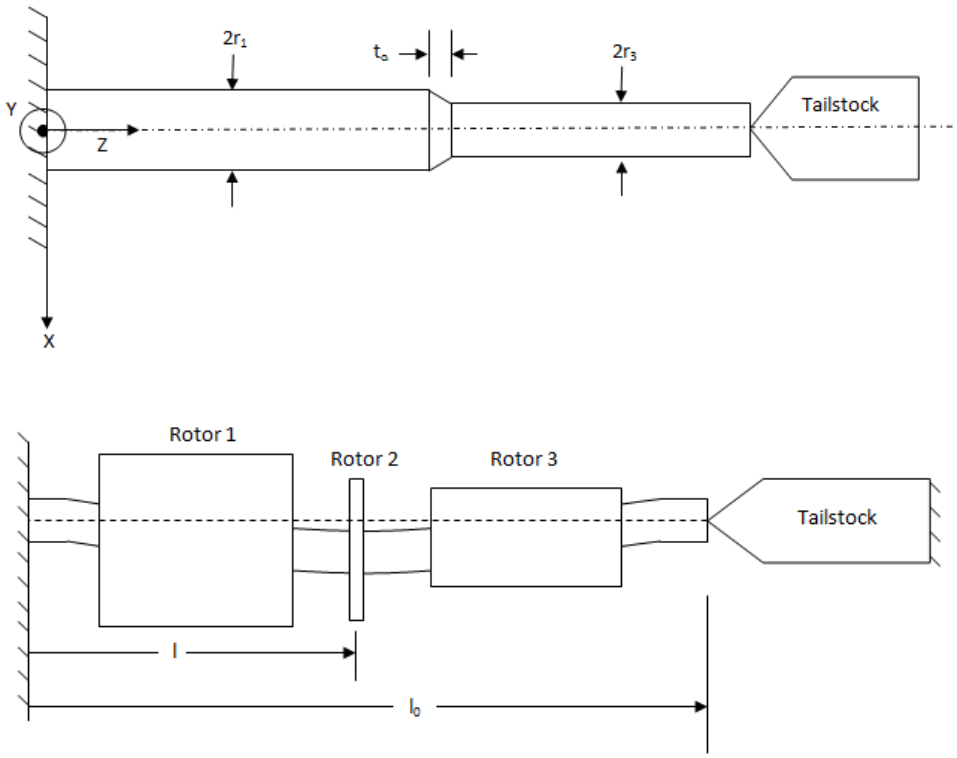

Fig. 3.1 Workpiece configuration (top) and workpiece modeled as 3 rotors (bottom)

The equations of motion for the model are given in Eqs. (3.1-3.3), where functions $f_i(t, x_2, y_2, z_t, z_t')$ are nonlinear functions defined in [24] and the subscript 2 corresponds to Rotor 2.

$$f_1(t)\ddot{x_2} + f_2(t)\dot{x_2} + f_3(t)x_2 = f_4(t, x_2, y_2, z_t, z_t') \tag{3.1}$$

$$f_5(t)\ddot{y_2} + f_6(t)\dot{y_2} + f_7(t)y_2 = f_8(t, x_2, y_2, z_t, z_t') \tag{3.2}$$

$$M_z\ddot{z_t} + k_z z_t + k_{zz} z_t^3 = f_9(t, x_2, y_2, z_t, z_t') \tag{3.3}$$

The tool is only considered in the Z-direction and workpiece motions in the Z-direction are assumed negligible. The force model used for the system is similar to the

3D force model developed in [23] except that the tool nose radius is not considered and a new method for calculating the instantaneous chip cross-sectional area and instantaneous DOC is developed. The base form for the force equations as a function of the normal, F_n, and frictional, F_f, forces are expressed in Eqs. (3.4-3.6) where γ_c is the chip flow angle, and coefficients b_{ij} are determined from the coordinate transformation matrices as functions of lead, inclination, and rake angles.

$$F_X = F_f(b_{x1}\sin(\gamma_c) + b_{x2}\cos(\gamma_c)) + b_{x3}F_n \tag{3.4}$$

$$F_Y = F_f\big(b_{y1}\sin(\gamma_c) + b_{y2}\cos(\gamma_c)\big) + b_{y3}F_n \tag{3.5}$$

$$F_Z = F_f(b_{z1}\sin(\gamma_c) + b_{z2}\cos(\gamma_c)) + b_{z3}F_n \tag{3.6}$$

As the DOC used is much larger than the tool nose radius, the effect of nose radius is considered negligible. Many models assume that either the chip thickness or DOC is constant; however, in reality the tool and workpiece vibrate simultaneously so the chip width changes due to the motion of the tool at the previous workpiece revolution and the DOC changes due to the instantaneous position of the workpiece and tool. In this model, the frictional and normal forces are assumed to be a function of the instantaneous chip thickness and DOC. In addition to the forces produced due to cutting, the workpiece has restoring forces which occur when the workpiece is deflected.

3.2 Experiment Design

The research in [24] demonstrates that the workpiece is critical to the underlying dynamics of the system and in [26] the detection of chatter is more prominent in the workpiece vibrations rather than the tool vibrations. However, tool vibration is predominantly the only variable investigated in research because it can easily be

obtained using contact sensors. Thus, in this research the objective is to investigate both the tool and workpiece vibrations. There are many different direct and indirect methods for monitoring the turning process as discussed in detail in [29]. Indirect measurements deal with measuring process variables such as motor current and then relating this to cutting force through mathematical and/or empirical relations. Direct methods allow for the direct measurement of the variable of interest which results in a high degree of accuracy. Tool vibrations can be directly measured using contact sensors such as force dynamometers, accelerometers, and strain gauges. However, contact sensors come with a mechanical resonance frequency that must be avoided. This limits the available sensing bandwidth and thus the ability to accurately capture high frequencies characteristic of a nonlinear process. Also, contact sensors are not applicable for measuring workpiece vibrations. Non-contact sensors such as eddy-current probes and displacement lasers can accurately capture vibration over a broad range of frequencies and are not limited by their mechanical resonance. Non-contact sensors also provide the advantage of ensuring the dynamics of the system is not altered since they are mounted independent of the process of interest. However, various non-contact sensors such as eddy-current probes require a very small measuring range which increases the probability of damaging the sensor during the event of tool failure or increased workpiece deflection. The availability of long range laser displacement sensors overcomes this difficulty.

The following experiment utilizes a laser displacement sensor which has a wide bandwidth and submicron resolution to capture both the tool and workpiece vibrations

during cutting. The tests were set up on a Victor lathe with 1,800 rpm capacity (Fig. 3.2). An NI6009 DAQ running at a sampling rate of 48 kHz was coupled with a Keyence LK-G 157 that was mounted above the workpiece on a rigid stand independent of the lathe and shielded from chips with an acrylic sheet (Fig. 3.3). For tool vibrations, the stand is adjusted so that the laser is mounted above the tool similar to the workpiece configuration. The laser controller was used to calibrate the system for the desired target material and to ensure no filtering of the data occurred. The DAQ was connected to a PC and a LabView program was built to continuously record and save the data. The details of the LabView program and the laser controller settings used are provided in Appendices A and B.

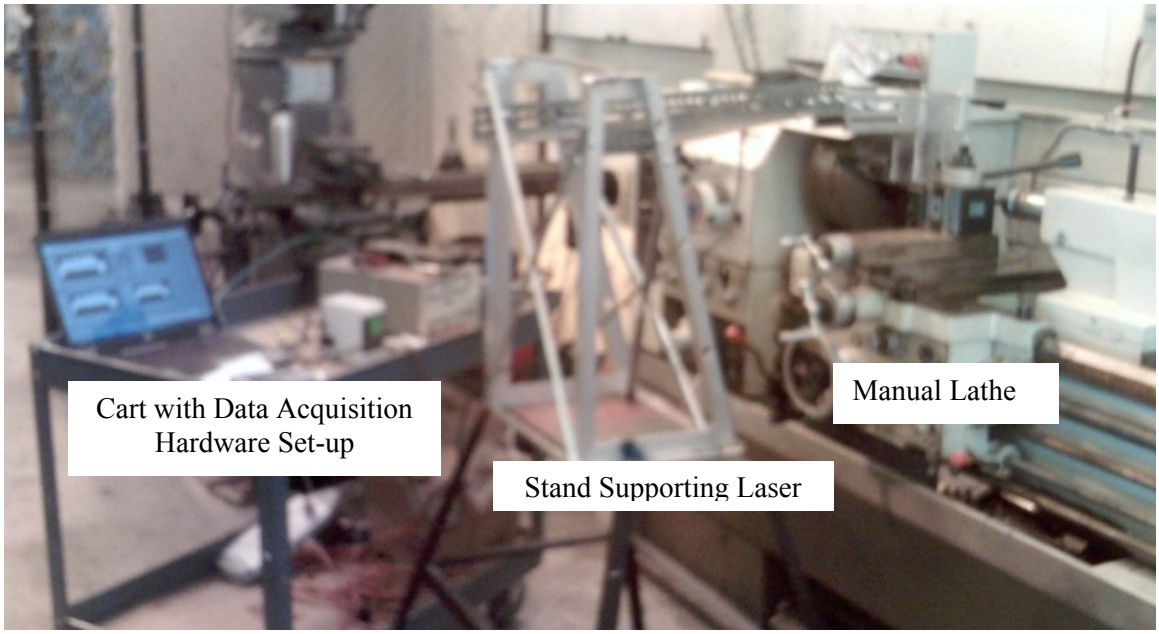

Fig. 3.2 Picture of experimental set-up

(A)

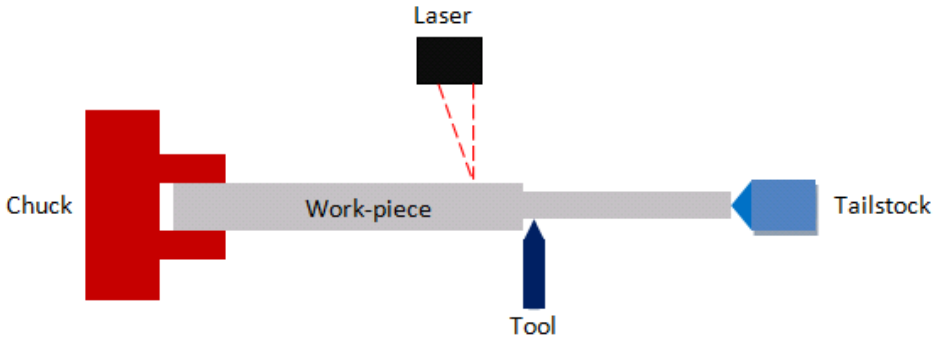

(B)

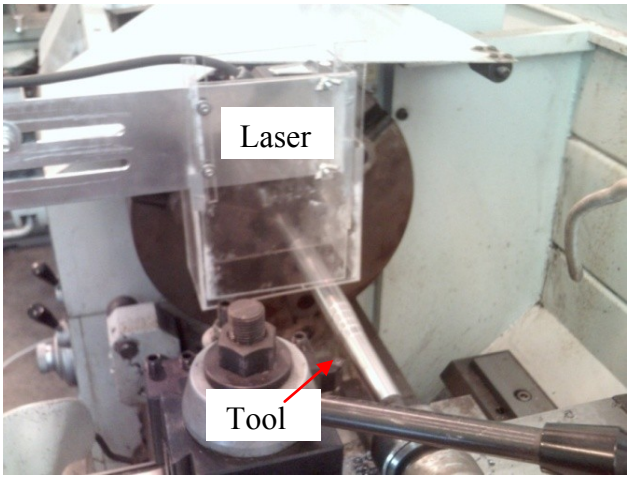

(C)

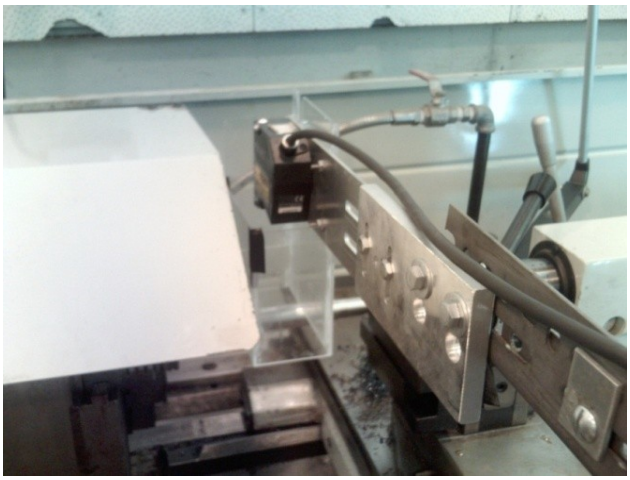

Fig. 3.3 (A) Schematic of laser set-up; (B) and (C) Experimental set-up of laser mounted above workpiece

3.3 Experiments

A Kennametal SSDC 45° tool holder with a SCMT-LF insert having a side cutting edge angle of 45°, inclination angle of 5°, rake angle of 5°, and a nose radius of 0.8mm was used for the cutting tests. The cutting was performed without coolant and a new insert was used for each test to ensure that tool wear did not affect the system. The workpiece material was a 25.4mm in diameter 4140 steel bar configured to be as similar as possible to the workpiece considered in [24] without wasting material. Here the workpiece has a significant un-machined section as well as a significant machined section as seen in Fig. 3.4 (A). However, to efficiently use the workpiece material available, the workpiece was set up with stepped sections for the changing DOC tests as shown in Fig. 3.4 (B). The section being machined was pre-configured to achieve about 10mm of cutting at different DOCs for approximately 5 tests before the workpiece had to be re-configured. The un-machined section was approximately 150mm while the machined section varied from ~50mm to ~100mm. This also placed the cutting and laser measurement towards the center of the workpiece where the largest deflection is experienced. To study turning dynamics, changing DOC tests were performed for different spindle speeds with a constant feed. The lathe was run at various spindle speeds to eventually have 885 and 1239 rpm determined along with a constant feed of 0.09mm/rev as the smoothest speed of operation. To accurately record the DOC of each cut, the diameter of the workpiece was measured before and after each cut. The tests performed along with the observations made are tabulated in Table 3.1. Figure 3.5 gives

the observations noted by the operator as excessive noise and chatter associated with poor workpiece surface finish.

(A)

(B)

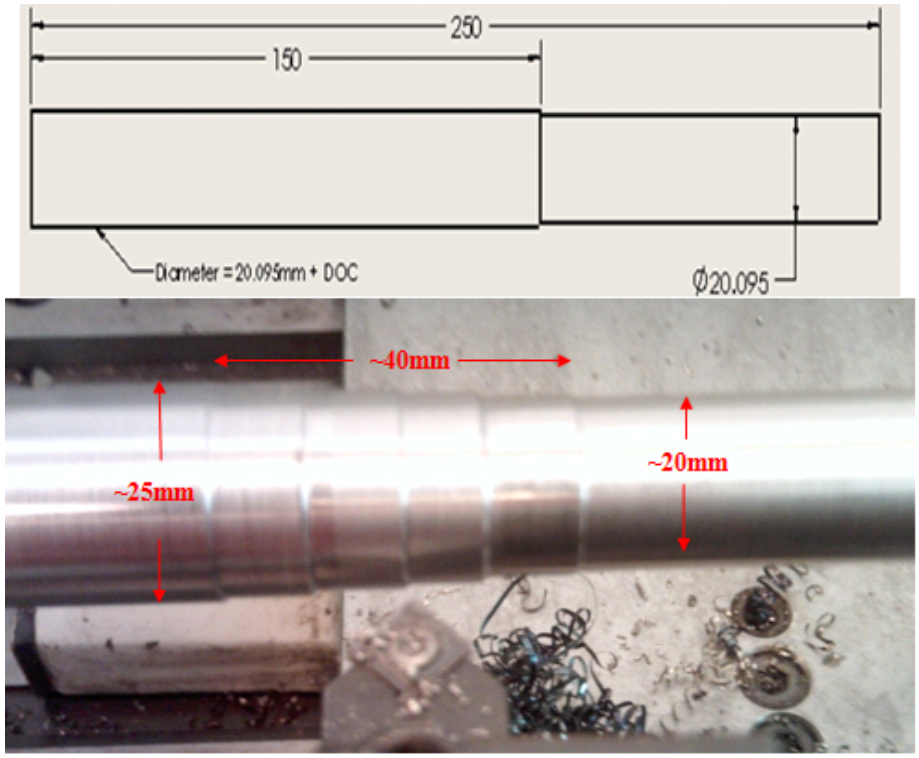

Fig 3.4 (A) Workpiece configuration for model in [24]; (B) Workpiece configuration for changing DOC tests used in experiment

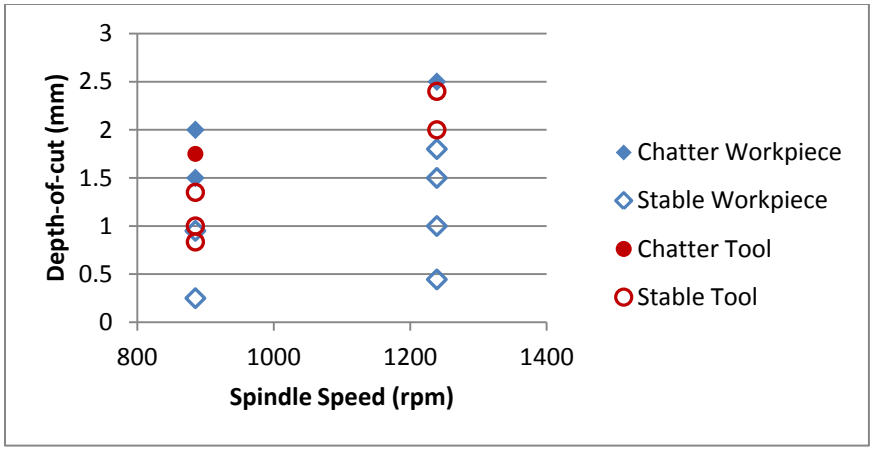

Fig. 3.5 Graph of operator observed stability points

Table 3.1 Cutting Tests Performed and Operator Observations

Machined Diameter (mm)	Unmachined Diameter (mm)	Depth of Cut (mm)	Observations
885 RPM Workpiece Vibrations			
20.4	20.9	0.25	stable cutting
20.3	22.2	0.95	stable cutting
20.2	23.2	1.5	noise/poor surface
20.2	24.2	2	noise/poor surface
885 RPM Tool Vibrations			
20.43	22.1	0.835	stable cutting
21.1	23.1	1	stable cutting
21.4	24.1	1.35	stable cutting
20.3	23.8	1.75	noise/poor surface
1239 RPM Workpiece Vibrations			
19.94	20.83	0.445	stable cutting
19.94	21.94	1	stable cutting
20.1	23.1	1.5	stable cutting
20	23.6	1.8	stable cutting
20.2	25.2	2.5	light noise/poor surface
1239 RPM Tool Vibrations			
20	24	2	stable cutting
20	24.8	2.4	stable cutting

3.4 Amplitude Analysis of Raw Vibration Data

The raw vibration signals are analyzed to determine the change in amplitude for the response under different cutting conditions. Since it is difficult to accurately quantify the vibration magnitude just by observing the raw signal, the root-mean-square (RMS) method is used. The RMS is a measure of the magnitude of a set of values, so as the vibration magnitude increases, the RMS values increase as well. The RMS plots presented account for the offset of the original signal.

The dry-run vibrations with the spindle off are compared to the dry-run vibrations of the workpiece with the workpiece rotating at 885 rpm and 1239 rpm in Fig. 3.6. The vibrations at 885 rpm have maximum values around 40 microns and the 1239 rpm has maximum values around 50 microns. The RMS for 1239 rpm is twice as large as that at 885 rpm suggesting that the whirling at 1239 rpm is much larger than what is portrayed by the vibration signal. This is because at 885 rpm there are just a few points which stray up to 40 microns in the vibration signal giving the image that the difference between the 885 rpm and 1239 rpm whirling isn't very large. However, the RMS provides insight about the overall magnitude of the entire set of values demonstrating that at 1239 rpm the vibration values consistently reach magnitudes much larger than the 885 rpm case. The dry-run vibrations for the tool at 885 rpm and 1239 rpm are shown in Fig. 3.7. The dry-run vibrations of the tool are slightly larger than the spindle not on vibrations in Fig. 3.6 and the 885 and 1239 rpm have similar vibration and RMS magnitudes. Thus, the lathe machine has similar vibration magnitudes at each speed but workpiece whirling is much larger at 1239 rpm.

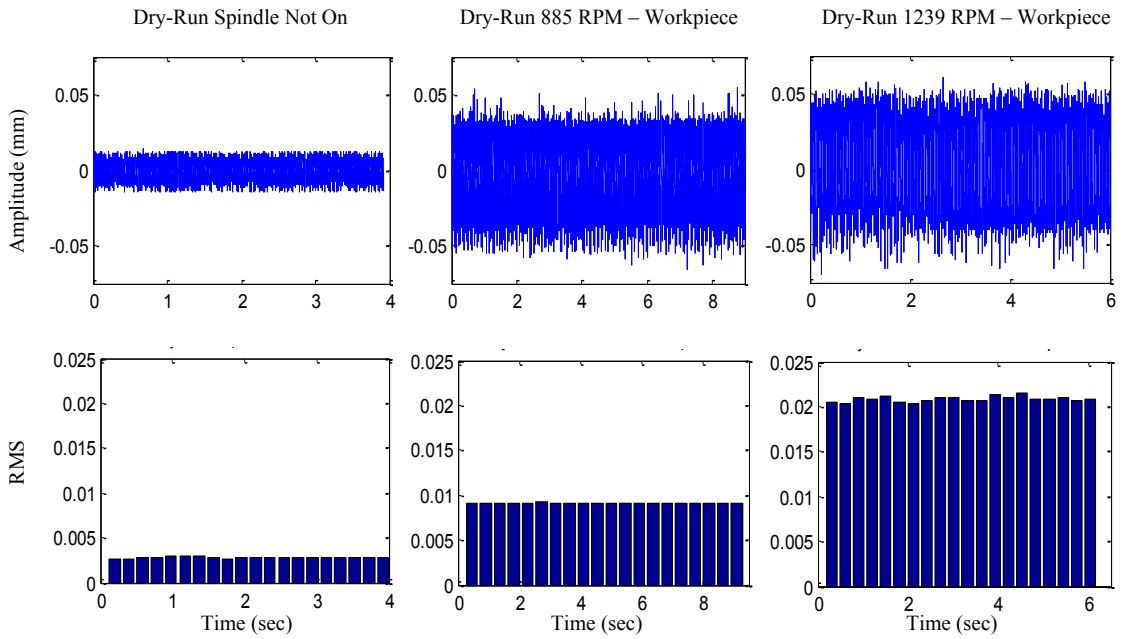

Fig 3.6 Vibration response for dry-run spindle not on (left), dry-run at 885 rpm for the workpiece (middle), and dry-run at 1239 rpm for the workpiece (right)

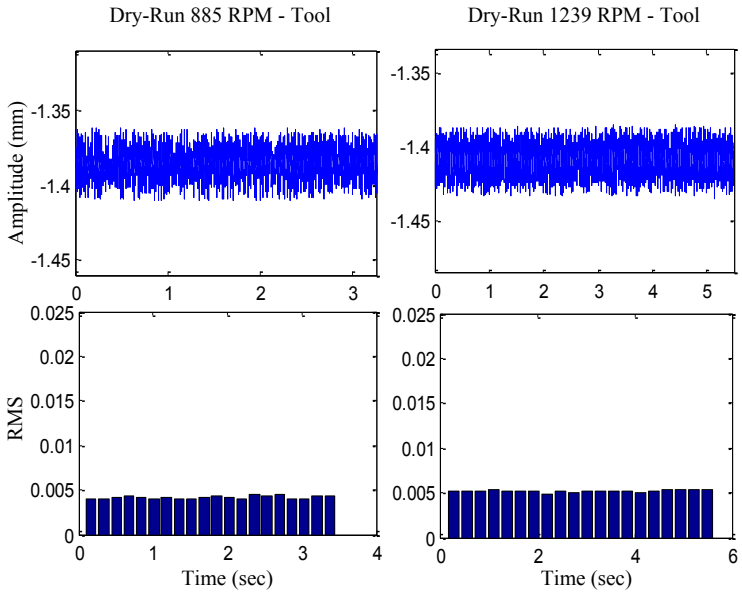

Fig. 3.7 Vibration response for dry-run at 885 rpm for the tool (left) and dry-run at 1239 rpm for the tool (right)

Chatter-free and chatter cutting workpiece vibrations at 885 rpm are compared in Fig. 3.8. The chatter-free vibrations at 0.25 and 0.95mm DOC have similar vibration magnitudes. The chatter cutting at 1.5mm DOC demonstrates a clear increase in vibration magnitude. The chatter-free vibrations for 1239 rpm at 0.445 and 1.5mm DOCs in Fig. 3.9 have different vibration magnitudes with the cutting at 1.5mm DOC having larger vibrations. The chatter cutting at 2.5mm DOC at 1239 rpm shows an increase in vibration magnitude. Here cutting did not last very long due to the intense chatter observed by the operator so enough time was not given for the vibration magnitude to continue to increase. The tool response in Fig. 3.10 shows similar vibrations for the chatter-free cases of 0.835mm and 1mm DOCs at 885 rpm. The chatter cutting at 1.75mm DOC and 885 rpm demonstrates an impulse in vibration magnitude at 4 seconds and increased sporadic vibrations in the vibration response. The two cases shown for 1239 rpm tool vibrations in Fig. 3.11 are chatter-free conditions and similar vibrations are observed in each case. The vibration responses shown demonstrate similar vibration magnitudes for chatter-free cutting except at low DOCs and increased vibrations for chatter cutting. Also, the workpiece vibrations are much larger than the tool vibrations for chatter-free and chatter cutting.

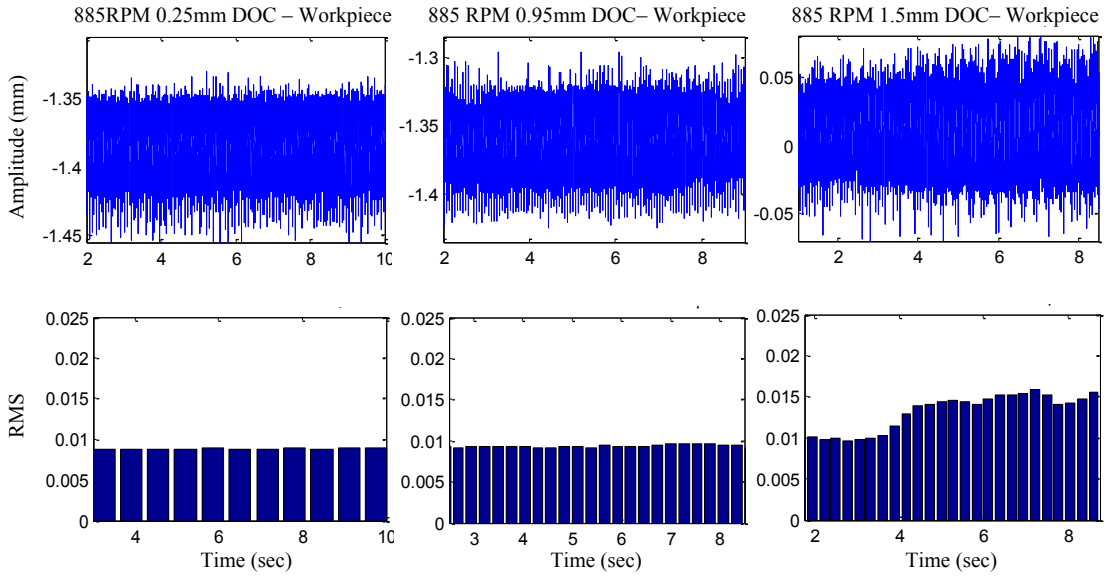

Fig. 3.8 Workpiece vibrations at 885 rpm for chatter-free cutting at 0.25mm (left) and 0.95mm (middle) DOC, and chatter cutting at 1.5mm (right) DOC

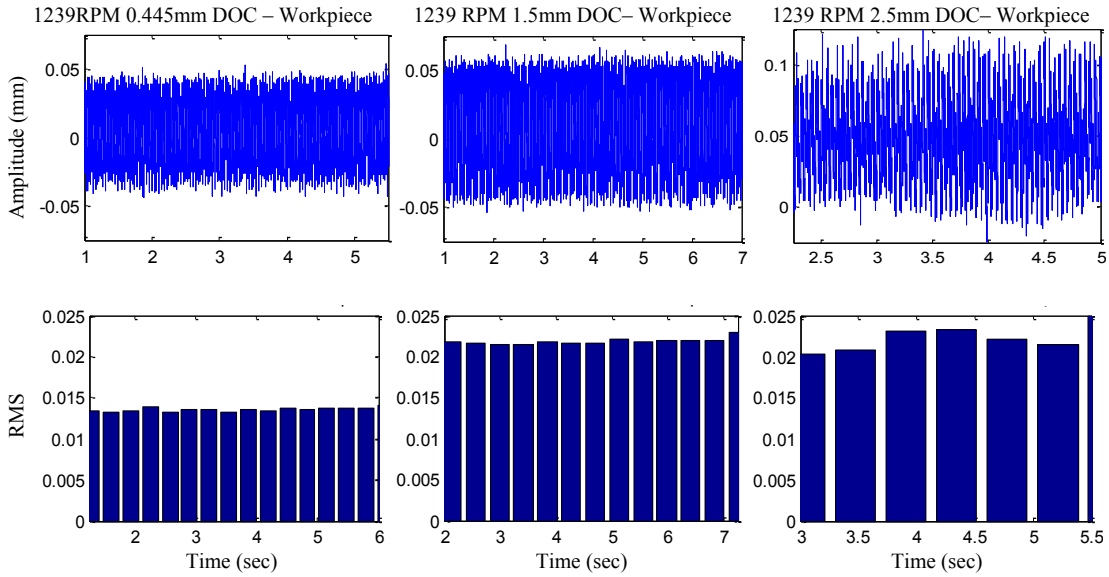

Fig. 3.9 Workpiece vibrations at 1239 rpm for chatter-free cutting at 0.445mm (left) and 1.5mm (middle) DOC, and chatter cutting at 2.5mm (right) DOC

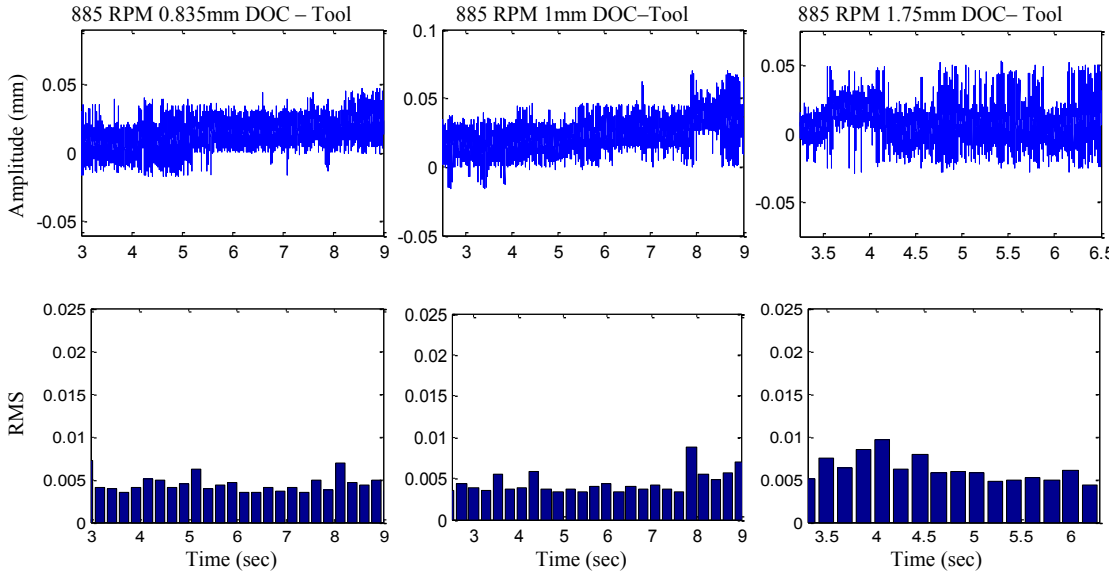

Fig. 3.10 Tool vibrations at 885 rpm for chatter-free cutting at 0.835mm (left) and 1mm (middle) DOC, and chatter cutting at 1.75mm (right) DOC

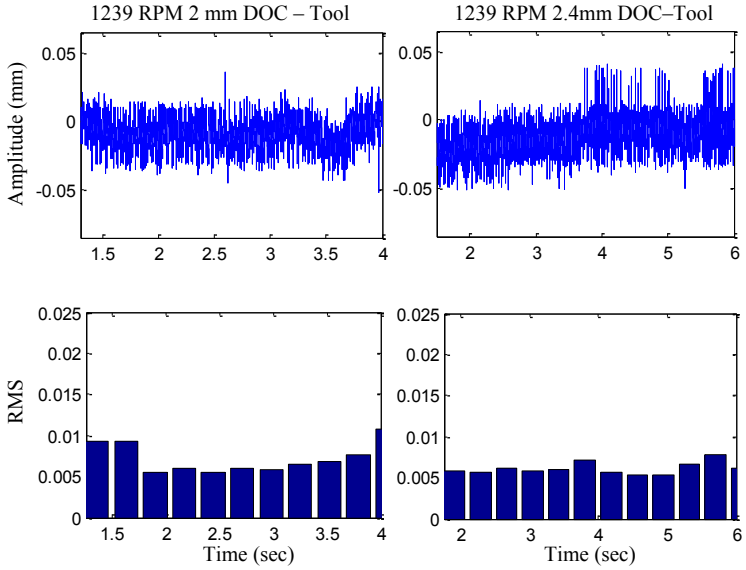

3.11 Tool vibrations at 1239 rpm for chatter-free cutting at 2mm (left) DOC and 2.4mm (right) DOC

4. EXPERIMENTAL VIBRATION ANALYSIS USING INSTANTANEOUS FREQUENCY

4.1 Analysis Procedure

Machining responses are nonlinear, non-stationary, and of time-varying amplitude and frequency. To meet the objective for studying machining instability, the concept of IF is adopted to resolve individual spectral components in time. Analysis of experimental cutting data using IF, however, is limited to non-existent in the literature. Thus, a procedure for analyzing experimental vibration data with IF is developed. The raw experimental data are highly nonlinear with multiple modes due to electrical and environmental noise as well as the vibration modes related to the system. Because IF provides all the modes inherent of the signal covering a wide range of frequencies, resolving the underlying dynamics using the tool is necessarily difficult. It would be beneficial to determine the important modes related to the process so only these modes and thus a more narrow range of frequencies are monitored. The normal process for eliminating noise in a signal is to filter the signal. However, filtering a signal alters the original response which could result in inaccurate observations made in the frequency domain as well as possibly filtering out nonlinear high frequency components. Since the motive is to provide insight into cutting dynamics, no signal filtering is performed to ensure that the inherent features are faithfully retained. Utilizing EMD, each decomposed mode that represents either measurement noise (environmental or electrical) or a vibration mode related to the system can then be separated accordingly. The

following procedure allows for the identification of the vibration modes related to noise so that only the modes related to the system are monitored for dynamic changes.

1. Perform Baseline Data Collection with the sensor in its desired position and environment
    a. Take vibration data with the system not running (spindle off)
    b. Take vibration data with the system running at each spindle speed (spindle on and no cutting)
    c. Take vibration data under stable conditions for each spindle speed (spindle on and cutting)
2. Compare the IFs to establish which modes are associated with measurement noise
3. Adjust the monitoring of the system to only the modes associated with the process

4.2 Baseline Analysis of Signal

4.2.1 885 RPM – Workpiece Vibrations

The IF for the top ten individual modes of the workpiece baseline data are plotted in Figs. 4.1- 4.3. These figures compare the IF plots for three different states of cutting in order to identify the modes related to noise and those related to the process. By comparing the plots, IF 1, 2, and 7 are difficult to make sense of and IF 3, 4, 5, 6, 8, and 9 indicate to have changed due to the presence of the lathe running and cutting. Each mode fluctuates around a dominate frequency with discontinuities that signify abrupt changes in dynamics and nonlinearity. These abrupt changes make it difficult to

quantitatively characterize and identify the noise modes by only using individual IF plots like in Fig. 4.1. To overcome this, it is assumed that if a mode remains unchanged then its basic distribution (shape) and dominant frequency will remain unchanged. Then to compare the IFs under different cutting conditions, the histograms (distribution) of the individual IFs are used to visualize changes in the individual modes. The histograms in Fig. 4.4 and 4.5 show that IF 1 and IF 2 essentially retain the same shape and dominate frequencies for each case suggesting they did not change from one case to the other and are thus modes related to noise. Modes 3 and 4 have shifted to lower frequencies of ~2500 and 1500Hz from the ~4000 and 2000Hz respectively when comparing the spindle-off to the spindle-on and stable cutting. This results in IF 3 and IF 4 to be associated with the workpiece natural frequency since there was not a change when cutting was present. It is observed that IF 5 and IF 6 are shifted lower when comparing the spindle-off to spindle-on (no cutting) histogram plots, suggesting that these modes are related to the process. Furthermore, when comparing the spindle-on (no cutting) to the stable cutting histograms, it shows that the distribution of IF 5 and IF 6 have altered again to approximately 750 and 400 Hz. This suggests that these modes are related to the tool being engaged in the workpiece and will then be considered the tool coupling frequencies. In Fig. 4.5 IF 7 and IF 8 essentially retain the basic shape and dominant frequency when comparing the three cases. The two modes, IF 9 and IF 10, become clear frequencies around 42Hz and 18Hz which is related to a lathe vibration and the spindle speed when the spindle is at 885 rpm. The modes below the spindle speed mode are recognized as low frequency noise and are not presented.

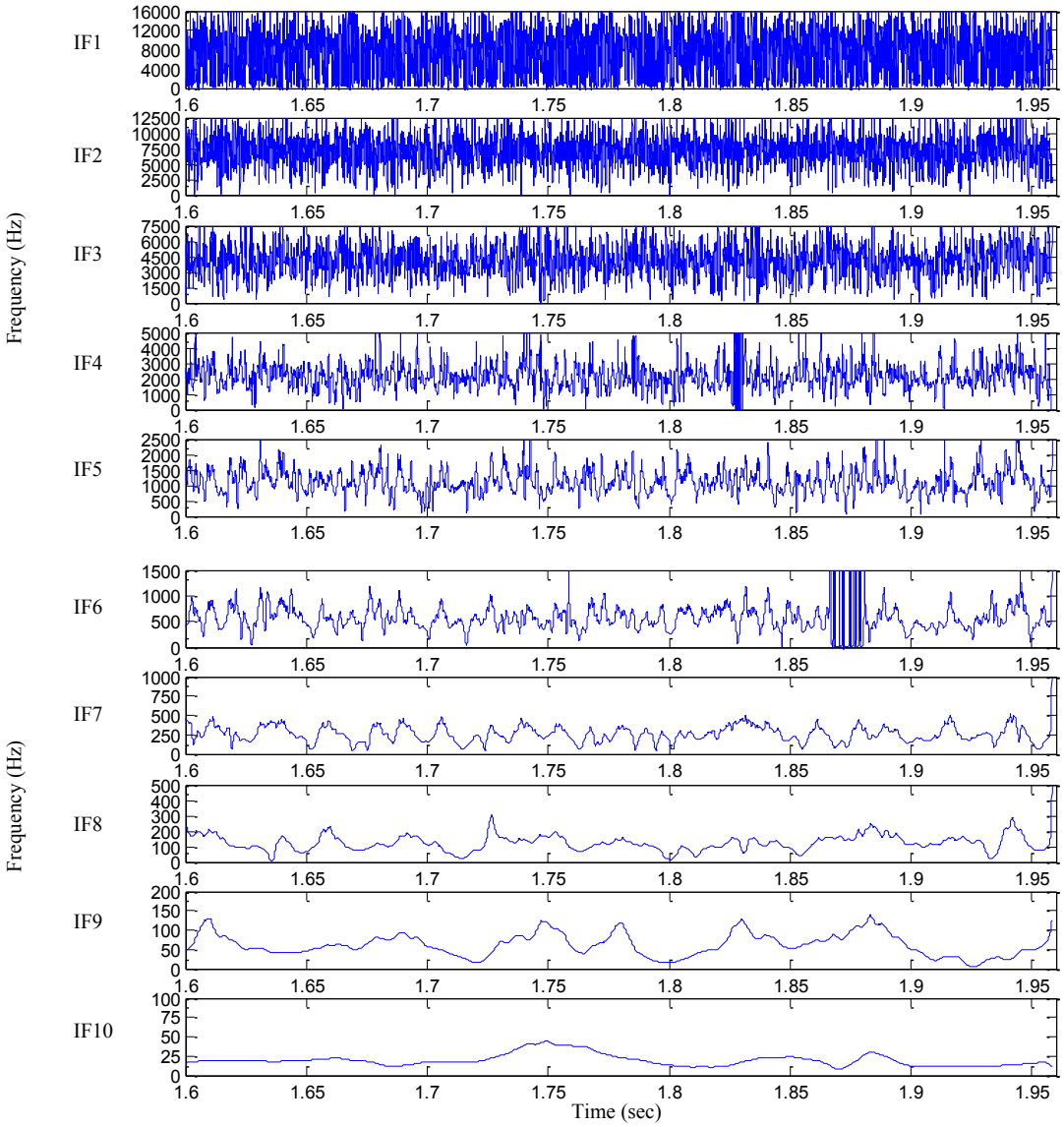

Fig. 4.1 Top ten frequency modes for spindle-off vibrations

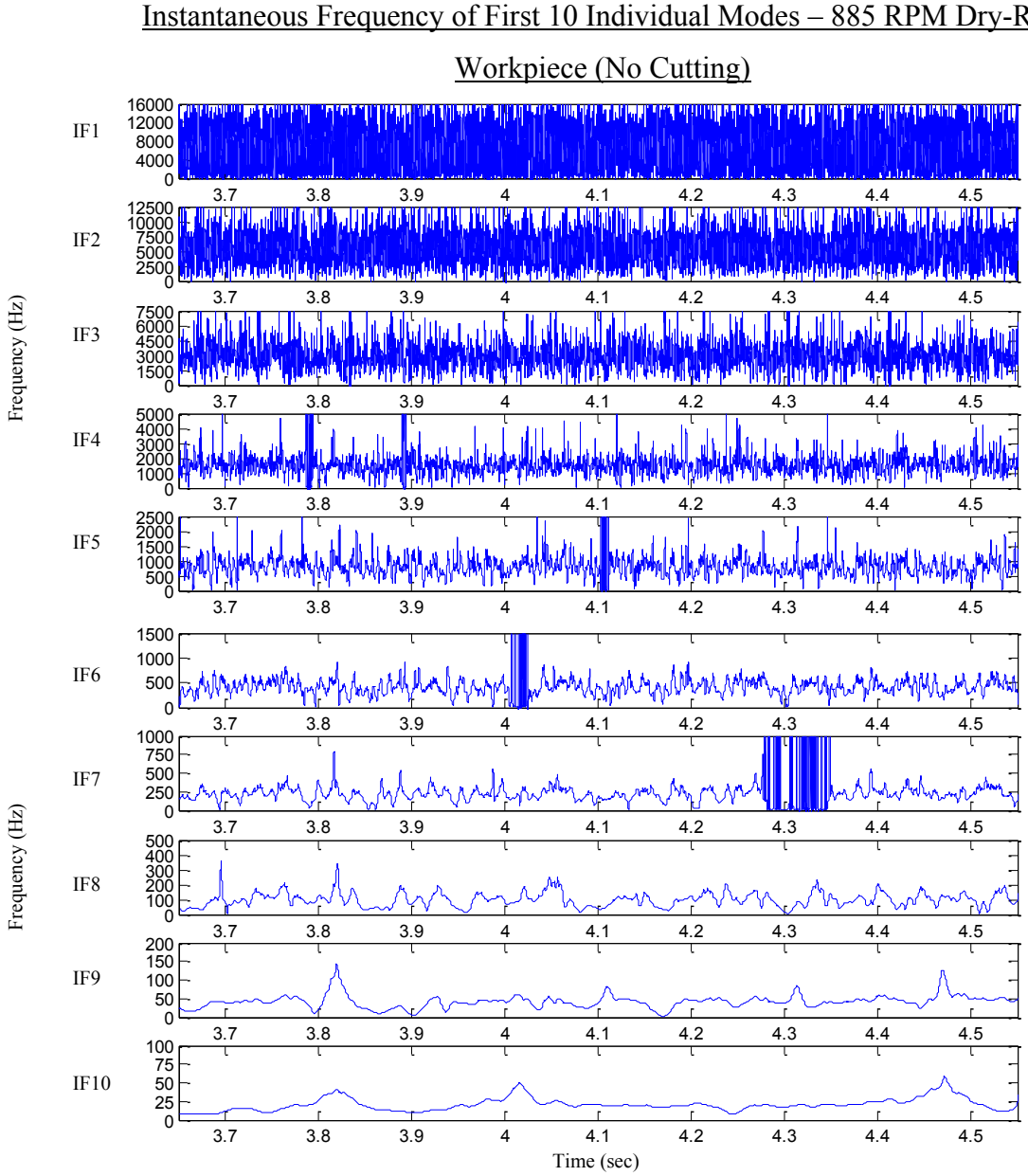

Fig. 4.2 Top ten frequency modes for 885 rpm dry-run workpiece vibrations

Instantaneous Frequency of First 10 Individual Modes – 885 RPM 0.95mm DOC Chatter-Free Cutting

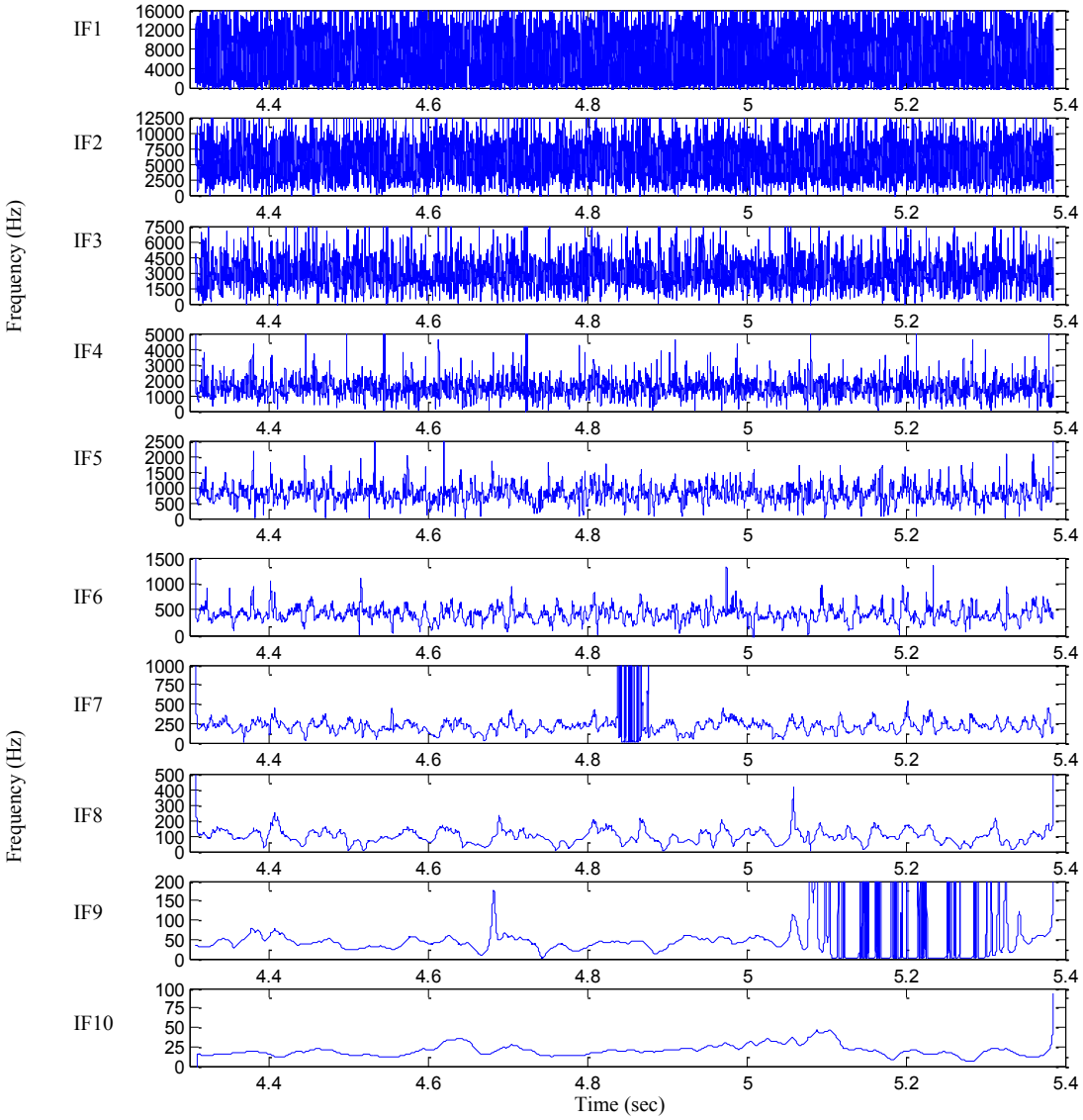

Fig. 4.3 Top ten frequency modes for 885 rpm and 0.95mm DOC chatter-free cutting

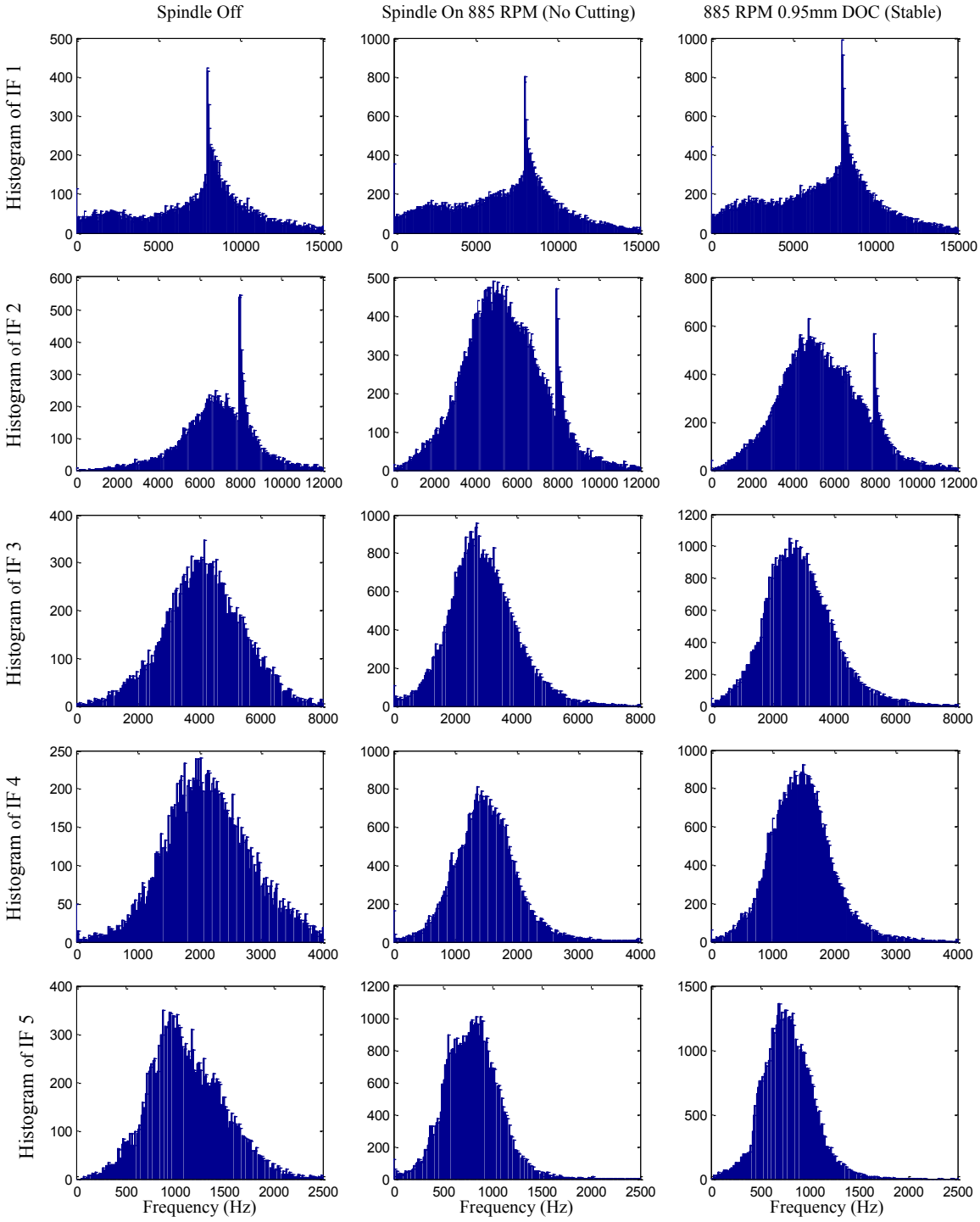

Fig. 4.4 Histogram plots of individual IFs 1-5 at 885 rpm – workpiece

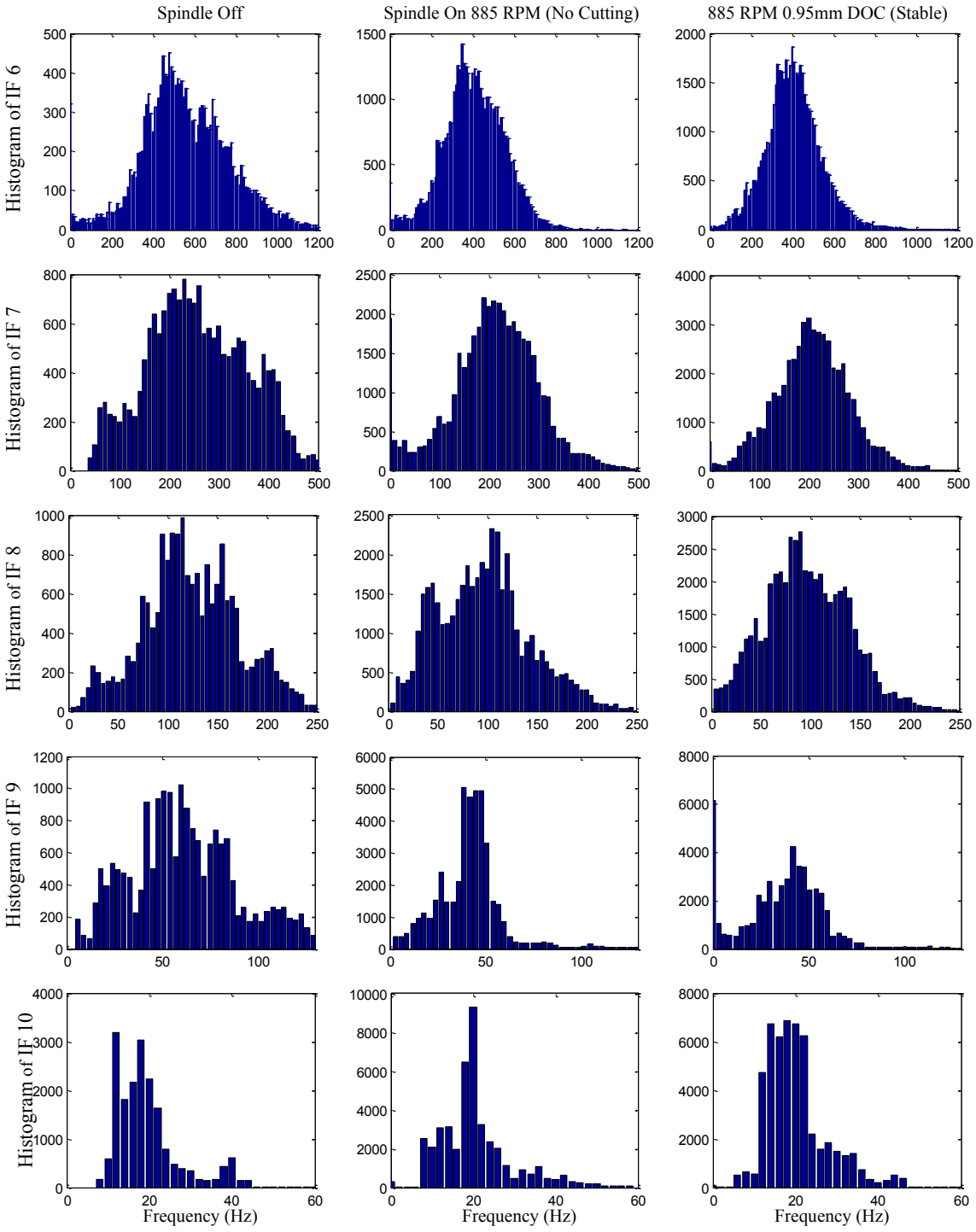

Fig. 4.5 Histogram plots of individual IFs 6-10 at 885 rpm – workpiece

4.2.2 1239 RPM – Workpiece Vibrations

The top ten individual IF plots for the baseline workpiece vibrations at 1239 rpm are provided in Figs. 4.6 - 4.7. When comparing Fig. 4.6 with the spindle off IF plots in Fig. 4.1, it is observed that due to the spindle rotating at 1239 rpm the spindle frequency of ~22 Hz is now IF 8, and IF's 9 and 10 are low frequency noise. This is further clarified in the histograms of Figs. 4.8 - 4.9 where there is a very clear spindle speed frequency in IF 8. This mode is a dominant mode at this spindle speed due to the increased whirling which occurs at 1239 rpm as identified in Section 3.4. In Fig. 4.8, IF 1 and IF 2 retain the same shape and dominant frequency rendering these as high frequency noise modes. Similar to the 885 rpm case, IF 3 and IF 4 have shifted to ~2800 and 1620Hz from the ~4000 and 2000Hz seen in spindle-off data (Fig. 4.4) when the spindle is at 1239 rpm and stable cutting is present. Thus, these modes are related to the workpiece natural frequency and bifurcation mode. In Figs. 4.8 and 4.9, IF 5 and IF 6 have altered due to the presence of the spindle-on and again when cutting is present, designating these as cutting related modes at ~900 and 450Hz.

Instantaneous Frequency of First 10 Individual Modes – 1239 RPM DOC Dry-Run Workpiece (No Cutting)

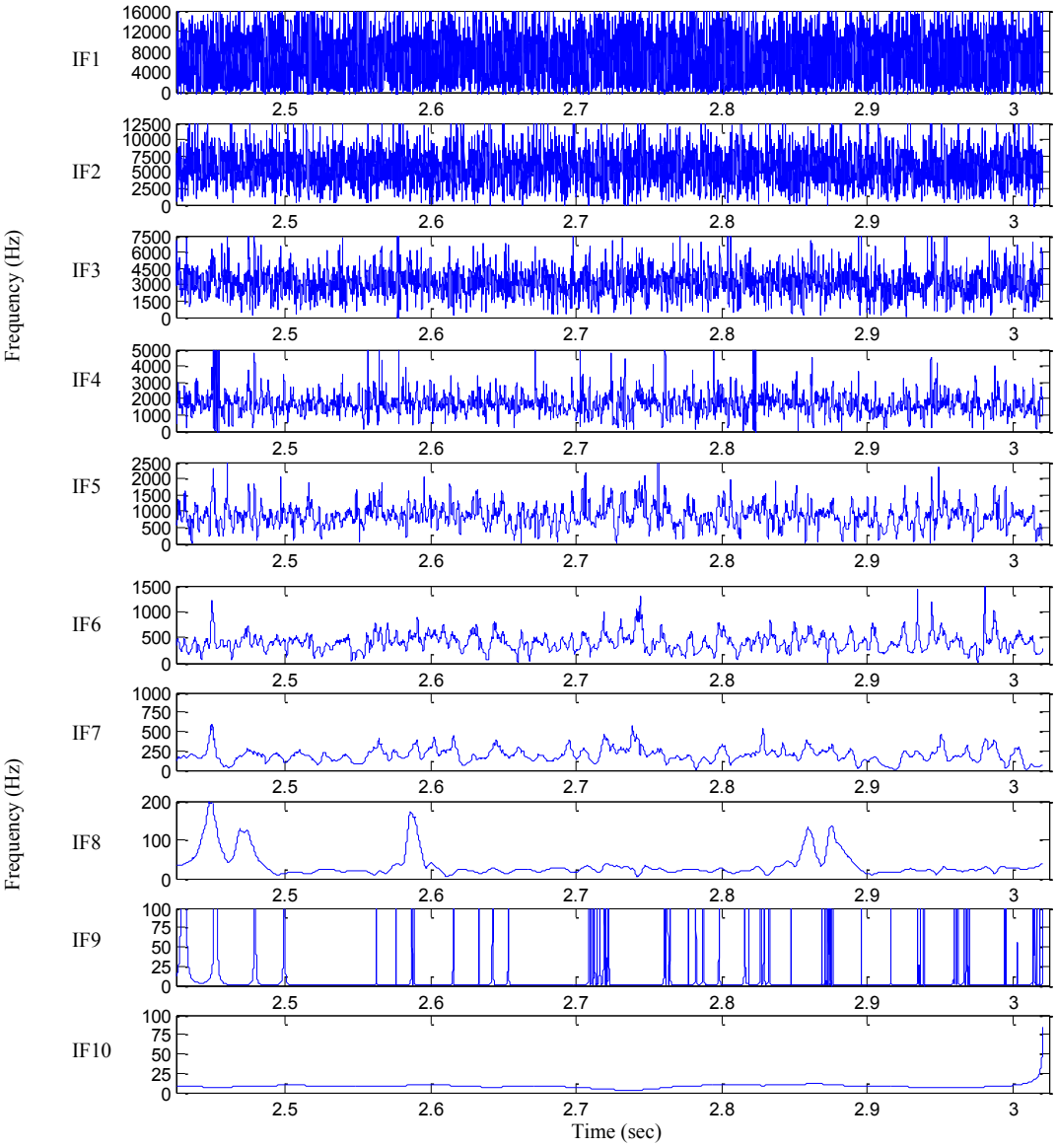

Fig. 4.6 Top ten frequency modes for 1239 rpm dry-run workpiece vibrations

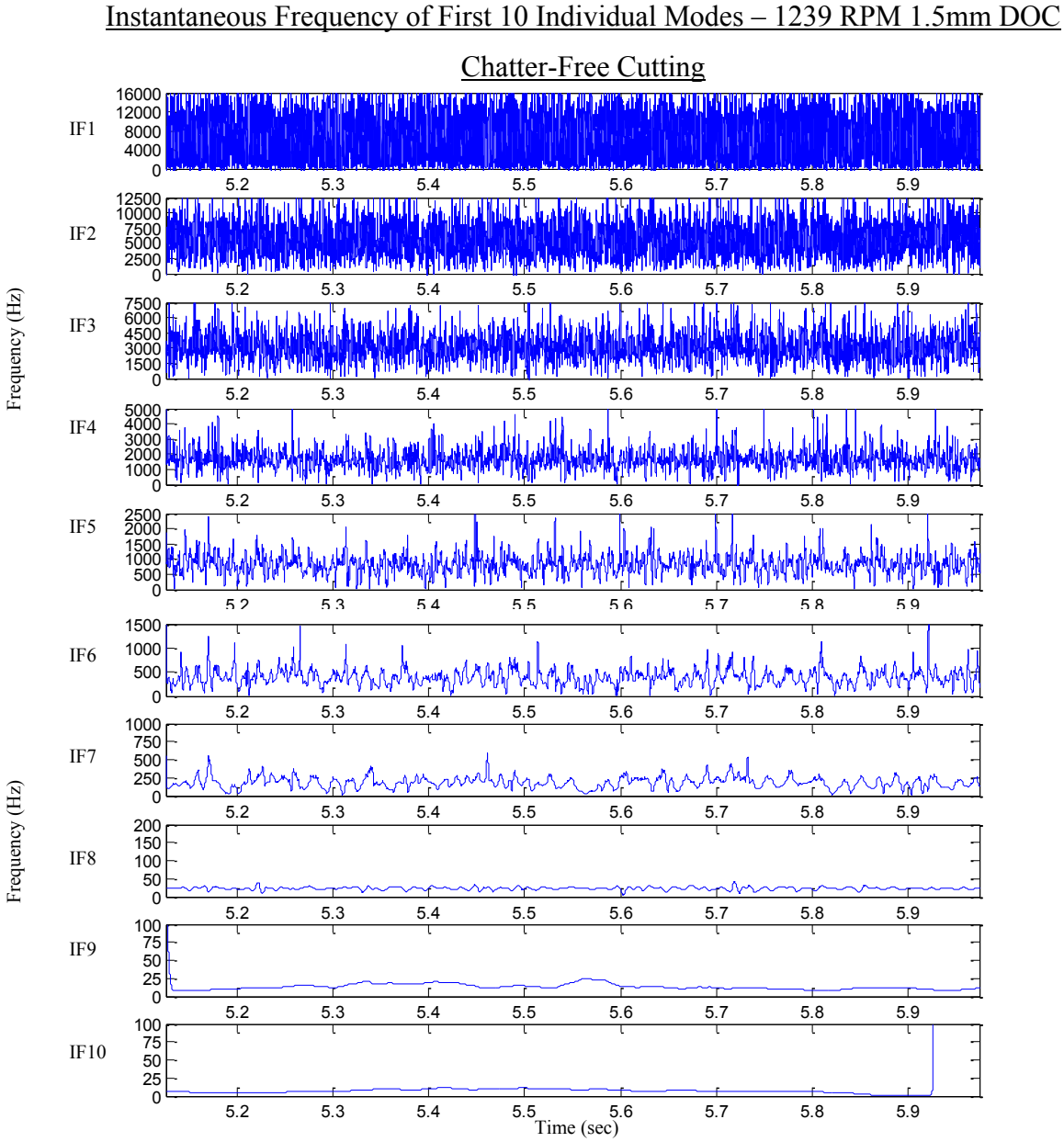

Fig. 4.7 Top ten frequency modes for 1239 rpm and 1.5mm DOC chatter-free cutting

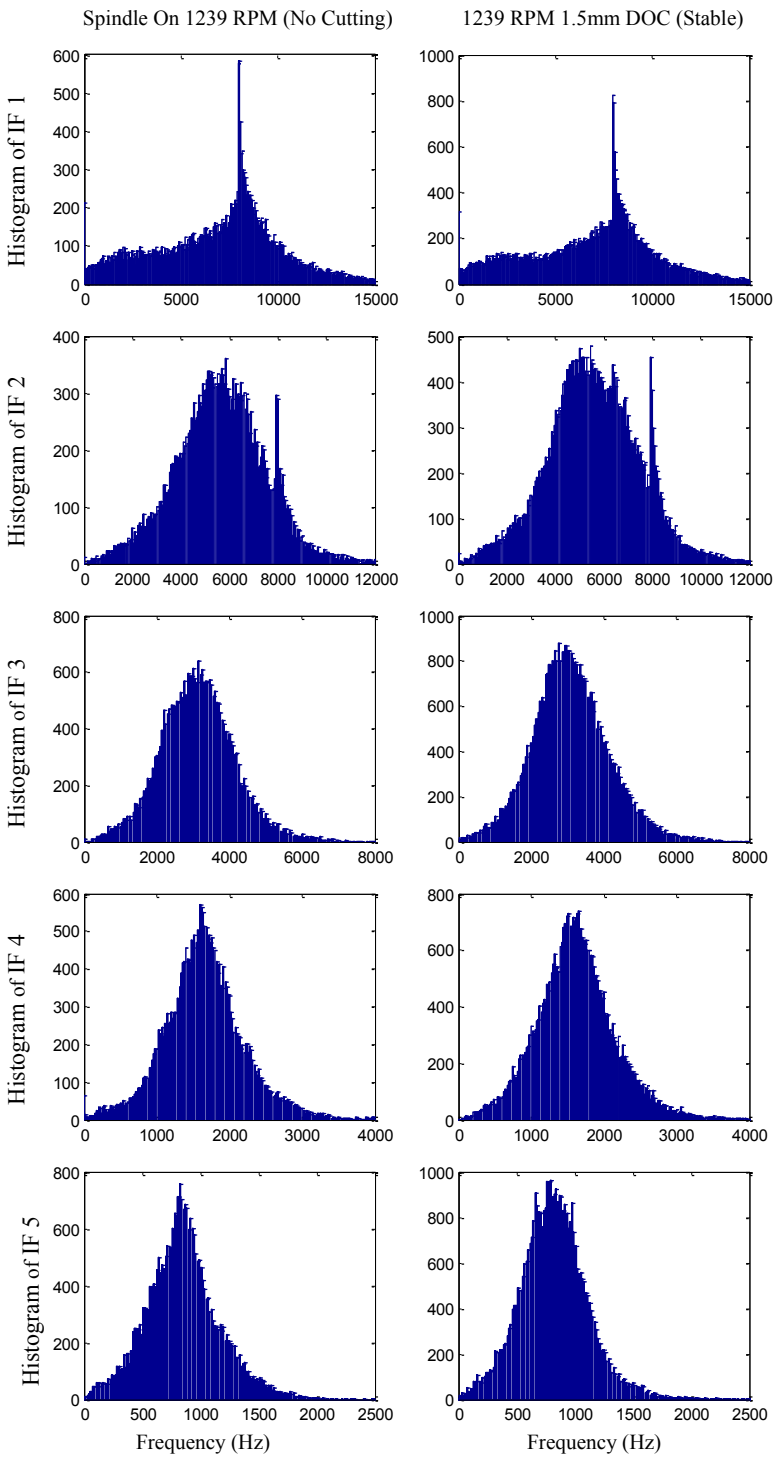

Fig. 4.8 Histogram plots of individual IFs 1-5 at 1239 rpm – workpiece

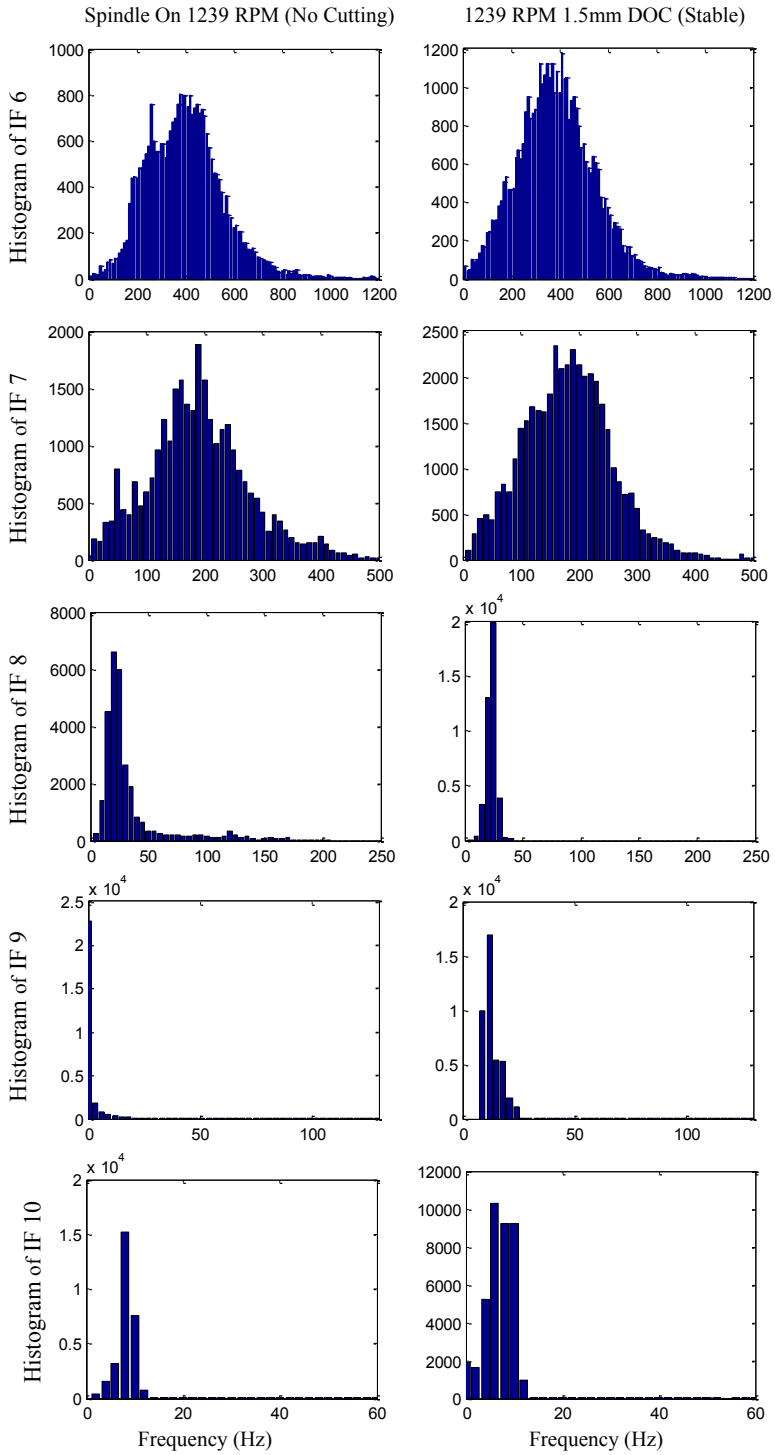

Fig. 4.9 Histogram plots of individual IFs 6-10 at 1239 rpm – workpiece

4.2.3 885 RPM – Tool Vibrations

The baseline data for the tool vibrations at 885 rpm is presented in Figs. 4.10-4.13. Compared to the spindle-off data in Fig. 4.1, IF 8, 9 and 10 in Fig. 4.10 are much lower when the spindle is running at 885 rpm. IF 8 is now a low frequency lathe vibration at ~50Hz, IF 9 is the spindle speed mode at ~16Hz, and IF 10 is low frequency noise. When cutting occurs, IF 8 shifts and appears to become a cutting related frequency where IF 9 is now the low frequency lathe mode and IF 10 is the spindle speed frequency. In Fig. 4.12, IF 1, 2, 3, and 4 appear to retain the same shape and dominant frequency as that of the spindle-off histograms in Fig. 4.4 rendering these modes as high frequency measurement noise. However, the dominate frequency of IF 5 has increased to ~1080Hz from ~800Hz and IF 6 has shifted to ~550Hz from ~400Hz due to the spindle being on and cutting being present which suggests that these are modes related to the cutting process. When cutting is present, IF 8 in Fig. 4.13 is now a very sporadic mode covering a wide range of frequencies from ~35-125Hz. In Fig. 4.13 IF 7 appears to essentially retain the same dominant frequencies when compared with the spindle-off case in Fig. 4.4.

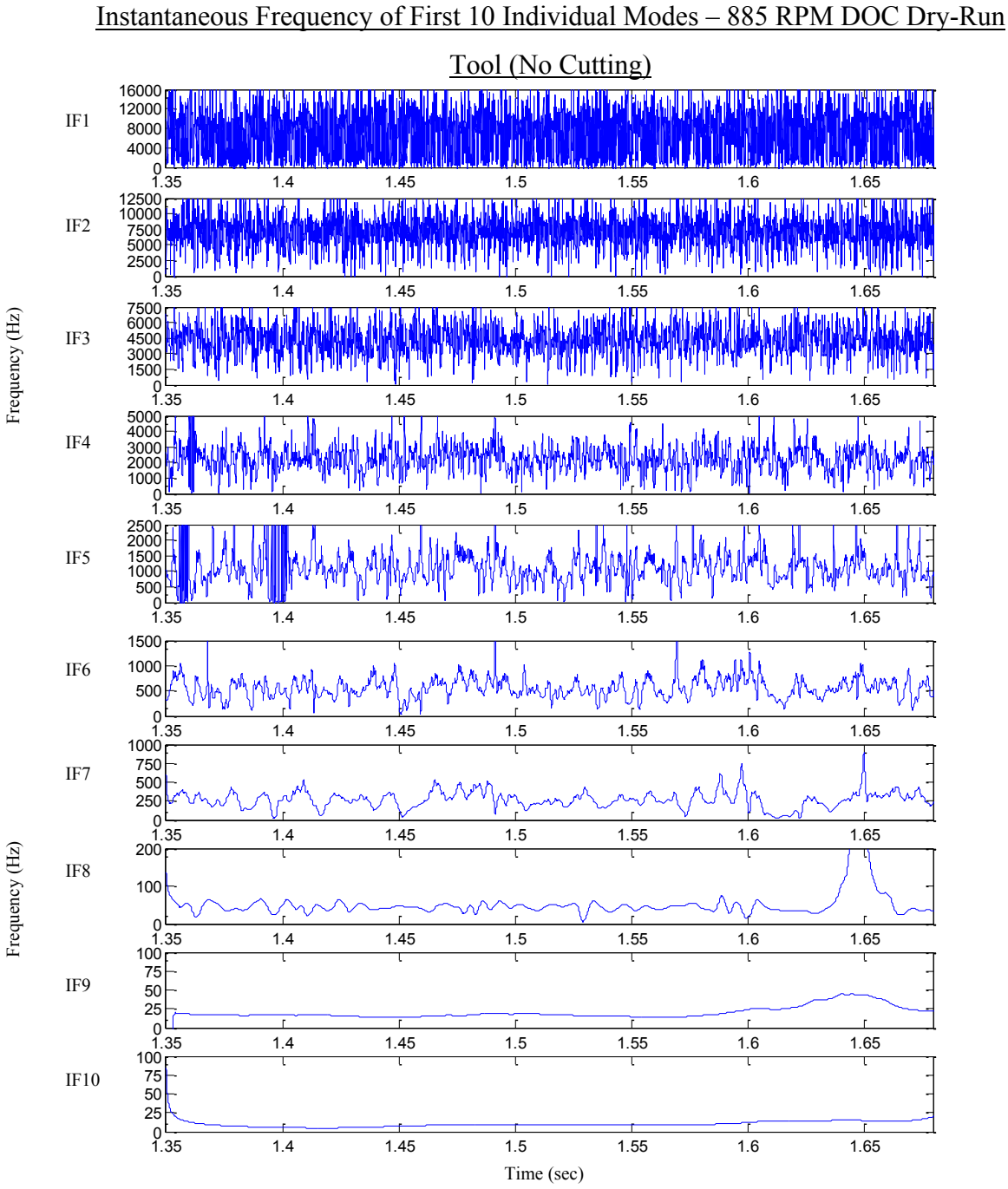

Fig. 4.10 Top ten frequency modes for 885 rpm dry-run tool vibrations

Instantaneous Frequency of First 10 Individual Modes – 885 RPM DOC 1.35mm DOC Tool

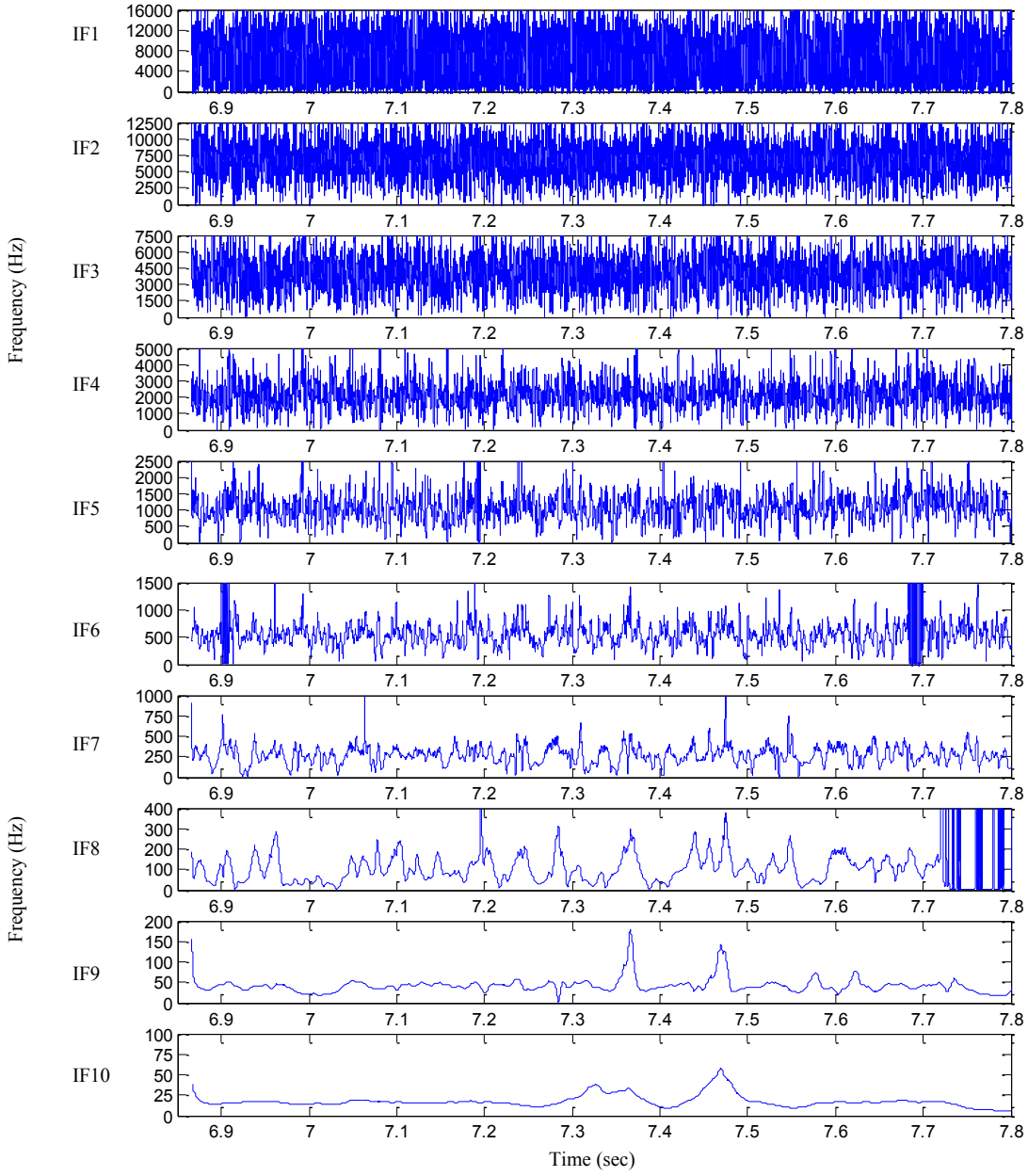

Fig. 4.11 Top ten frequency modes for 885 rpm and 1.35mm DOC tool vibrations

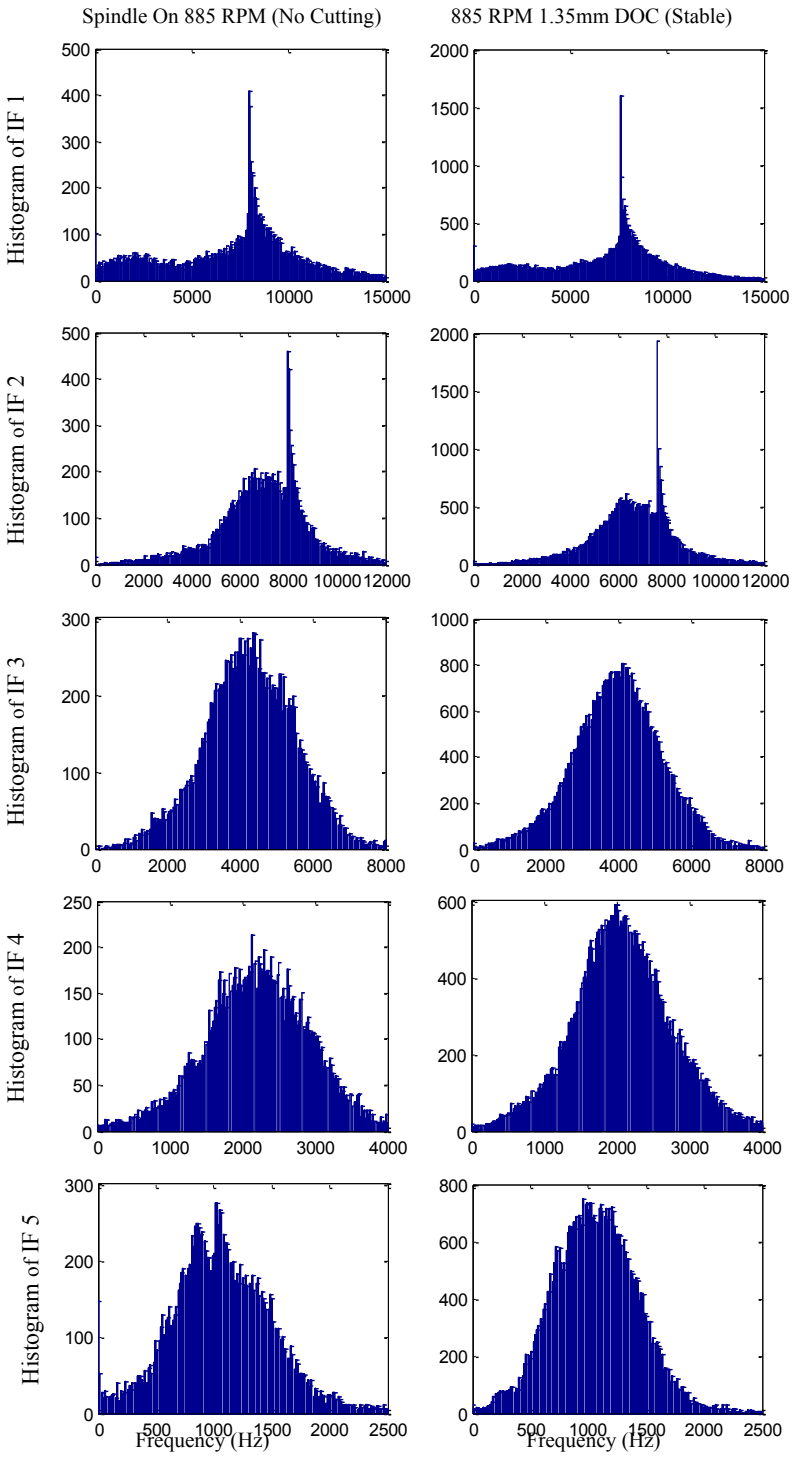

Fig. 4.12 Histogram plots of individual IFs 1-5 at 885 rpm – tool

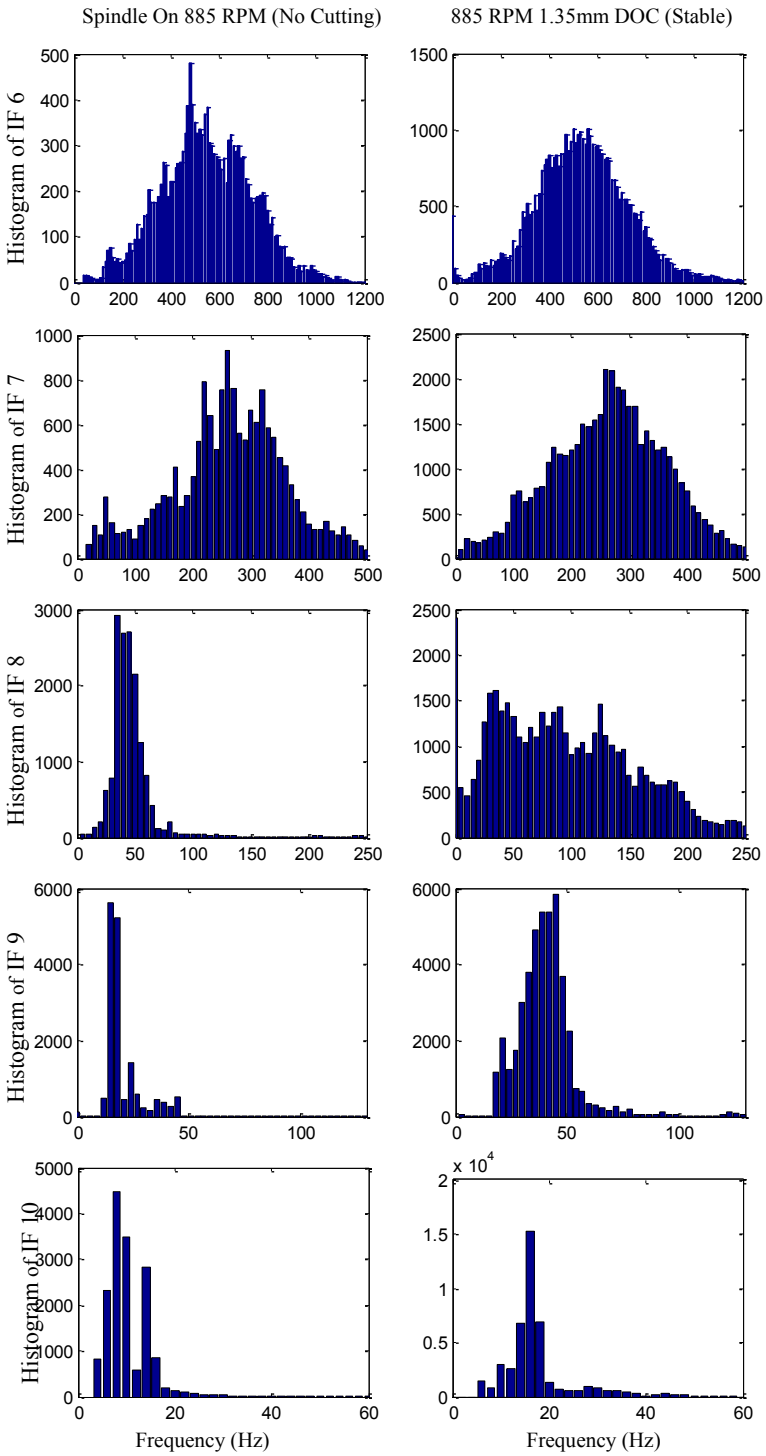

Fig. 4.13 Histogram plots of individual IFs 6-10 at 885 rpm – tool

4.2.4 1239 RPM – Tool Vibrations

The baseline IF analysis for tool vibrations at 1239 rpm is presented in Figs. 4.14 – 4.17. It is observed by comparing the figures with the spindle-off case in Fig. 4.4 that IF 1, 2, 3, and 4 remain unchanged and are again classified as high frequency measurement noise. The dominant frequencies in IF 5 have shifted to ~1080Hz from ~800Hz and the dominant frequencies in IF 6 have increased to ~550 Hz from ~400Hz due to the presence of the spindle being on and chatter-free cutting. Mode 7 continues to retain its dominant frequency of ~250 Hz and is considered measurement noise. When compared with the spindle-off in Fig. 4.5, IF 8 has shifted down and has main components around 50 and 100 Hz which makes IF 8 a cutting related mode. Mode 9 becomes a clear spindle speed frequency in Fig. 4.17 and IF 10 is low frequency noise.

The summary of the important modes related to the process identified during the baseline analysis is provided in Table 4.1. The dominant frequency in Table 4.1 is the peak value of the distribution for these modes. This peak value helps to identify what each mode physically represents (spindle speed, etc.). The numerical results in [24] similarly show that the workpiece natural frequency is much higher than the tool natural frequency and that there is a distinct spindle speed frequency related to workpiece whirling. The workpiece vibrations in [24] also have a mode related to coupling with the tool which is near the natural frequency of the tool, and the tool vibrations show modes related to the natural frequency and spindle speed. This along with the FFTs of the stable cutting presented in Section 4.3 confirms the physical meaning of the modes identified using IF.

Instantaneous Frequency of First 10 Individual Modes – 1239 RPM DOC Dry-Run Tool (No Cutting)

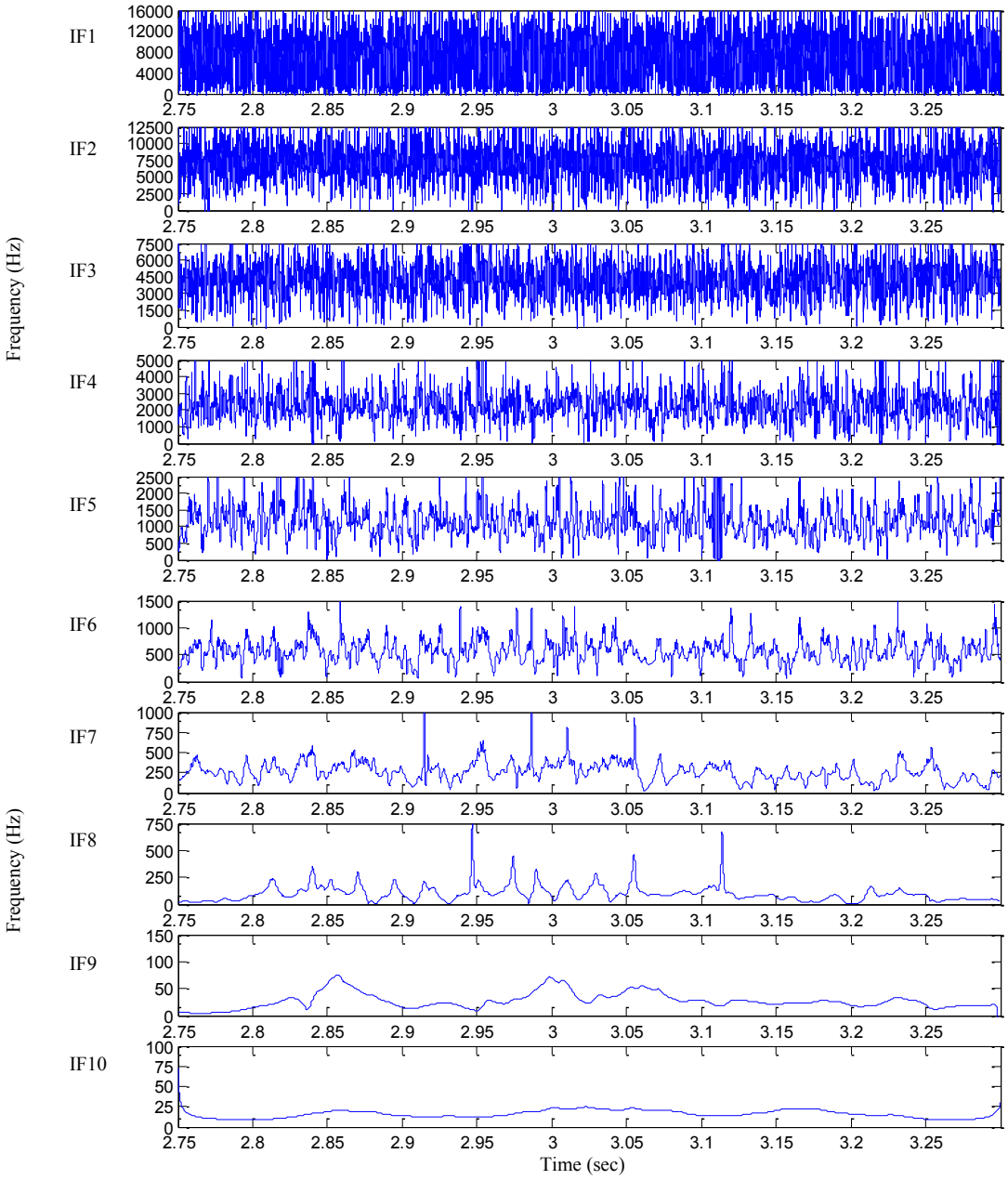

Fig. 4.14 Top ten frequency modes for 1239 rpm dry-run tool vibrations

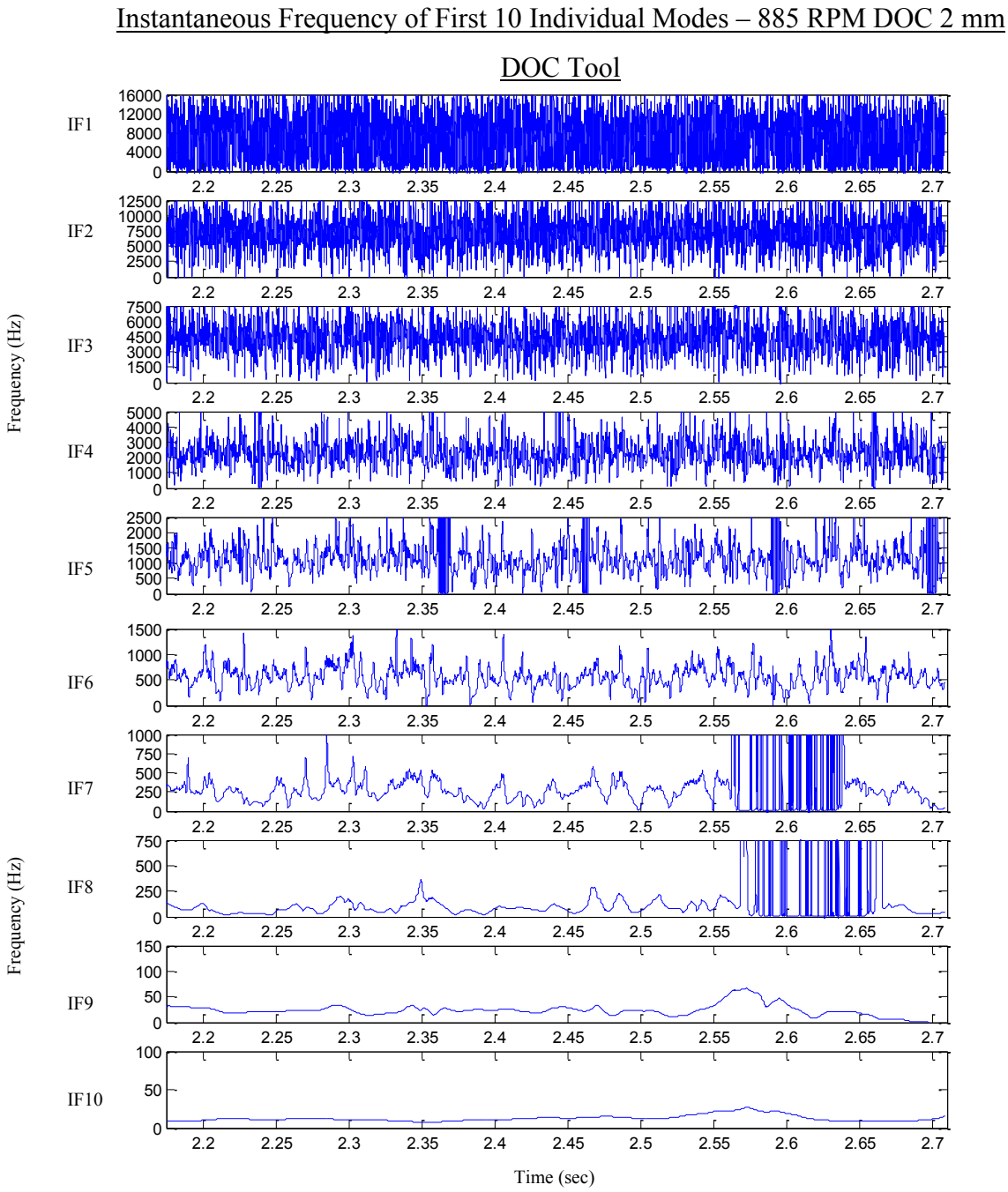

Fig. 4.15 Top ten frequency modes for 1239 rpm and 2 mm DOC tool vibrations

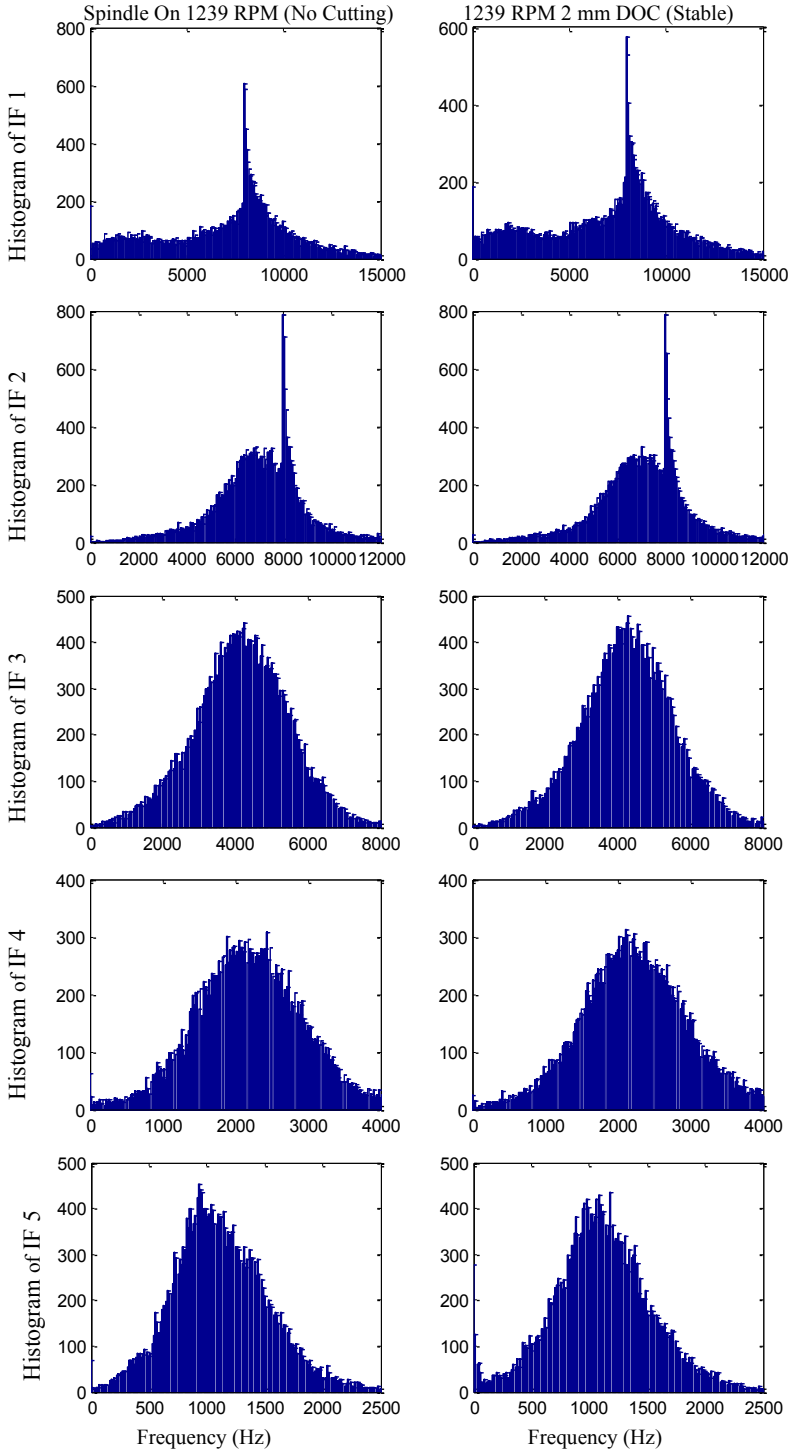

Fig. 4.16 Histogram plots of individual IFs 1-5 at 1239 rpm – tool

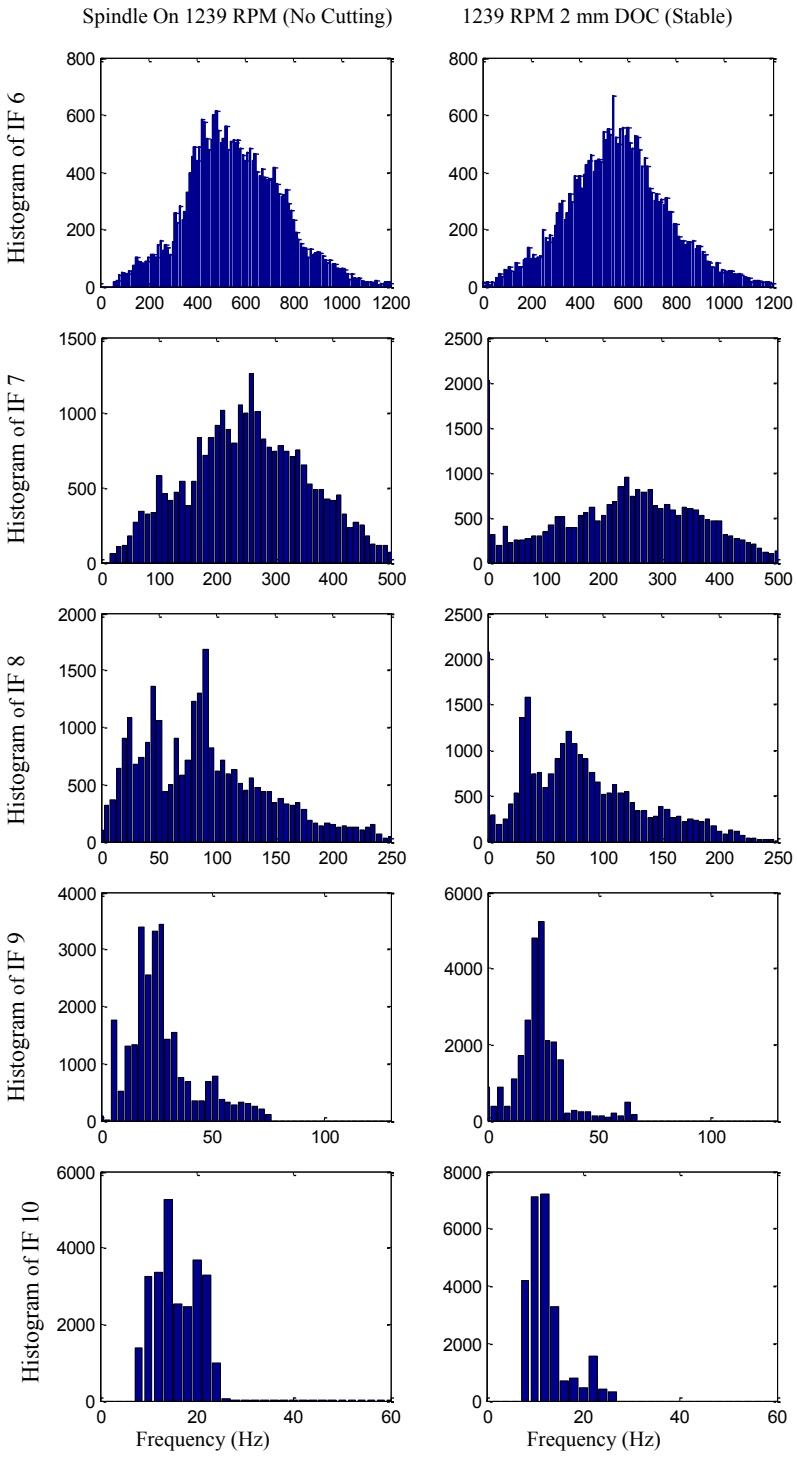

Fig. 4.17 Histogram plots of individual IFs 6-10 at 1239 rpm – tool

Table 4.1 Important Vibration Modes for the Workpiece and Tool

Workpiece Vibration Modes related to the Process		
885 RPM Spindle Speed		
Mode	**Approximate Main Freq.**	**Description**
IF 3	2500 Hz	Workpiece Nat. Freq.
IF 4	1500 Hz	Workpiece Nat. Freq. Bifurcation
IF 5	750 Hz	Tool Coupling Freq.
IF 6	400 Hz	Process Related
IF 9	42 Hz	Lathe Related Freq.
IF 10	18 Hz	Spindle Speed
1239 RPM Spindle Speed		
Mode	**Approximate Main Freq.**	**Description**
IF 3	2800 Hz	Workpiece Nat. Freq.
IF 4	1620 Hz	Workpiece Nat. Freq. Bifurcation
IF 5	900 Hz	Tool Coupling Freq.
IF 6	450 Hz	Process Related
IF 8	22 Hz	Spindle Speed
Tool Vibration Modes related to the Process		
885 RPM Spindle Speed		
Mode	**Approximate Main Freq.**	**Description**
IF 5	1080 Hz	Tool Nat. Freq.
IF 6	550 Hz	Tool Bifurcation
IF 8*	35-125Hz	Cutting Related Frequency
IF 9	45 Hz	Lathe Related Frequency
IF 10	16 Hz	Spindle Speed
1239 RPM Spindle Speed		
Mode	**Approximate Main Freq.**	**Description**
IF 5	1080 Hz	Tool Nat. Freq.
IF 6	550 Hz	Tool Bifurcation
IF 8*	35-80Hz	Cutting Related Frequency
IF 9	24 Hz	Spindle Speed
*As the DOC increases for 885 RPM, IF 8 becomes more broadband away from the 35Hz value increasing to higher frequencies around 125 Hz. The same is for 1239 RPM.		

4.3 Characterizing Chatter-Free vs. Chatter Cutting

As the state of motion of a dynamic system changes or deteriorates towards instability, the modes related to the process undergo bifurcations [28, 32]. These dynamic changes can be identified and characterized by IF in the time-frequency domain. To observe this, the vibration response, RMS, FFT, IF, phase portrait, and Poincare section for chatter-free and chatter cutting are compared. The offset of the vibration response is accounted for in both the RMS and phase plots.

4.3.1 Workpiece Chatter-Free vs. Chatter

Comparing chatter-free and chatter cutting for workpiece vibrations at 885 rpm in Fig. 4.18 shows that chatter cutting is associated with increased vibration amplitude which begins around the 4 second mark in the RMS. The FFT for the chatter-free cutting represents a system with multiple frequencies ranging between 0-5,000Hz and does not provide detailed dynamic information about the system. This is representative of the multiple modes related to the process as identified using IF during the baseline analysis. However, the FFT for chatter cutting shows that a chatter frequency at 808 Hz has appeared as the dominant component in the spectrum. The FFT still shows the presence of the high frequency components related to the workpiece natural frequency as well as the low frequencies identified in Table 4.1. The IF for chatter-free cutting shows a spectrum which does not change for the duration of the cut. However, the IF plot for chatter cutting has a distinct change in the frequency domain just after the 3.5 second mark in IF 4, IF 5, and IF 6. Subtle mode changes due to chatter can be clearly made out in the histograms in Fig. 4.19, where the main workpiece natural frequency, IF 3, is seen

to remain unchanged during chatter cutting. The workpiece period-doubling mode (IF 4) at 1500 Hz disappears and a new mode at approximately 840 Hz appears. Also, IF 5 and IF 6 have shifted down to approximately 450 and 250 Hz, respectively. Thus, a very clear dominant "chatter" frequency, IF 4, and its bifurcations, IF 5 and IF 6, are present during chatter. This corresponds to the same chatter frequency identified using FFT. The lower frequency IF 9 has become more sporadic with the lathe frequency of approximately 42 Hz jumping in and out, and IF 10 has developed into a very stable 16Hz spindle frequency.

The change in the state of motion as identified using IF is confirmed by the phase portraits and Poincare sections in Fig. 4.20. The phase diagram for chatter-free cutting at 885 rpm describes a system with multiple frequencies but is constrained within a limit cycle. The phase portrait for chatter cutting covers a wider range of magnitudes and deviates away from the original state of motion. The Poincare section for chatter-free cutting, which is sampled at the workpiece natural frequency of 2500Hz, interestingly has a different distribution with a negative slope from the corresponding phase plot. The Poincare section for chatter cutting is much more dispersed with a changing distribution. These plots confirm the presence of multiple frequencies as well as indicate a change in the state of motion when chatter appears.

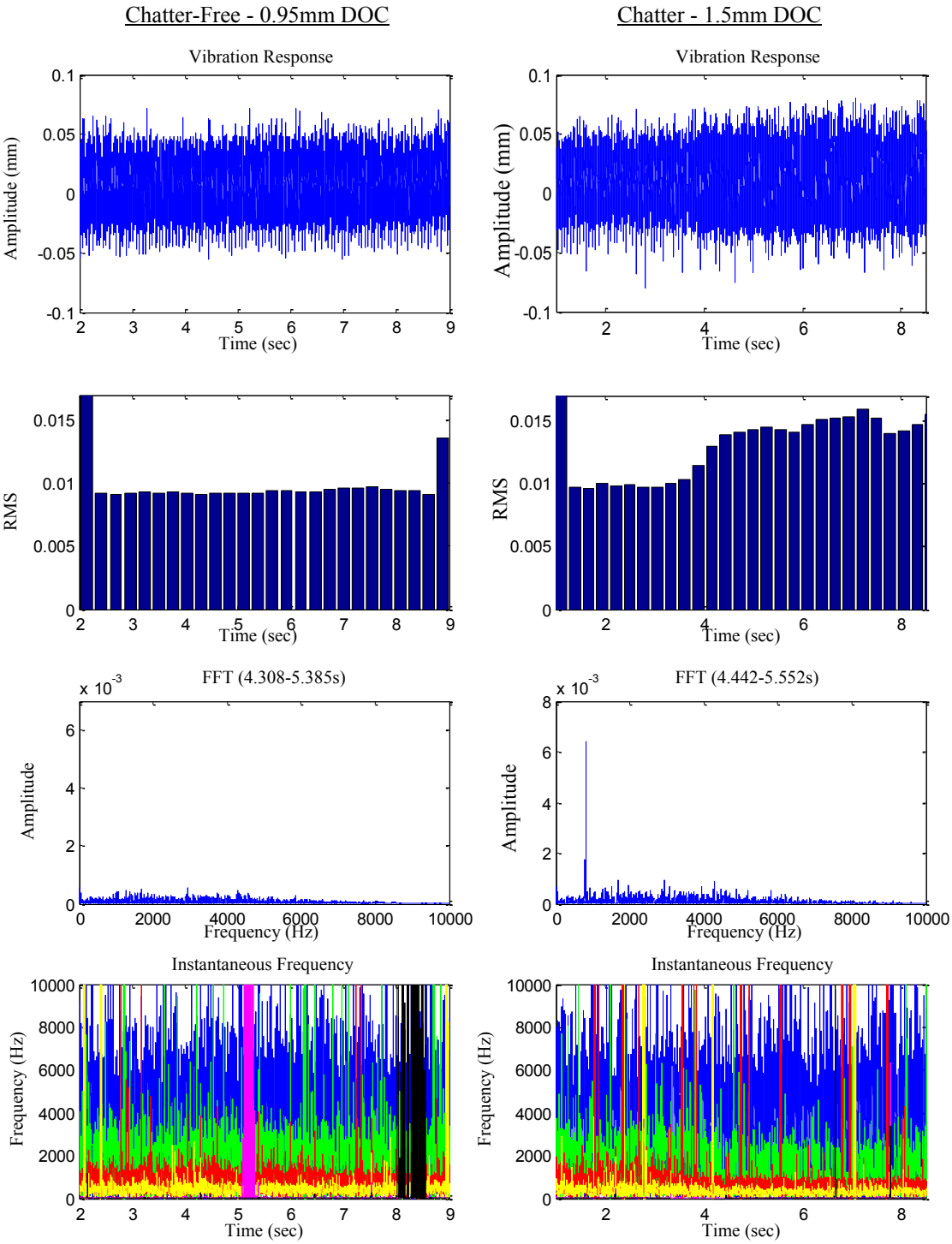

Fig. 4.18 Comparison of chatter-free (left) vs. chatter (right) cutting for workpiece at 885 rpm

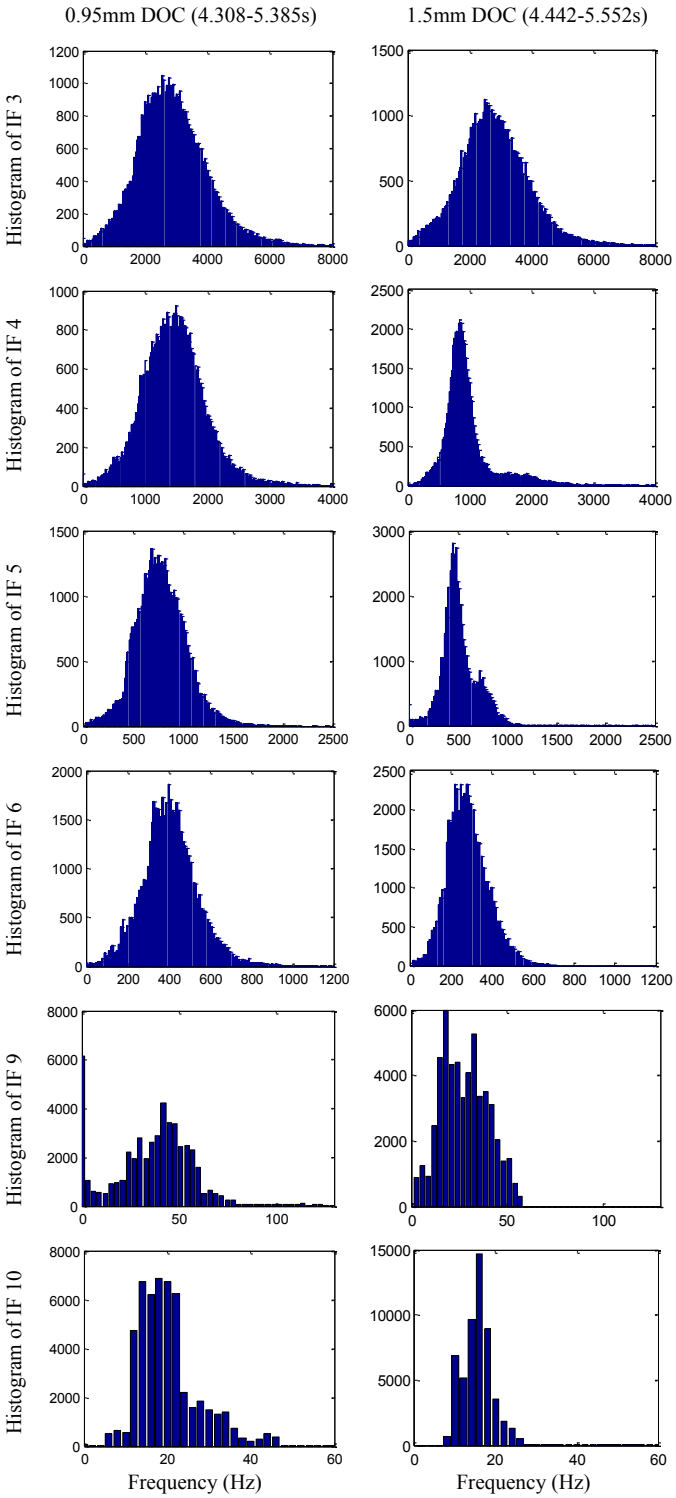

Fig. 4.19 Histogram plots of important modes for chatter-free (left) and chatter (right) workpiece vibrations at 885 rpm

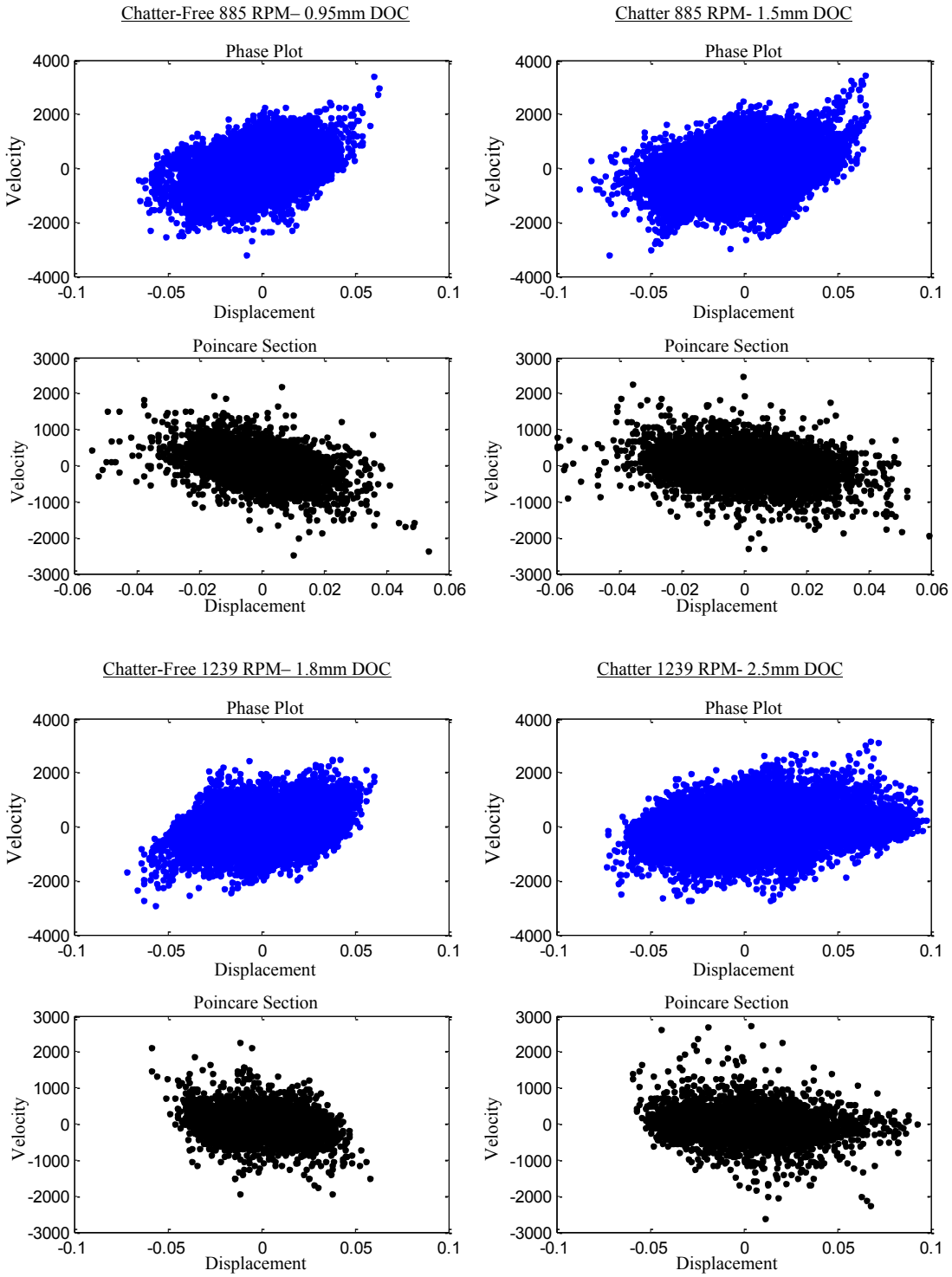

Fig. 4.20 Phase plot and Poincare section of chatter-free (left) vs. chatter (right) cutting for the workpiece at 885 rpm (top) and 1239 rpm (bottom)

The same procedure is followed to monitor the modes related to workpiece vibrations at 1239 rpm, as seen in Figs. 4.21-4.22. An increase in the vibration magnitude is observed in the RMS and the FFT plot reveals the appearance of a chatter frequency at 812 Hz. The IF shows a change in the frequency spectrum just after the 3.25s mark preceding the increase in vibration amplitude. Similar to the 885 rpm cutting, the workpiece natural frequency mode, IF 3, is unchanged as shown in Fig. 4.22. The 1600Hz IF 4 has disappeared for chatter cutting and an 820Hz frequency appears. Also, IF 5 and IF 6 have shifted to approximately 450 and 240Hz, respectively. The spindle speed mode is still seen as IF 8. Chatter at 1239 rpm displayed similar characteristics to chatter at 885 rpm with the appearance of a chatter frequency in IF 4 and its bifurcations in IF 5 and 6. The value of the chatter frequency obtained by IF is confirmed with the FFT, and the phase diagram in Fig. 4.20 for the 1239 rpm case is similar to the 885 rpm case. For chatter-free cutting at 1239 rpm the system is vibrating within a limit cycle and the chatter case covers a broader range of values deviating away from the original state of motion. The Poincare sections in Fig. 4.20 for 1239 rpm cutting also show an interesting shift in the slope of the distribution and the chatter case covers a wider range of values than the chatter-free case.

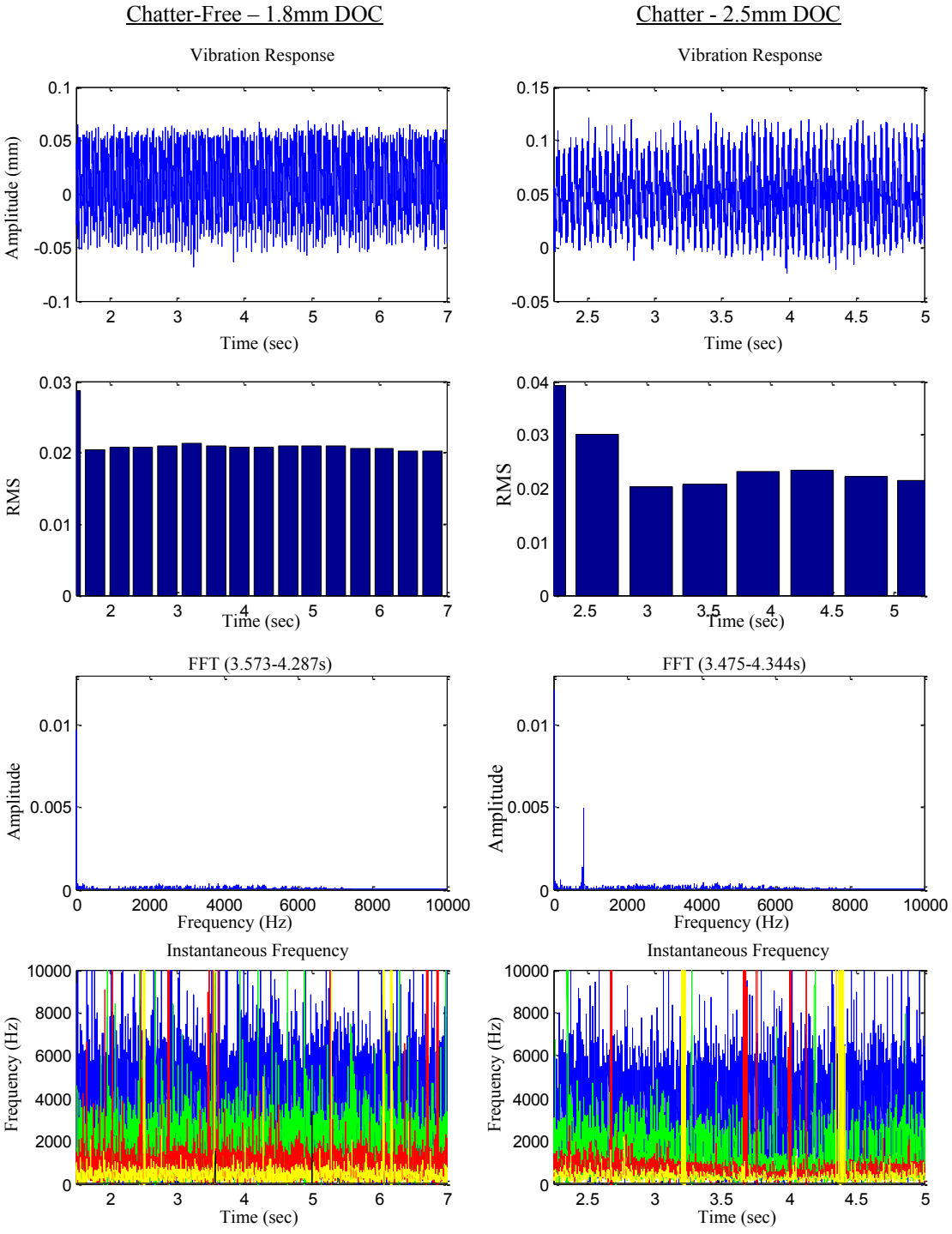

Fig. 4.21 Comparison of chatter-free (left) vs. chatter (right) cutting for workpiece at 1239 rpm

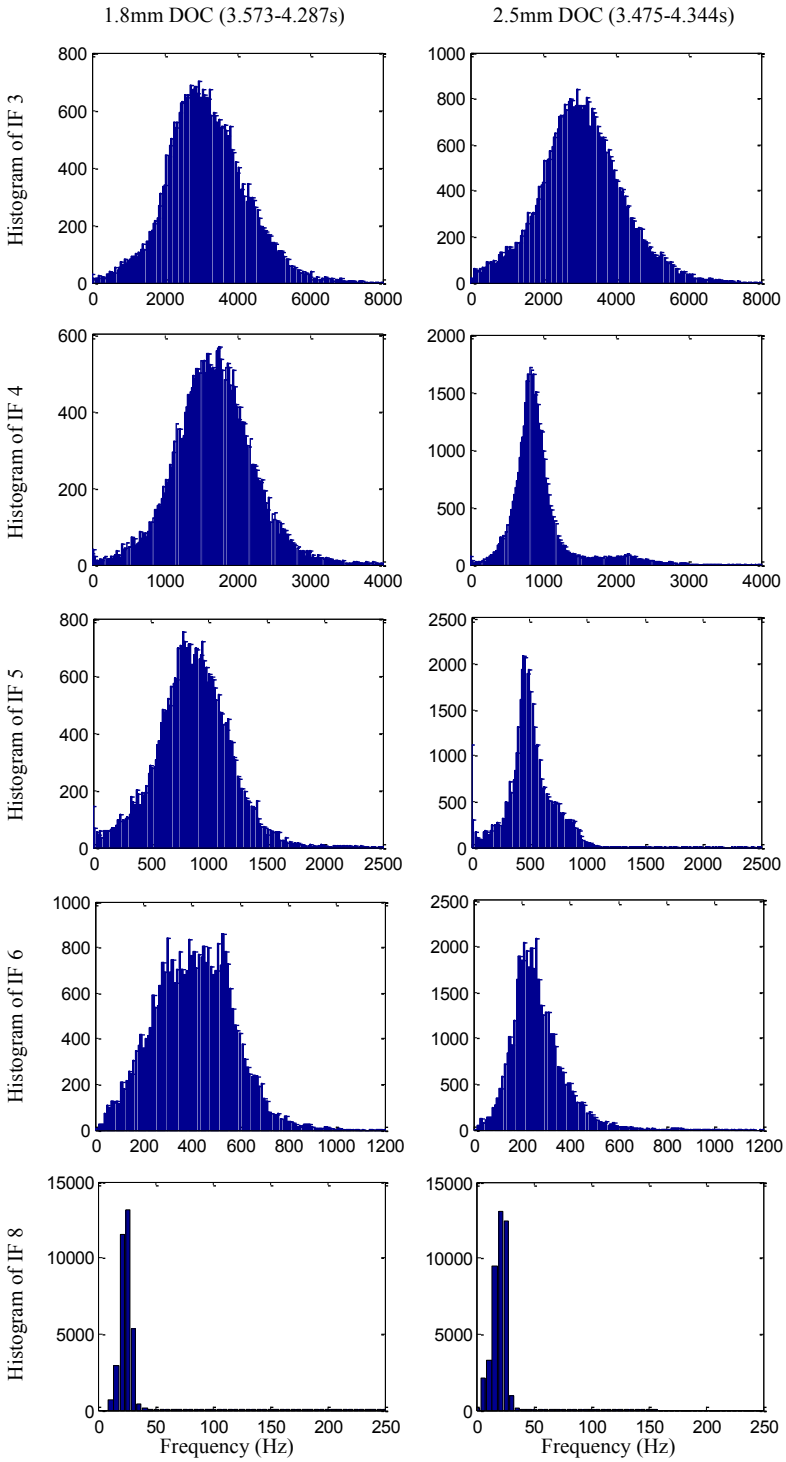

Fig. 4.22 Histogram plots of important modes for chatter-free (left) and chatter (right) workpiece vibrations at 1239 rpm

4.3.2 Tool Chatter-Free vs. Chatter

The tool vibrations are investigated in the same manner as the workpiece to identify and characterize chatter-free and chatter cutting (Figs. 4.23 - 4.25). Comparing the FFTs for chatter-free and chatter cutting in Fig. 4.24 clearly shows the presence of chatter at DOC = 1.75mm due to the appearance of a chatter frequency peak at 792 Hz along with higher frequency peaks at 934 and 1584 Hz. The FFT of chatter-free cutting has dominant low frequencies corresponding to the spindle speed as well as a small harmonic near the tool natural frequency. The chatter cutting is not clearly observed in the vibration response or the RMS plots. The large values at the beginning of the RMS plots are due to the offset of the vibration response when cutting began and the system was settling out. Early in the signal there appears to be a sharp increase in the vibration magnitude around the 4 second mark which then begins to decrease. Unlike the vibration response, the onset of chatter is easily identified in the IF time-frequency domain. The IF for the chatter-free response has a steady frequency spectrum and the IF for the chatter response has a clear change in the dynamics of each mode around the 4 second mark. This corresponds to the moment in time that the peak vibration amplitude occurred. The histograms in Fig. 4.25 reveal that many of the modes are altered due to the onset of chatter. The mode, IF 5, which corresponds to the tool natural frequency, deteriorates into a well-defined chatter frequency at 840 Hz, and IF 6 becomes the period-doubling bifurcation of the chatter frequency at approximately 420 Hz. Also, the IF 8 in chatter-free cutting disappears and the low frequency modes around 42 Hz and the spindle frequency remain unchanged. The frequency mode in IF 10 for chatter

cutting is the low frequency measurement noise identified during the baseline analysis of the process. The phase plots in Fig. 4.23 show that during chatter cutting the dynamics of the system have changed as identified by IF. Sampled at tool natural frequency of 1000Hz, the Poincare sections indicate a transition from chatter-free to chatter cutting. Thus, the IF analysis of chatter cutting is associated with the appearance of a chatter frequency and its bifurcations.

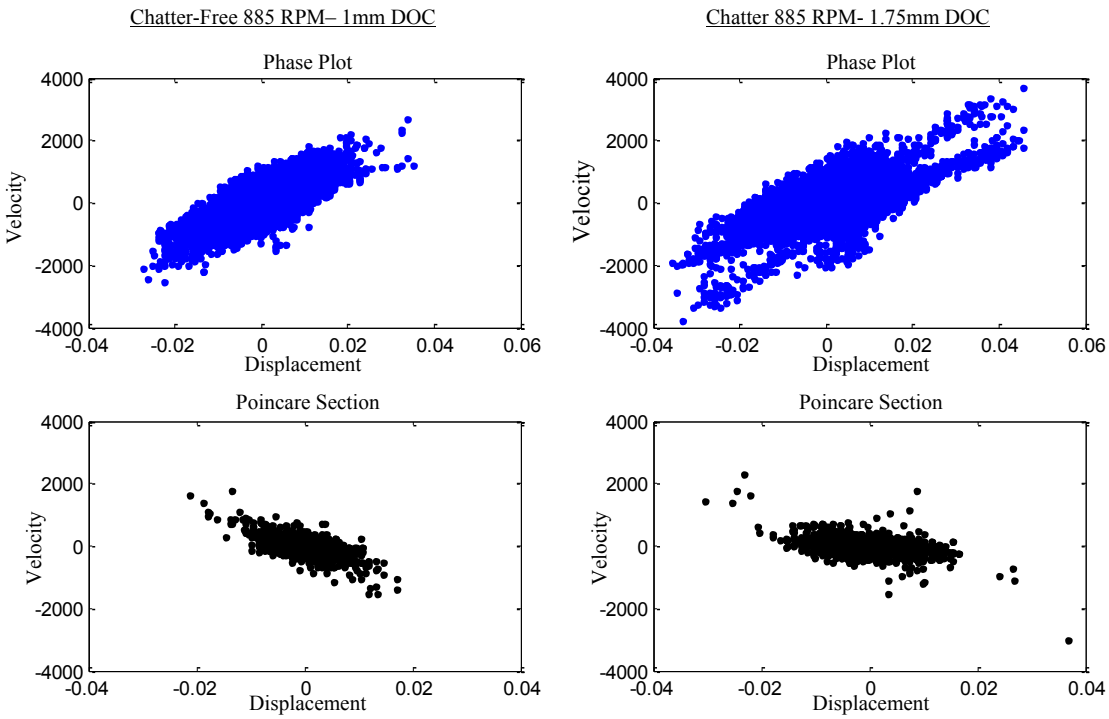

Fig. 4.23 Phase plot and Poincare section of chatter-free (left) vs. chatter (right) cutting for the tool at 885 rpm

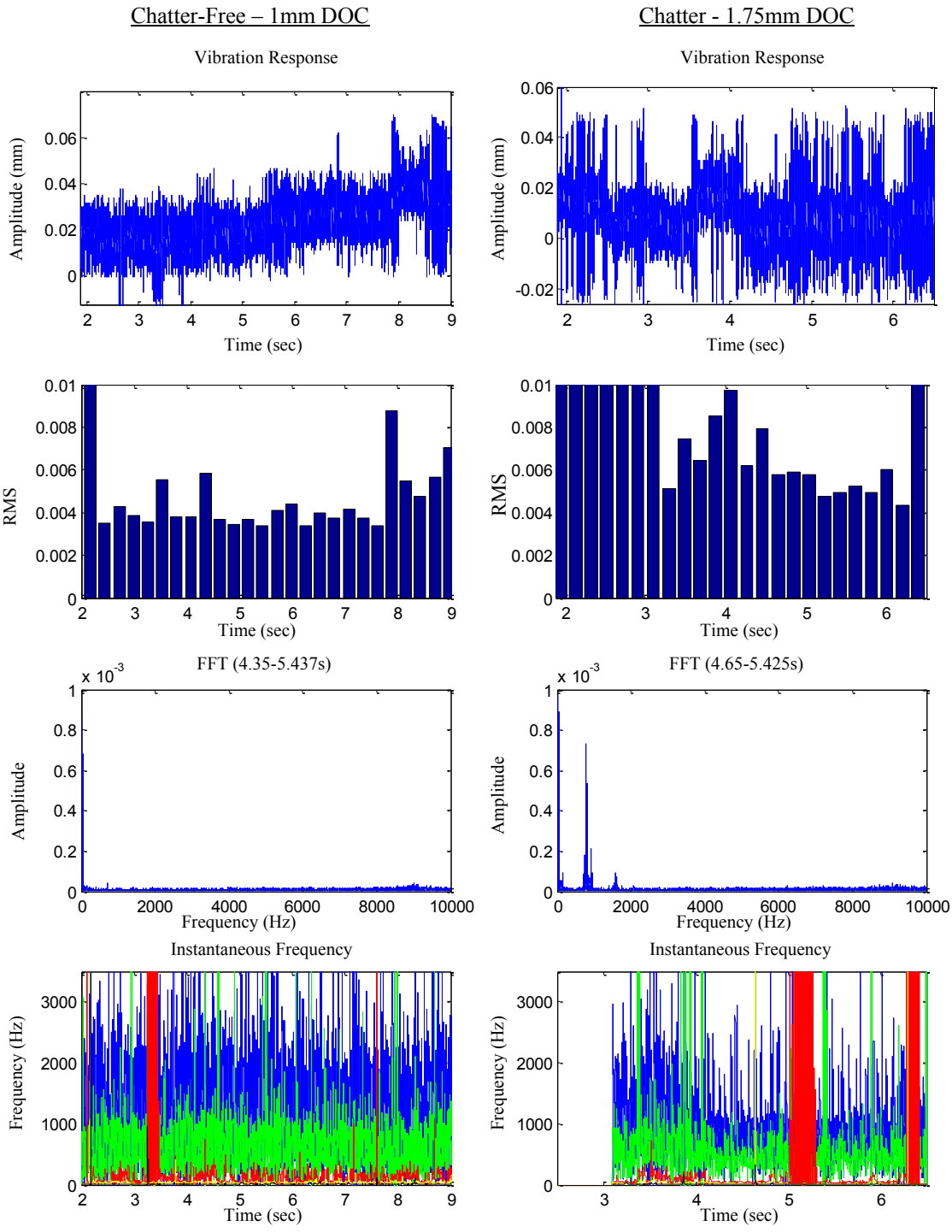

Fig. 4.24 Comparison of chatter-free vs. chatter cutting for tool at 885 rpm

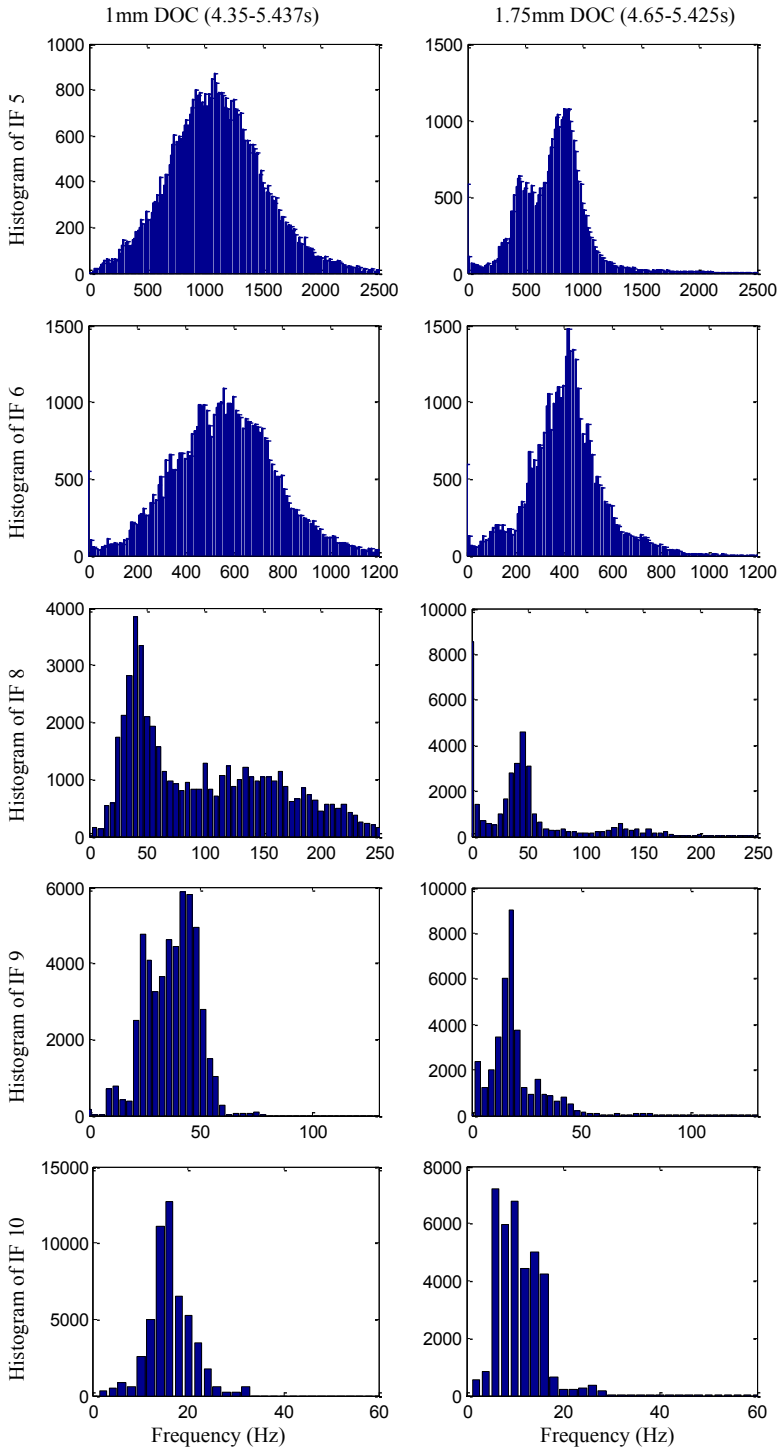

Fig. 4.25 Histogram plots of important modes for chatter-free (left) and chatter (right) tool vibrations at 885 rpm

4.3.3 Transition to Chatter

It was noted that chatter occurred when the DOC became too large. To better visualize the birth of chatter cutting, a few selected modes for chatter cutting in Figs. 4.18 and 4.24 are extracted and revisited. They are plotted on their own axis in Figs. 4.26 and 4.27 to make clear the transition moment when chatter developed. The workpiece natural frequency mode is not included because it did not change when chatter transpired. Both figures show that the dynamic response of the system undergoes changes in its frequency response which suggests ongoing bifurcation and impending instability. Another interesting observation is the effectiveness of IF to pin-point the instant of chatter. The RMS in Fig. 4.18 shows no clear increase in the vibration magnitude of the workpiece until the 4 second mark; however, the IF plot in Fig. 4.26 shows that the modes have begun to shift around the 3.75 second mark. The lowest mode, IF 10 in Fig. 4.26(D), completely disappears at approximately 3.4 seconds which indicates the onset of the changing dynamics. This is followed by the development of chatter in the frequency domain and an increase in vibration amplitudes. Also, the RMS in Fig. 4.24 for tool vibrations has a sharp impulse around the 4 second mark but doesn't indicate sustained vibrations. The mode IF 5 in Fig. 4.27(A) begins to shift down at 4 seconds and by 4.2 seconds this mode has fully developed into chatter, with the lower frequencies also shifted. Mode 8 in Fig. 4.27(C) makes a very abrupt and clear shift at 4.2 seconds and becomes a bounded mode just below 50Hz. For workpiece vibrations, the corresponding IF identifies the inception of chatter before it evolves into a state of instability recognized by the excessive vibration amplitude. For tool vibrations, the IF

identifies chatter at the same moment in time as the impulse seen in the vibration magnitude but the vibrations then decrease where the IF plot continues to illustrate a bifurcated system. Transition of motion from one dynamic state to the other is accompanied by the appearance of new modes, the disappearance of old modes, or both [32]. This means that different states of motions (periodic, period-doubling, quasi-periodic, etc.) can be spectrally identified. The changing of the dynamic state depicted in Figs. 4.26 and 4.27 are accompanied by the disappearance of modes, the appearance of new modes, and period-doubling bifurcation of the chatter frequency.

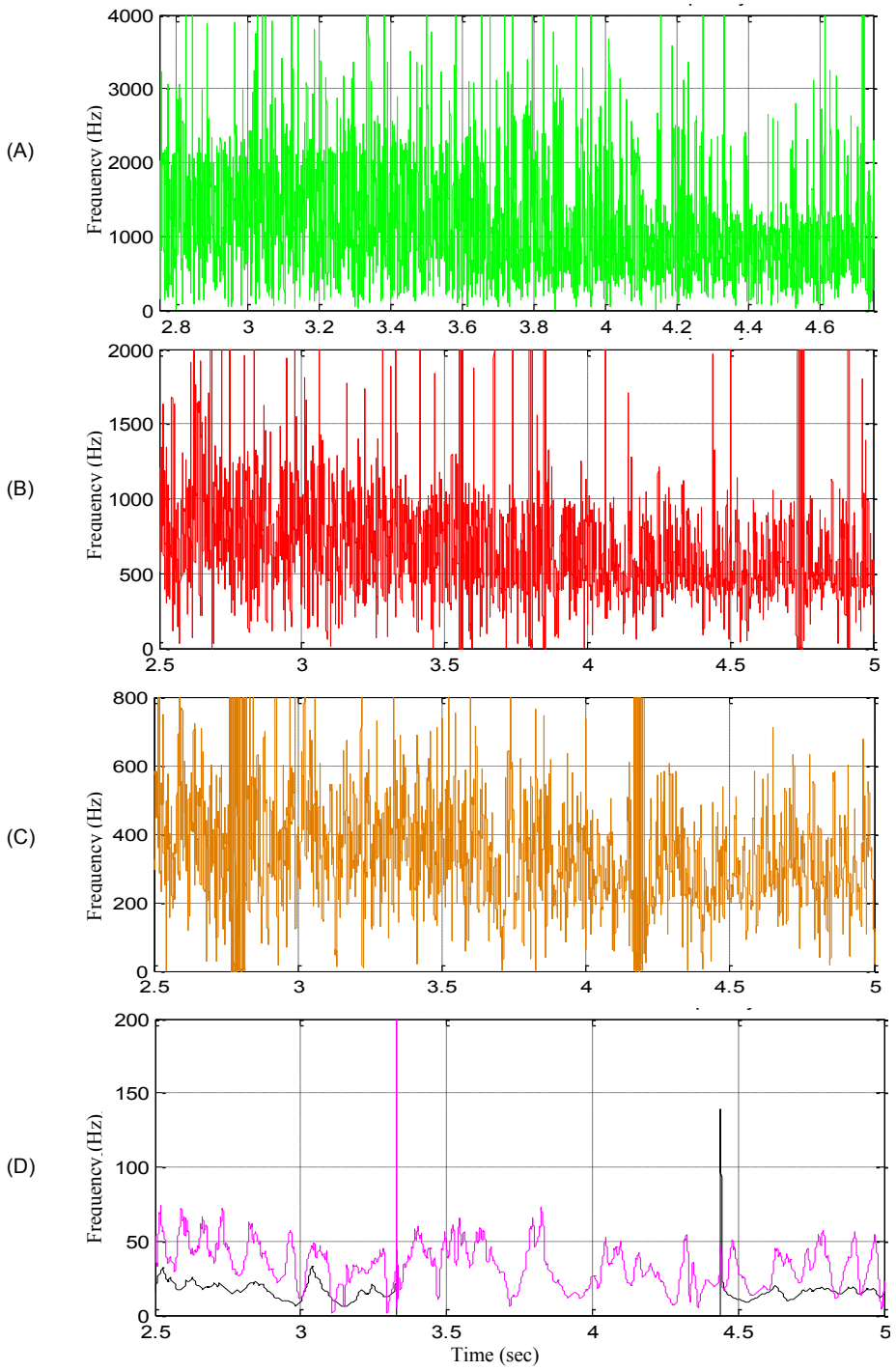

Fig. 4.26 Zoomed-in plots of individual IFs for chatter cutting workpiece vibrations at 885 rpm which show the development of chatter; Modes as noted in Table 4.1: (A) IF 4; (B) IF 5; (C) IF 6; (D) IF 9 & IF 10

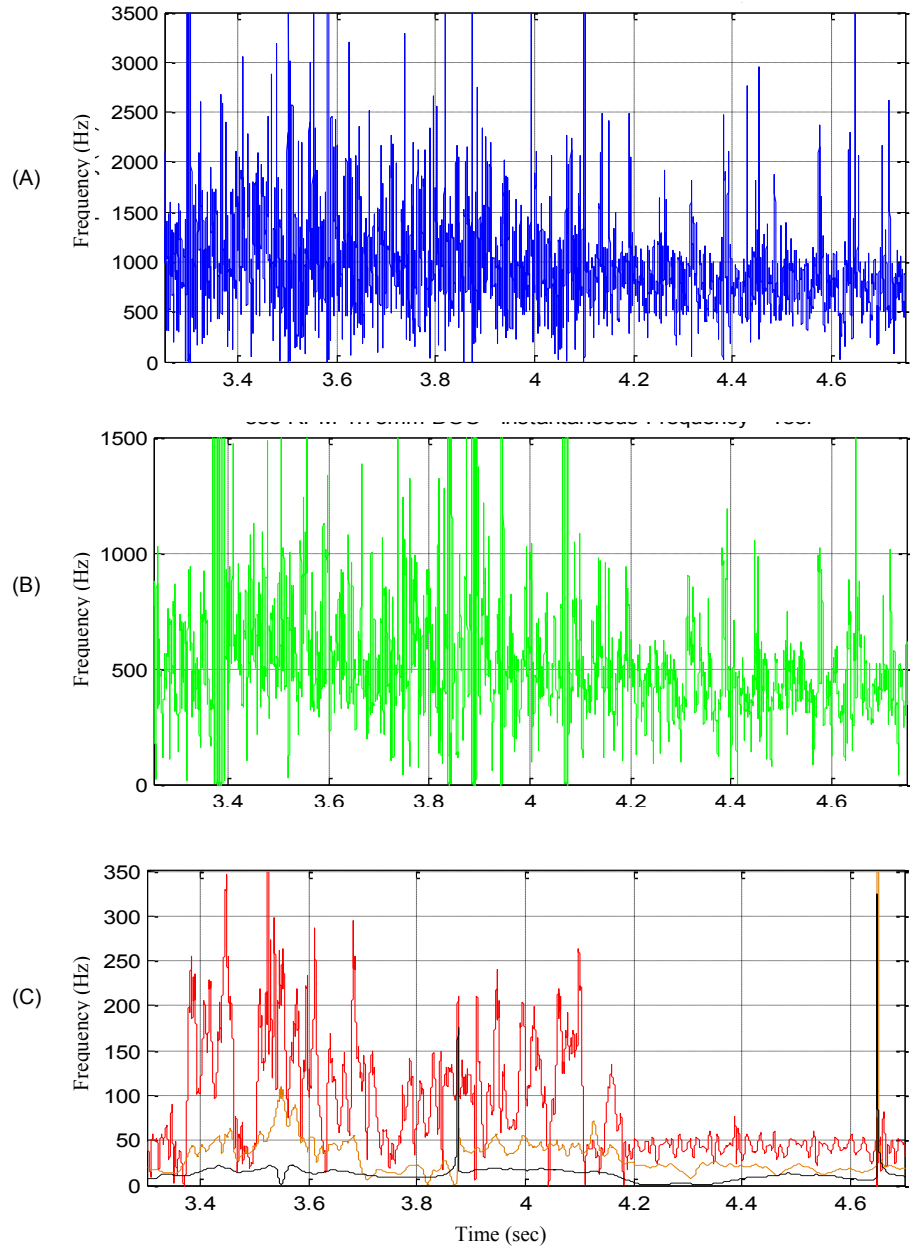

Fig. 4.27 Zoomed plots of the individual IFs for chatter cutting tool vibrations at 885 rpm which show the development of chatter; Modes as noted in Table 4.1: (A) IF 5; (B) IF 6; (C) IF 8, IF9 & IF10

5. VALIDATION OF MODEL

5.1. Chatter-Free Comparison

To begin the validation of the model in [24], experimental vibrations from Section 4 are compared to the numerical simulations for chatter-free cutting to investigate the ability of the model to simulate the underlying dynamics of the system. The model is run with a workpiece material property of 4140 steel and a geometry similar to what was used in the experiment. The identical values used in the experiment for the lead, inclination, and rake angles of 45°, 5°, and 5°, respectively, are followed to simulate the model. The modal properties used for the tool also follow those of [25], in which M_z = 9kg, k_z = 5.7x107N/m, and k_{zz} = 1.34x1017 N/m^3. The experimental data for a spindle speed of 885 rpm had a maximum whirling of 20 micron so this value is used. Numerical simulations are considered chatter-free if there are no increasing amplitude vibrations. The experimental chatter-free conditions were determined in Section 3. It should be noted that the experimental tool vibrations are obtained in the X-direction while the model simulates the tool motion in the Z-direction. Thus, a direct comparison of tool vibrations along the same axis cannot be performed. Since the tool used in Section 3 has a square cross-section of 20x20mm^2, then it is assumed that the moment of inertia in the X- and Z-direction will be similar and the tool will dynamically respond similarly in both directions. Based on this assumption, the characteristics of the experimental and numerical tool vibrations will be discussed.

The plots in Fig. 5.1 compare the numerical and experimental tool vibration responses under the identical cutting parameters with a DOC of 1.35mm, where the vibration response and frequency spectrum indicate chatter-free cutting. The 3 modes at 420Hz, 35-300Hz, and 0-12Hz are tool natural frequency, nonlinear stiffness, and spindle speed, respectively. The mode related to spindle speed is not sustained throughout the simulation and the nonlinear stiffness mode is lower than the natural frequency mode and fluctuates over a wide range of frequencies. The modes for the experimental data are the tool natural frequency, tool bifurcation, lower frequency cutting, lathe frequency, and spindle speed mode. The experimental data has an additional mode at ~42Hz which is related to the lathe machine as identified in Section 4. The model presented accounts for tool linear and nonlinear stiffness and thus would not produce the lathe related mode at ~42 Hz seen experimentally. The tool and workpiece motions interact, so the spindle frequency vibrations due to workpiece whirling are transmitted from the workpiece to the tool in the numerical simulations. However, this mode isn't prominent during chatter-free cutting. In reality, the lathe machine structure could vibrate at the spindle frequency making this mode more prominent in experimental data. The tool vibrations in the simulation and the experiment data similarly produce a mode related to the tool natural frequency, but due to the high nonlinearity of the tool in real life, the natural frequency mode is bifurcated experimentally but doesn't occur numerically. Interestingly, the nonlinear stiffness term in the model corresponds to the low frequency cutting mode identified experimentally which also varies over a wide range of frequency values. The numerical and

experimental results do not have similar frequency values for the various modes of the system because the exact modal properties of the tool were unknown. A summary of the comparison for chatter-free cutting between the numerical and experimental data for the tool is displayed in Table 5.1.

Table 5.1 Tool Experimental and Numerical Chatter-Free and Chatter Modes

Chatter-Free Conditions			
Tool			
Numerical		**Experimental**	
Tool Nat. Freq.	~420 Hz	Tool Nat. Freq.	~ 1000Hz
Tool Nonlinear Freq.	~35-300Hz	Tool Bifurcation Freq.	~ 500Hz
Spindle Freq.	~12 Hz	Cutting Related Freq.	~ 35-125 Hz
		Lathe Related Freq.	~ 42Hz
		Spindle Freq.	~16 Hz
Chatter Conditions			
Tool			
Numerical		**Experimental**	
Chatter	~550-850Hz	Chatter Freq.	~ 840Hz
Unstable Mode*	~70-700Hz	Chatter Bifurcation Freq.	~ 440Hz
Unstable Mode*	~50-400 Hz	Lathe Related Freq.	~ 42Hz
Unstable Mode*	~20-150Hz	Spindle Freq.	~16 Hz
Low Freq. Components	~13-50 Hz		
*Increases with severity of chatter			

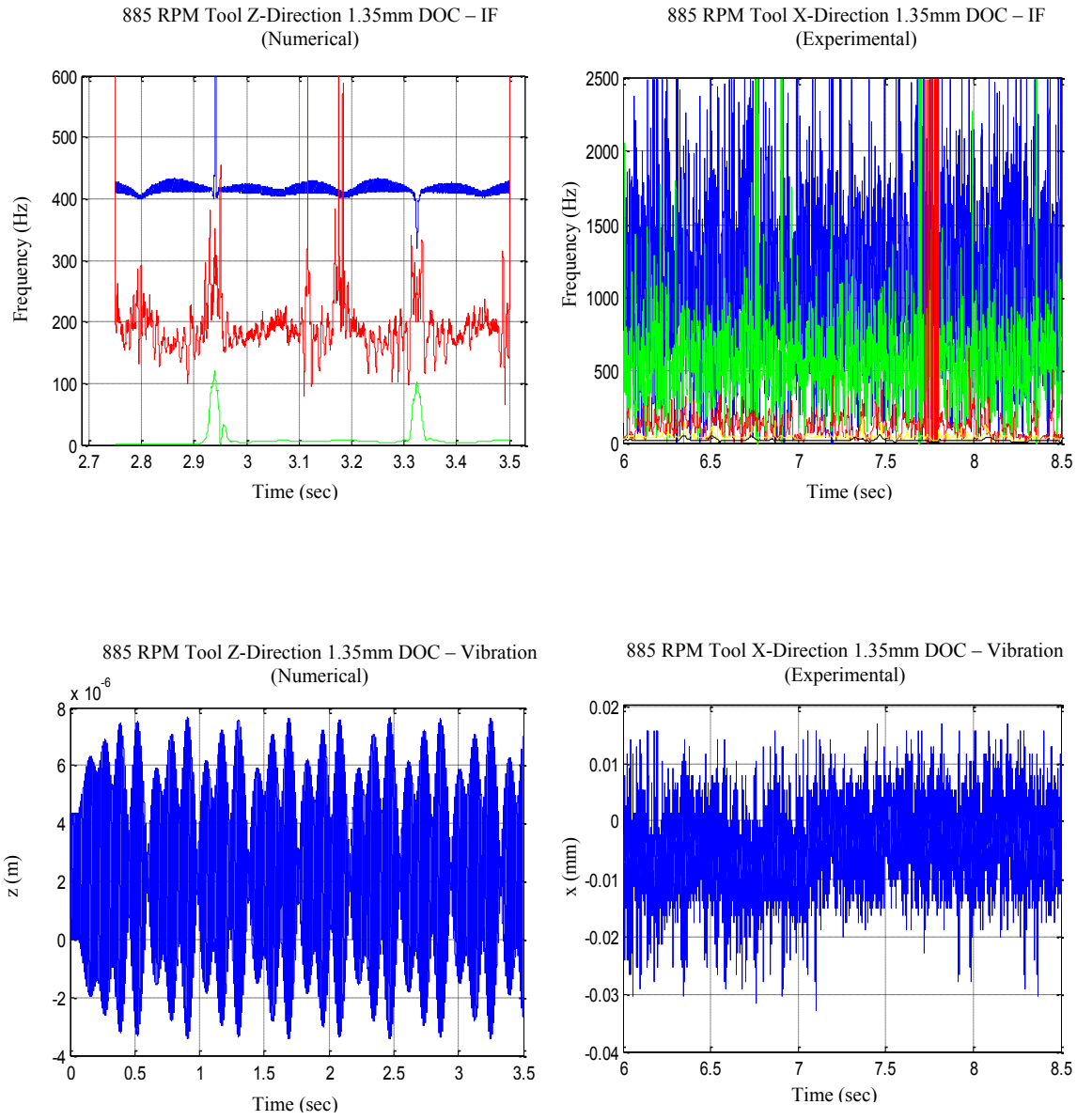

Fig. 5.1 Comparison of numerical (left) and experimental (right) tool vibration signals for chatter-free cutting

The workpiece numerical and experimental vibrations under chatter-free cutting at DOC = 0.95mm and a spindle speed of 885 rpm are plotted in Fig. 5.2. The experimental and numerical workpiece motions are similarly compared in the X-direction and the vibration response demonstrates chatter-free cutting. The IF plot for the numerical signal has modes for the workpiece natural frequency, tool natural frequency, lower cutting frequencies, and the spindle speed. The lower frequency modes are highly modulated and the spindle speed mode is not constant due to the relatively low whirling at 885 rpm. The experimental results have modes at the workpiece natural frequency, workpiece bifurcation, tool natural frequency, lower process related frequency, lathe related frequency, and spindle speed. The numerical simulations do not contain the workpiece bifurcation mode but they do have lower frequency modes which are below the tool natural frequency similar to what is seen experimentally. The frequency values for the workpiece modes are different from the experimental values because the modeling of the workpiece doesn't incorporate changes in workpiece stiffness due to chuck clamping and the tailstock applying an axial load onto the workpiece. The numerical model accurately simulates the modes of the system under chatter-free cutting except for the workpiece and tool bifurcation modes. These modes are due to the high nonlinearity of the real-world system which is difficult to fully simulate. In addition, the tool nonlinear stiffness term corresponds to a varying lower frequency mode related to cutting and observed experimentally. This suggests that the assumption of the tool having a nonlinear stiffness in the development of the model is

accurate. A summary of the comparison for chatter-free cutting between the numerical and experimental data for the workpiece is compiled in Table 5.2.

Table 5.2 Workpiece Experimental and Numerical Chatter-Free and Chatter Modes

Chatter-Free Conditions	
Workpiece	
Numerical	**Experimental**
Workpiece Nat. Freq. ~1850 Hz	Workpiece Nat. Freq. ~2500 Hz
Tool Nat. Freq. ~420 Hz	Workpiece Bifurcation ~1500 Hz
Tool Nonlinear Freq. ~50-200Hz	Tool Coupling Freq. ~750 Hz
Spindle Freq. ~13Hz	Process Related ~400 Hz
	Lathe Related Freq. ~42 Hz
	Spindle Speed ~18 Hz
Chatter Conditions	
Workpiece	
Numerical	**Experimental**
Workpiece Nat. Freq. ~1850 Hz	Workpiece Nat. Freq. ~2500 Hz
Chatter* ~560-850 Hz	Chatter ~840 Hz
Unstable Mode* ~160-600 Hz	Chatter Bifurcation ~450 Hz
Unstable Mode* ~25-500Hz	Chatter Bifurcation ~250 Hz
Low Freq. Components ~13-50 Hz	Lathe Related Freq. ~42 Hz
	Spindle Speed ~16 Hz
*Increases with severity of chatter	

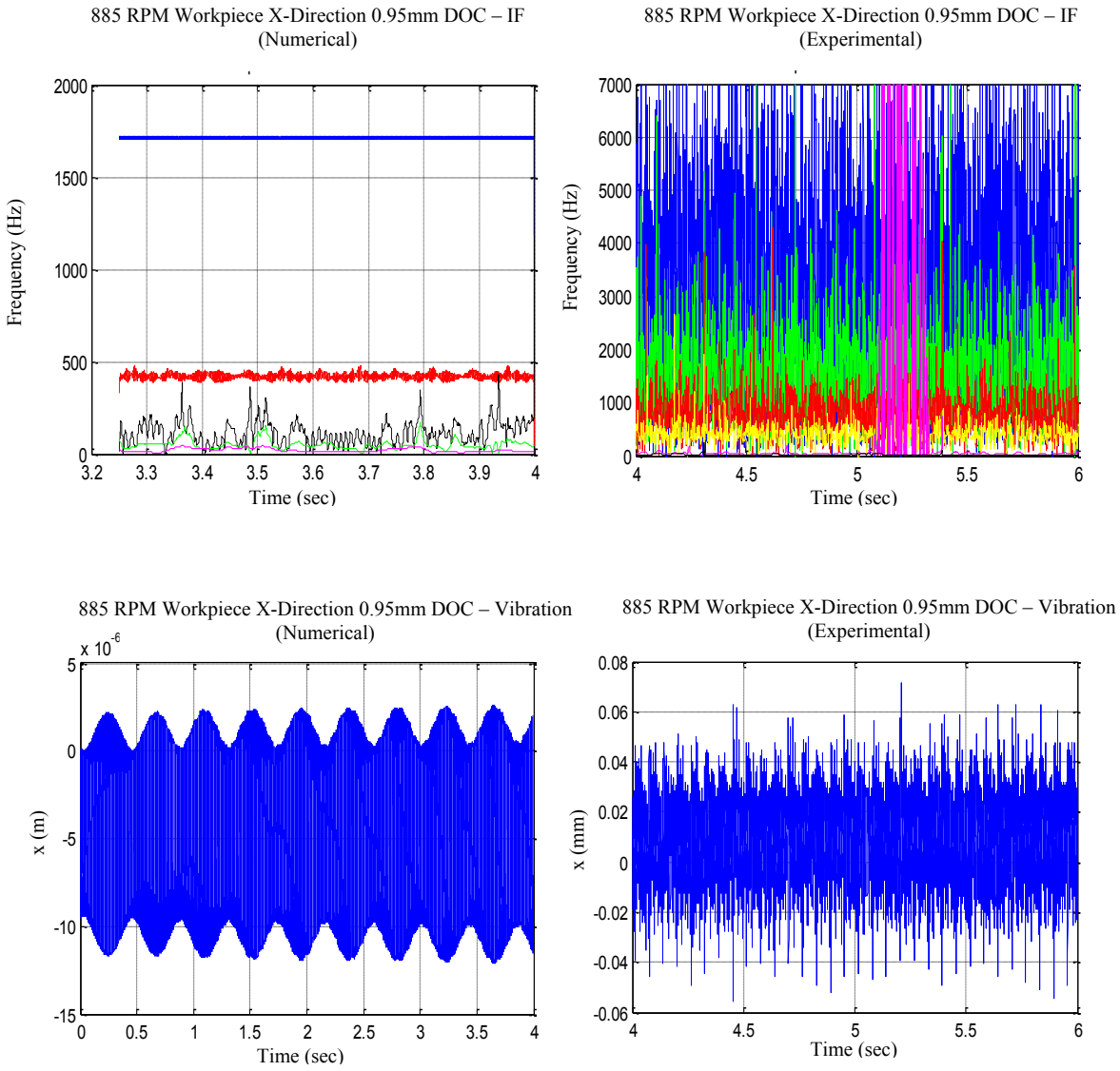

Fig. 5.2 Comparison of numerical (left) and experimental (right) workpiece vibration signals for chatter-free cutting

5.2 Chatter Comparison

The importance of mathematical models is to study the dynamic instability of a system in order to develop methods to prevent or avoid instability which could be harmful to the process. With the underlying dynamics captured, numerical and experimental chatter cutting is compared to determine if the model accurately accounts for the mechanisms that lead to chatter. Chatter was observed in the numerical and experimental tool vibrations for a DOC of 1.75mm as seen in Fig. 5.3. The numerical vibration response shows increased finite amplitude vibrations and the experimental vibrations are slightly increased when compared to the amplitude in Fig. 5.1. The difference in the IF plots between chatter-free and chatter cutting can be identified when comparing Fig. 5.1 with Fig. 5.3. The experimental IF demonstrates a frequency spectrum which now incorporates a chatter frequency around 840 Hz and its corresponding bifurcations as demonstrated in Section 4 as well as the low frequency lathe mode and the spindle speed mode. The numerical IF has a very dense mode around 700 Hz and the lower frequency modes fluctuate drastically covering a wide range of frequencies. There is an additional lower frequency mode and the spindle speed frequency isn't consistent throughout the signal. The numerical IF plot demonstrates a broadband unstable frequency spectrum corresponding with an unstable state of motion.

The workpiece motions for chatter cutting at approximately 1.5mm DOC are plotted in Fig. 5.4. The numerical vibration response doesn't demonstrate a very large increase in vibrations, but the vibrations are steadily increasing and becoming unstable as cutting continues. This is a set of parameters near the critical point of chatter-free

cutting. The experimental vibration response has increased vibrations when compared to Fig. 5.2. The experimental IF plot demonstrates a frequency spectrum which has changed when compared to Fig. 5.2 and now has a dense chatter mode around 840Hz and its associated bifurcations as discussed in Section 4. The numerical IF plot now has a much denser tool natural frequency mode that has slightly increased along with a lower frequency mode which fluctuates at higher frequency values when compared to chatter-free cutting. The numerical and experimental IF plots both show that the workpiece natural frequency doesn't change when chatter develops, and the chatter frequency develops near a dominant mode of the lathe. For the numerical model, the lathe is simply modeled as the tool and thus the chatter frequency develops near this mode. The numerical simulations for the tool and workpiece do not demonstrate period-doubling bifurcation of the chatter frequency as seen experimentally but rather include lower frequency modes which fluctuate drastically and are associated with the nonlinear stiffness term that is included in the modeling of the tool.

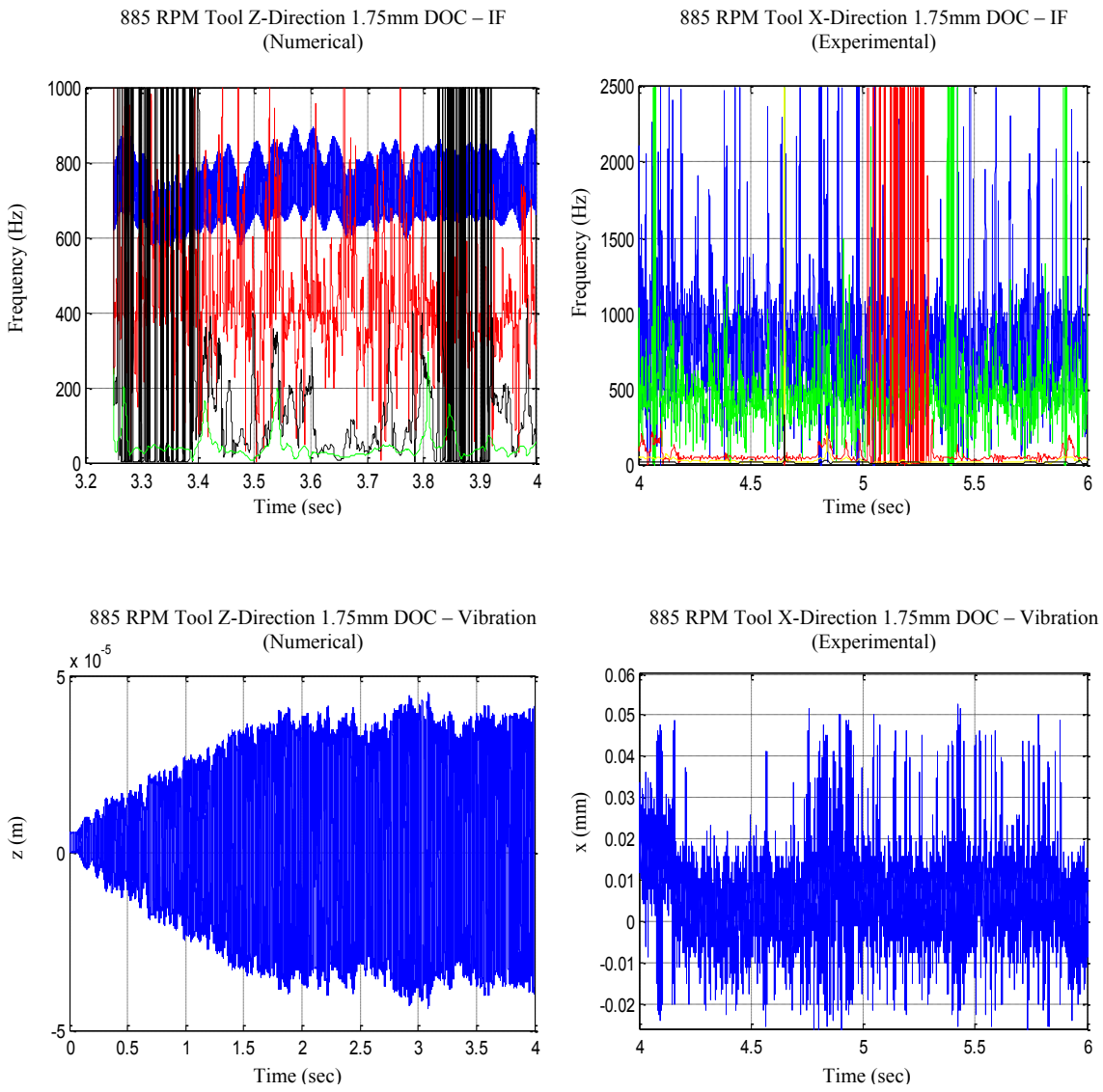

Fig. 5.3 Comparison of numerical (left) and experimental (right) tool vibrations for chatter cutting

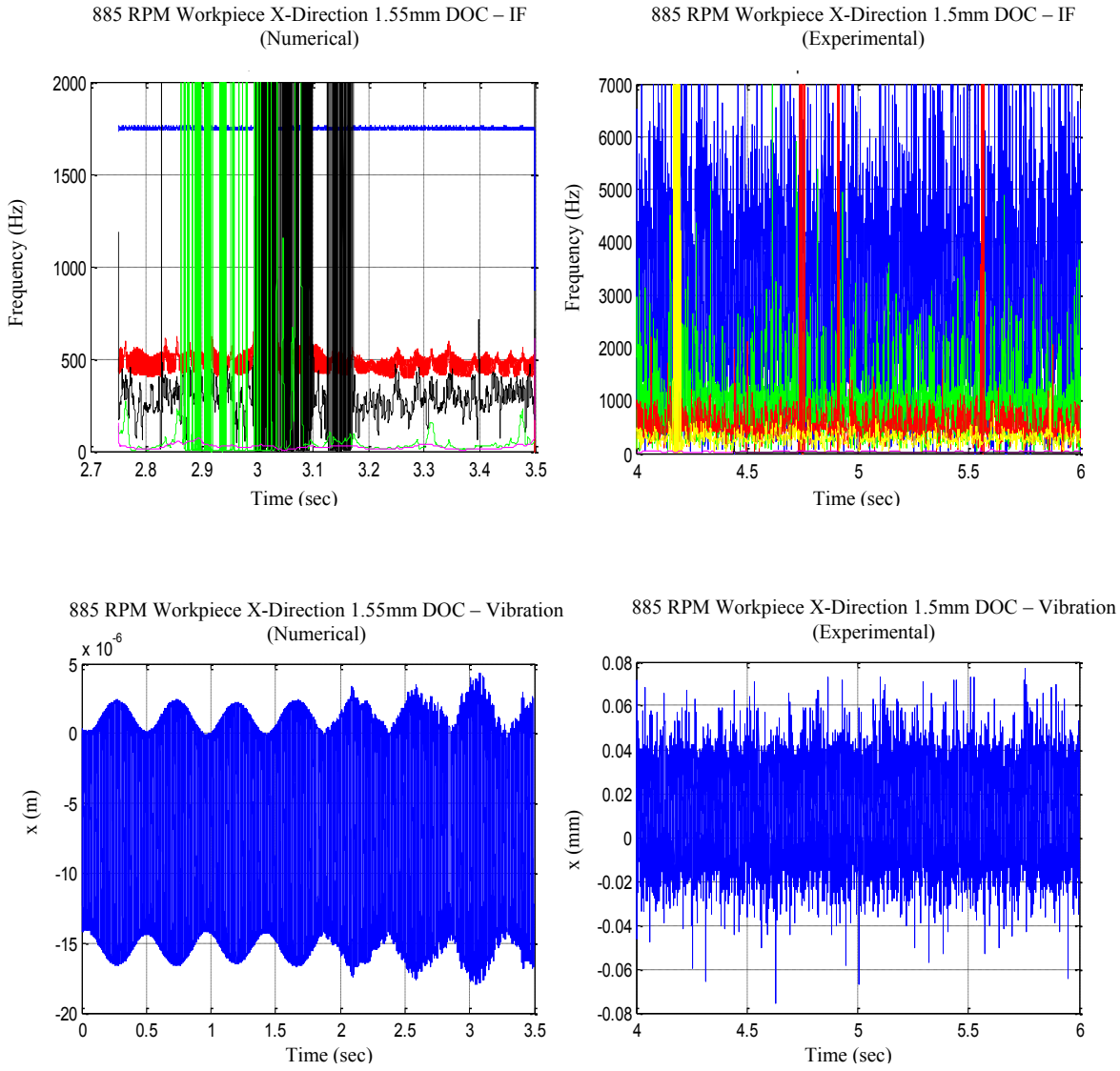

Fig. 5.4 Comparison of numerical (left) and experimental (right) workpiece vibrations for chatter cutting

The IF plots in Figs. 5.3 and 5.4 demonstrate a change in the dynamic response of the system when chatter develops. This illustrates the effectiveness of the model to accurately predict chatter cutting in both the vibration amplitude and frequency spectrum. In Section 4, it was observed that for chatter cutting the tool and workpiece demonstrated coupled vibrations at a "chatter frequency" near the tool natural frequency. The model simulated increased chatter vibrations of the tool and workpiece at a DOC of 1.55mm and at 1.75mm the chatter developed further. These two cases are presented in Fig. 5.5 to analyze the relationship between the tool and workpiece vibrations. The 1.55mm case shows that the tool and workpiece have identical modes at the tool natural frequency and that these modes have a similar structure. The tool and workpiece also have the lower and highly fluctuating frequencies; however, this mode is not sustained in the tool vibrations. As chatter further developed at 1.75mm DOC, the chatter frequency has increased to a dense mode around 750 Hz in both the tool and workpiece. Also, the lower frequency modes and spindle speed exhibit similar characteristics for the tool and workpiece demonstrating coupled vibrations. It is also observed that the workpiece natural frequency mode is retained during chatter cutting which was observed experimentally. The results in Section 4 demonstrated tool and workpiece vibrations which were uncoupled during chatter-free cutting and chatter-free numerical simulations are presented in Fig. 5.6. The tool IF has modes related to the tool natural frequency, nonlinear stiffness, and a varying spindle speed mode. The workpiece contains a natural frequency, a tool natural frequency, and lower frequency modes. The tool and workpiece both have the identical tool natural frequency but the lower frequency modes

do not have similar characteristics. This indicates that for the numerical simulations the tool and workpiece exhibit uncoupled vibrations except the tool natural frequency. The model accurately simulates the coupled tool and workpiece vibrations at the chatter frequency during chatter cutting and more uncoupled vibrations during chatter-free cutting.

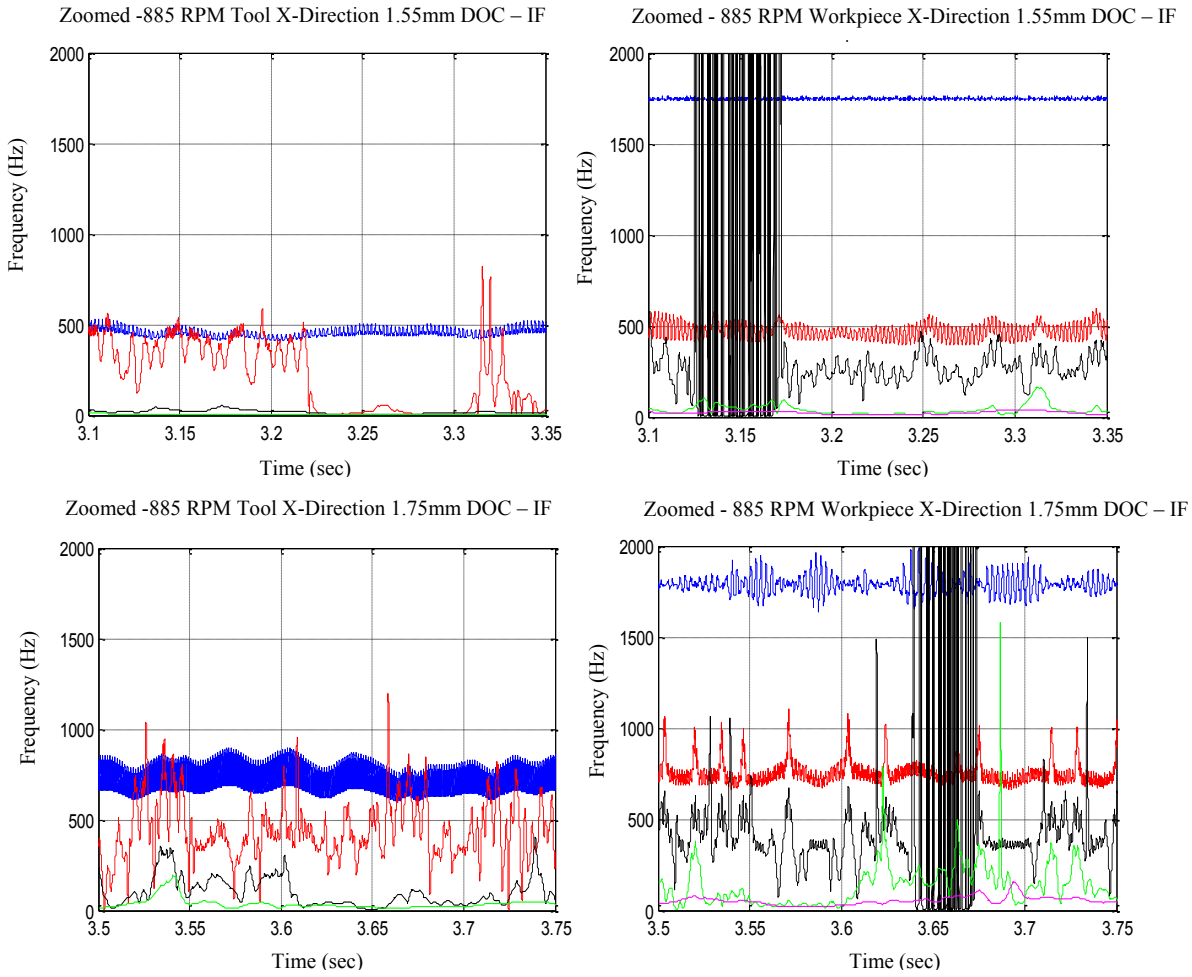

Fig. 5.5 Comparison of tool (left) and workpiece (right) numerical chatter vibrations for the onset of chatter (top) and further developed chatter (bottom)

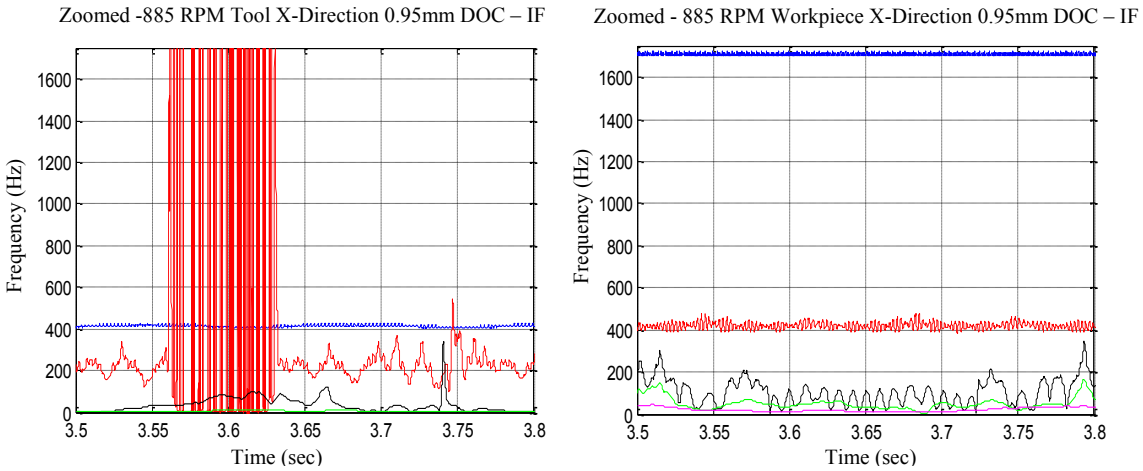

Fig. 5.6 Comparison of tool (left) and workpiece (right) numerical chatter-free vibrations

5.3 Cutting Stability

The model simulated the underlying dynamics of chatter cutting defined by having increased vibration amplitude for the tool and workpiece and coupled vibrations at a chatter frequency. Using this definition of chatter, the model was run for varying spindle speeds and DOCs to develop chatter limits and investigate high speed dynamics. The stability diagram presented in Fig. 5.7 demonstrates that as the spindle speed increases the chatter-free DOC limit increases and begins to exponentially level out at high speeds. This was perceived experimentally in Section 3 and was also observed in [7, 59] where the critical DOC increased with cutting speeds. In [12] the stability lobes for lathe turning with process damping are similar, where the chatter-free DOC gradually increases with spindle speed until 1,000 rpm where the lobes then level out. However, the experimental data in [12] shows stable cutting well above the stability lobes at higher

spindle speeds. This suggests at higher spindle speeds there could be pockets of unstable cutting below the absolute critical DOC limit. The stability diagram in Fig. 5.7 shows that at speeds above 1,500 rpm there are locations in which excessive frequencies and excessive workpiece vibrations occurred. These cases could represent pockets of instability at higher spindle speeds. The excessive frequency cases are parameters which result in frequency spectra indicative of nonlinear vibrations such as period-doubling bifurcation, broadband frequencies, and high frequencies that are different from the chatter and chatter-free cutting cases. These cases can still exhibit stable tool and workpiece vibration amplitudes. The excessive workpiece vibrations are conditions where the workpiece vibrations are stable but have a magnitude at least three times greater than the chatter-free conditions. These cases occur at higher speeds and could have a highly nonlinear frequency spectrum but do not exhibit chatter cutting in the time or frequency domain. In the machine shop, excessive workpiece vibrations such as these would greatly affect the tolerances and roundness of the workpiece and would be unacceptable. The excessive workpiece vibrations present a second limit case in the stability diagram as shown by the dashed line in Fig. 5.7. It is important to acknowledge workpiece motion when developing methods to increase cutting speeds and still retain adequate tolerances. The stability diagram shows that for the presented workpiece configuration, the workpiece motions dominate the system at high spindle speeds.

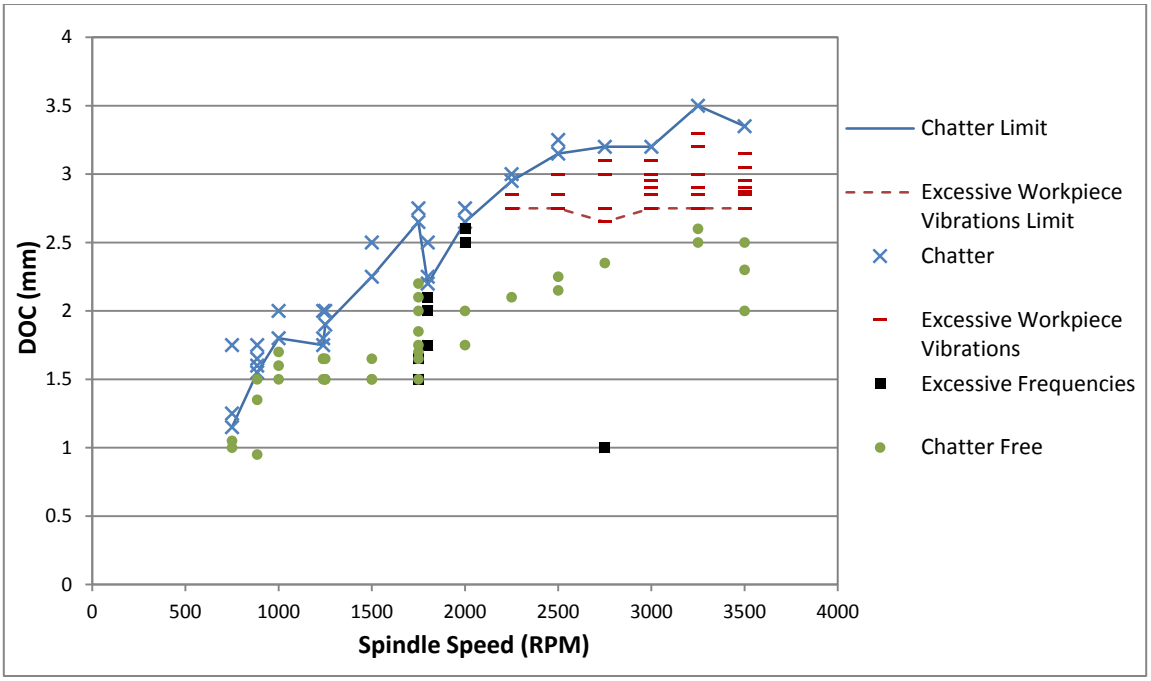

Fig. 5.7 Stability diagram for depth-of-cut vs. spindle speed with a constant feed rate of 0.09mm/rev

The simulations at 1,800 rpm and DOCs of 2.0, 2.1, and 2.2mm are shown in Figs. 5.8 and 5.9. The 2.0 and 2.1 mm DOC workpiece cases in Fig. 5.8 have stable vibrations. However, the IF plots show two different states of motion. The 2.0mm case has period-doubling bifurcation of the workpiece natural frequency which covers a broad frequency range, and the tool natural frequency mode isn't constant. The 2.1mm DOC case has a bounded mode that ranges from 1000-1250Hz similar to the period-doubling bifurcation frequency in the 2.0mm case. There is also a bounded tool natural frequency mode and lower frequency mode below the tool natural frequency. The 2.2mm case is a

chatter cutting case in which the workpiece vibrations exhibit chatter cutting with increasing amplitude. A chatter frequency has appeared and when compared to the tool motion IF in Fig. 5.9, the tool and workpiece are vibrating at the same chatter frequency. The tool response in Fig. 5.9 at 2.0mm DOC has a chatter-free frequency spectrum and stable vibration amplitudes. The 2.1mm tool response has stable vibration amplitude but the IF shows that the tool now has a workpiece natural frequency mode and frequencies just below the tool natural frequency. These modes oscillate over a wider range of frequencies than that of the case at 2.0mm DOC. The 2.2mm DOC case for the tool response is chatter cutting which demonstrates increased chatter vibrations and the appearance of a chatter frequency. These cases illustrate that at higher spindle speeds chatter-free cutting still exhibits unstable states of motion as defined in nonlinear dynamics. These are pockets of instability which will increase the rate of tool wear and the probability of tool failure.

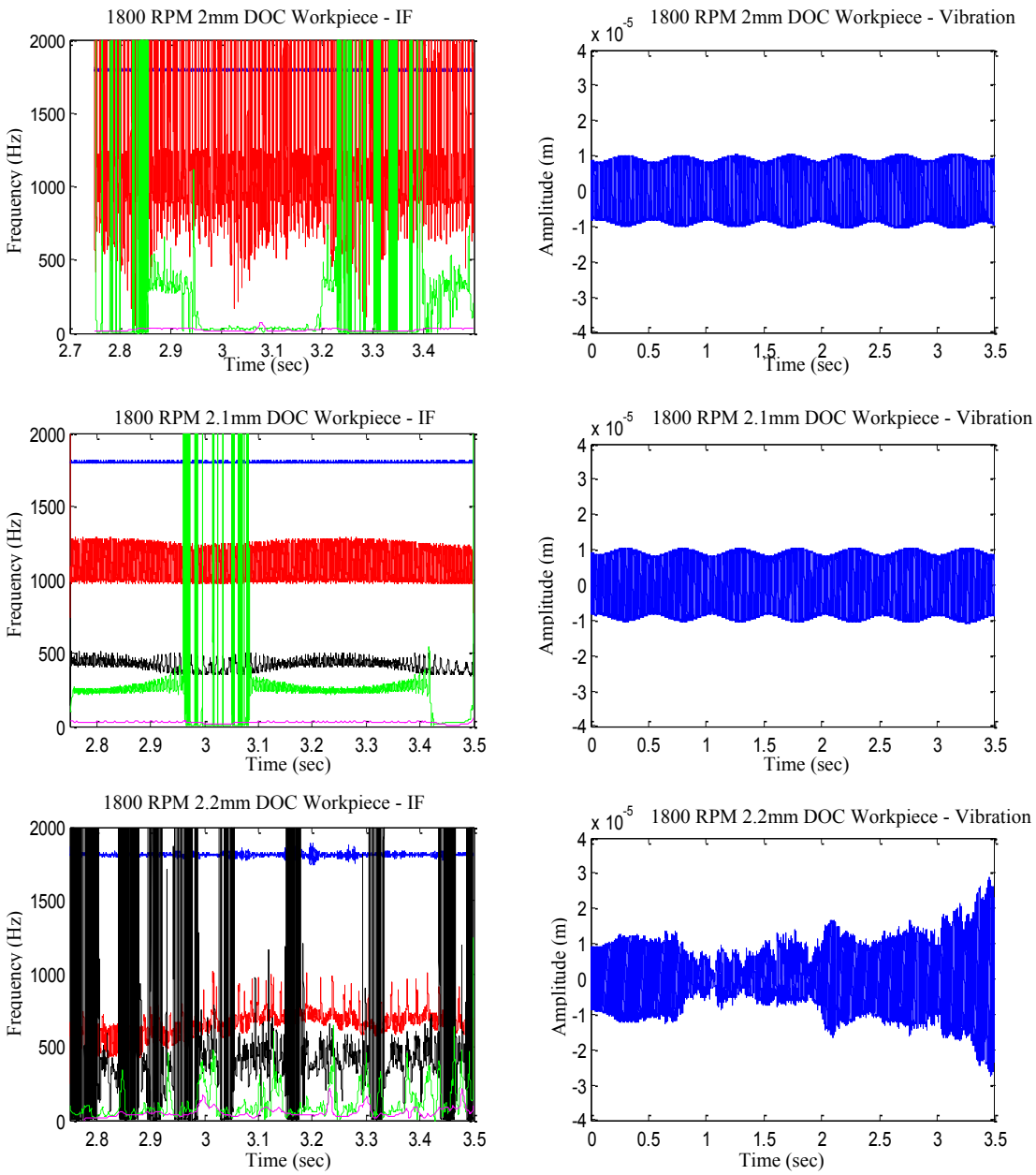

Fig. 5.8 Workpiece response at 1800 rpm and 2.0mm (top), 2.1mm (middle), and 2.2mm (bottom) DOCs

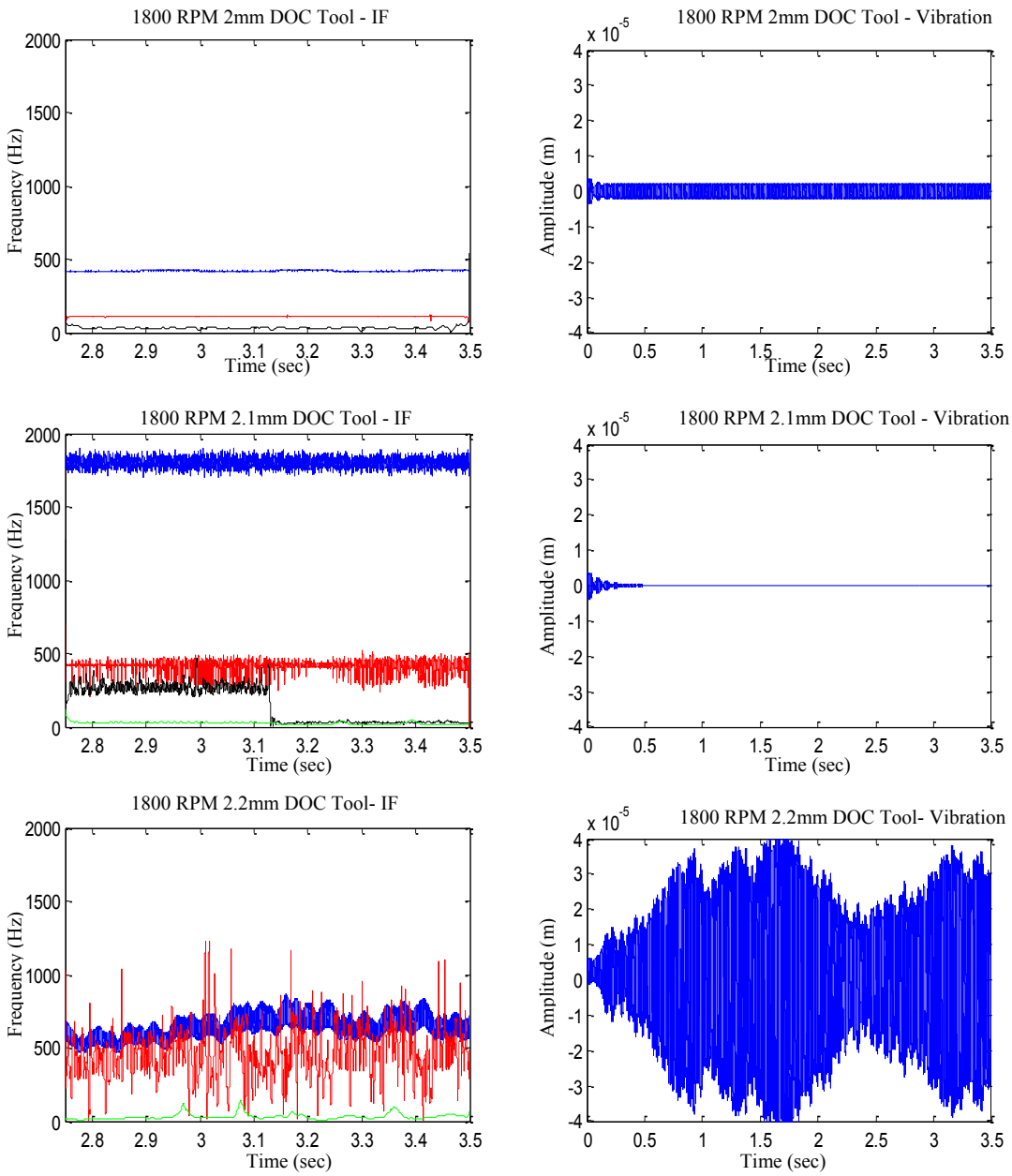

Fig. 5.9 Tool response at 1800 rpm and 2.0mm (top), 2.1mm (middle), and 2.2mm (bottom) DOCs

The 2.85, 2.95, and 3.0mm DOC cutting at 2250 rpm is presented in Figs. 5.10 and 5.11 to investigate excessive workpiece vibrations. The 2.85mm workpiece response in Fig. 5.10 has stable vibrations and an IF plot with a chatter-free frequency spectrum. The 2.95 mm case in Fig. 5.10 has increasing vibrations which have not reached a steady-state magnitude. The IF plot of the 2.95mm DOC workpiece response in Fig. 5.10 has a tool natural frequency mode which fluctuates over a wide range and is increasing with time. The 3.0mm case demonstrates workpiece motion which has finite amplitude chatter vibrations and a chatter frequency. The 2.85mm DOC tool vibrations in Fig. 5.11 are chatter-free with stable vibrations and a chatter-free IF plot. As the DOC increases to 2.95mm, the tool vibrations in Fig. 5.11 have stable amplitude but now the frequency spectrum has a high frequency mode at the workpiece natural frequency as seen in the IF plot. This mode covers a wide range of frequencies and is developing towards a broadband mode as cutting continues. High frequency vibrations which are growing broadband are detrimental to the life of the tool even though the process is not experiencing chatter. The 3.0mm case for the tool vibration is chatter cutting where the vibration amplitude of the tool is unstable and the IF plot has a chatter frequency coupled with the workpiece. These three cases compare simulations that are chatter-free, excessive workpiece vibrations, and chatter cutting. At higher spindle speeds excessive workpiece vibrations occur due to the imbalance and configuration of the workpiece.

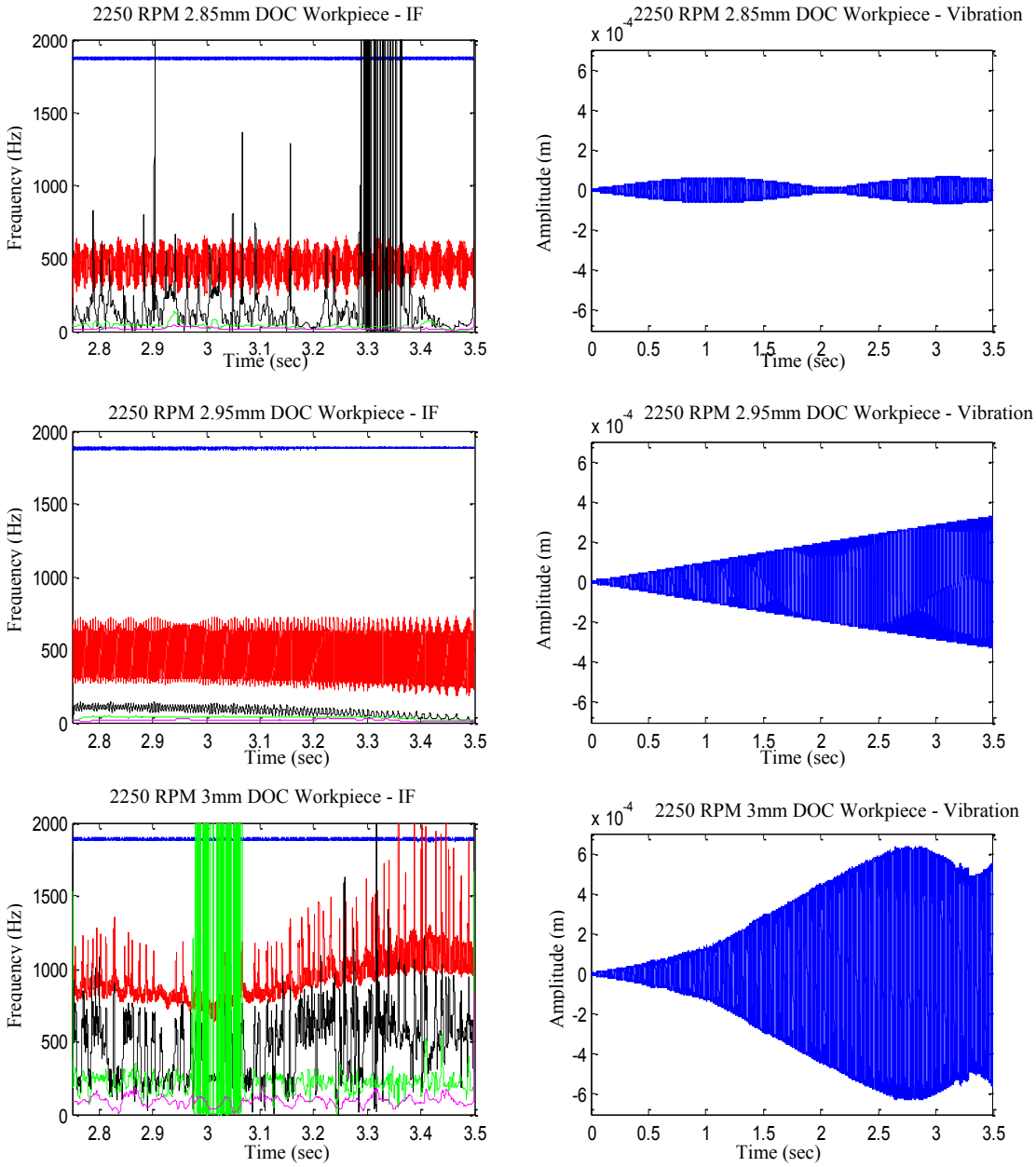

Fig. 5.10 Workpiece response at 2250 rpm and 2.85mm (top), 2.95mm (middle), and 3.0mm (bottom) DOCs

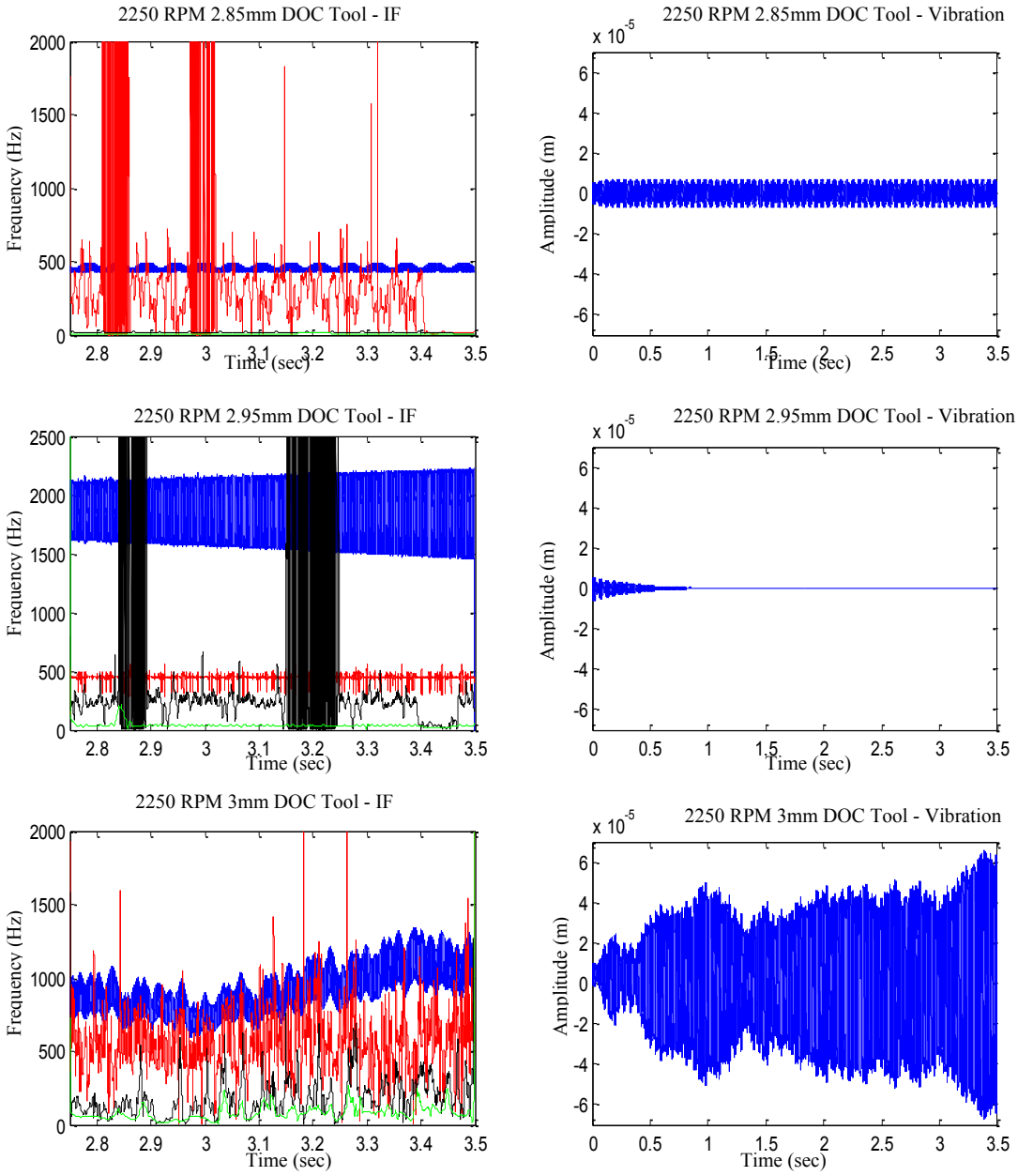

Fig. 5.11 Tool response at 2250 rpm and 2.85mm (top), 2.95mm (middle), and 3.0mm (bottom) DOCs

The maximum spindle speed used to develop the stability diagram is 3500 rpm and was run at DOC = 1.5mm, which is a stable DOC for lower speeds. The workpiece response in Fig. 5.12 has chatter-free vibrations. The corresponding IF plot has a mode that stables out near the tool natural frequency and covers a wide range of frequencies. The tool response for 1.5mm DOC in Fig. 5.13 has stable tool vibrations but the IF plot has high frequency vibrations at the workpiece natural frequency. The appearance of this mode in the tool IF is due to the increased impact that the workpiece motion has on the system at high spindle speeds and would negatively impact the tool. The 3.05mm DOC case for workpiece motion in Fig. 5.12 has excessive vibration amplitudes which would affect the tolerances of the workpiece, and the IF plot has a varying tool natural frequency. Chatter is not occurring at these conditions but the tolerances of the workpiece could be unacceptable. The 3.35mm DOC case for the workpiece vibrations in Fig. 5.12 are much larger than the chatter-free cutting case and reached steady state quickly at this spindle speed. The workpiece IF associated with DOC = 3.35mm indicates chatter vibrations coupled with the vibrations of the tool, but is at the onset of chatter because the chatter frequency is just above the tool natural frequency. The 3.05mm case for the tool in Fig. 5.13 shows chatter-free cutting of the tool. The tool vibrations at DOC = 3.35mm is clearly chatter cutting in which the tool vibrations are much larger than the chatter-free case and reaches the finite chatter amplitude very quickly. The corresponding IF also demonstrates coupled chatter vibrations with the workpiece.

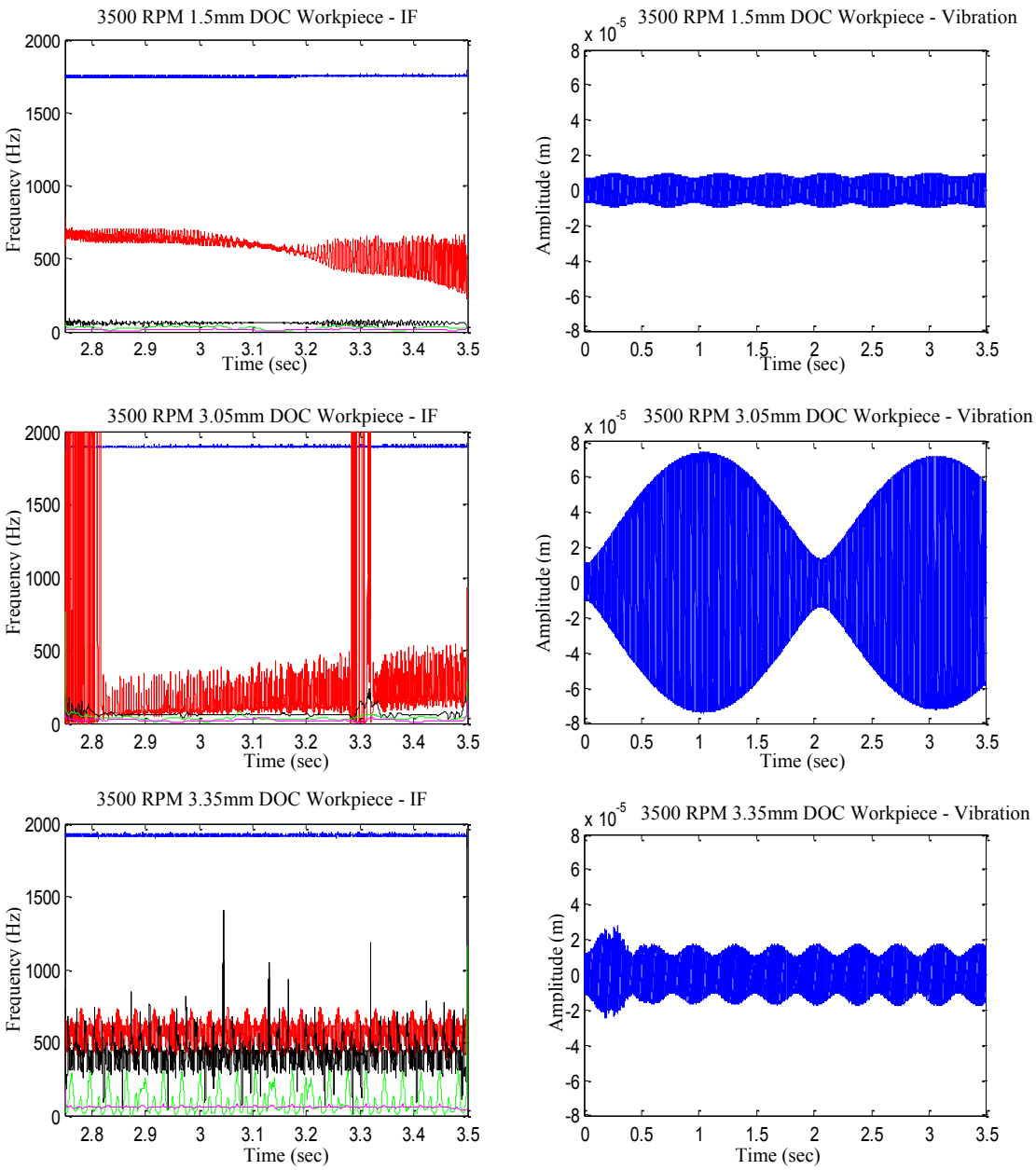

Fig. 5.12 Workpiece response at 3500 rpm and 1.5mm (top), 3.05mm (middle), and 3.35mm (bottom) DOCs

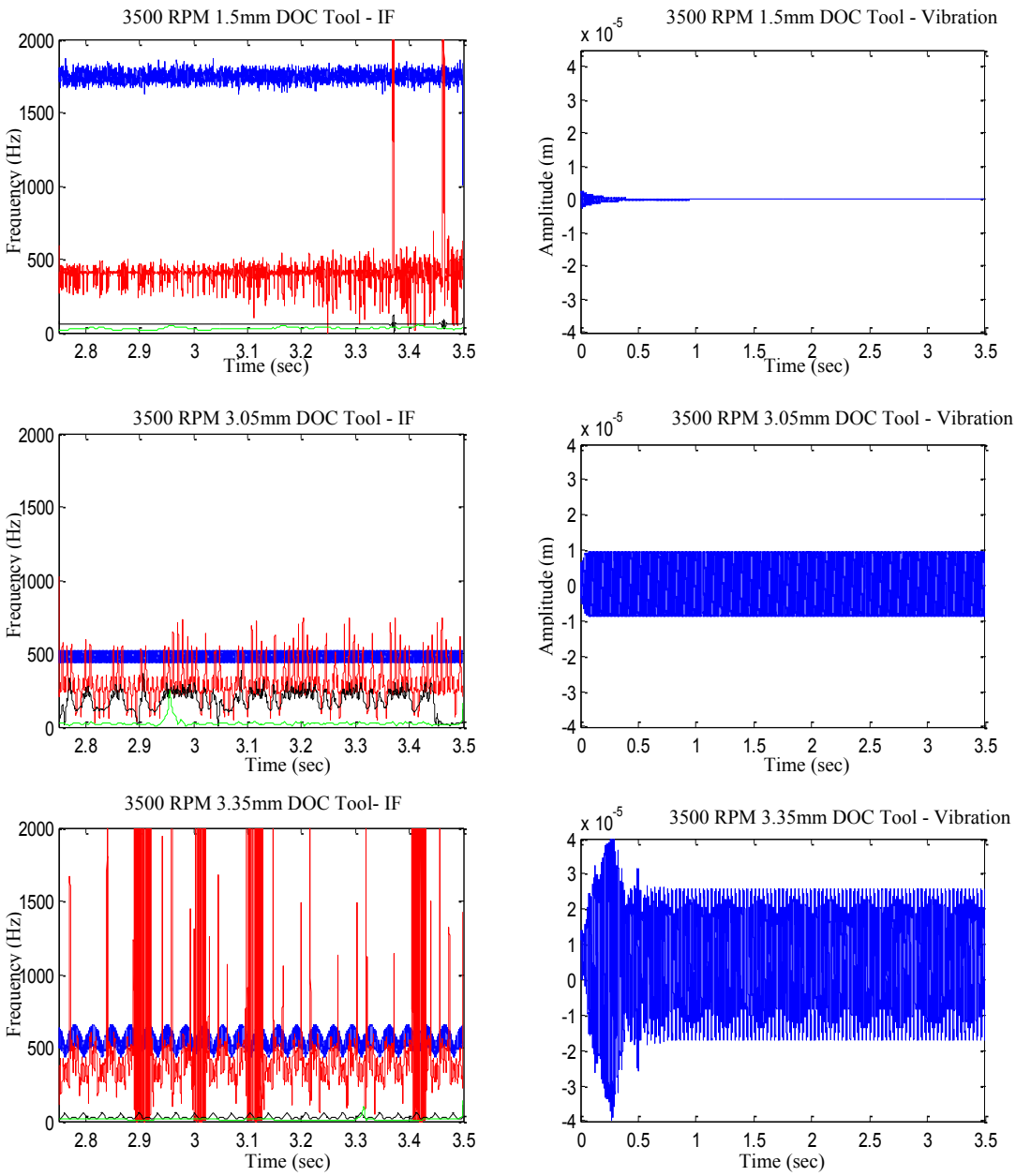

Fig. 5.13 Tool response at 3500 rpm and 1.5mm (top), 3.05mm (middle), and 3.35mm (bottom) DOCs

6. MICRO-MILLING MODEL DEVELOPMENT

6.1 Force Mechanism

The force mechanism used for the micro-milling model is adopted from [54]. The model in [54] expanded on the slip-line model in [53] by accounting for the dead metal cap and by adding an additional slip-line on the clearance face of the tool. The additional slip-line on the clearance face of the tool assumes that the material elastically recovers fast enough to create additional plowing forces when the chip thickness (tc) is less than the critical chip thickness (tc_{min}). However, since material takes time to recover, and micro-milling utilizes high spindle speeds, it will be assumed that the additional plowing forces produced on the clearance face can be neglected. Also, the feedrates used are larger than the tool nose radius. The slip-line theory has the following assumptions: 1) deformation is under plane-strain conditions, 2) workpiece material is elastic perfectly plastic (does not change with strain, strain rate, and temperature), and 3) orthogonal and continuous cutting is performed [51, 52]. The derivation for the shearing and plowing forces utilize the hodographs in [54] and a process similar to what was given in [53]. When the chip thickness is greater than the critical chip thickness, it is assumed that both shearing and plowing forces are present. The differential shearing forces in the cutting and thrust directions as given in [54] are

$$dF_{sc} = \tau\, da\, [(\cos\varphi_s + a_\theta \sin\varphi_s) l_s + (\cos(2\eta_2)\sin\alpha_e + a_2 \cos\alpha_e) l_b] \tag{6.1}$$

$$dF_{st} = \tau\, da\, [(a_\theta \cos\varphi_s - \sin\varphi_s) l_s + (\cos(2\eta_2)\cos\alpha_e - a_2 \sin\alpha_e) l_b] \tag{6.2}$$

where τ is the material shear flow stress, da is the axially depth-of-cut, φ_s is the shear angle, α_e is the effective rake angle, r_e is the tool nose radius, l_s is the shear plane length, l_b is the plowing length, and a_θ, a_1, a_2, η_2, η_1, ρ, and ψ are the slip-line field variables defined as follows [54, 60]

$$l_s = (tc(t) - r_e(1 + \sin\alpha_e) + h_{prow})/sin\,\varphi_s \tag{6.3}$$

$$l_b = r_e \tan(\pi/4 + (\alpha_e - \psi)/2) \tag{6.4}$$

$$h_{prow} = \sqrt{2} r_e \sin\rho\, (\sin\eta_1 + \cos\eta_2) \tan((\pi + 2\alpha_e - 2\psi)/4) \tag{6.5}$$

$$a_\theta = 1 + 2\theta \tag{6.6}$$

$$a_2 = (1 + 2\theta + 2\delta + \sin(2\eta_2)) \tag{6.7}$$

$$\theta = \pi/4 - \rho - \varphi_s \tag{6.8}$$

$$\delta(t) = \varphi_s - \alpha_e(t) - \eta_2 \tag{6.9}$$

$$\gamma(t) = \eta_1 + \eta_2 + \alpha_e(t) - \psi \tag{6.10}$$

$$\psi = \sin^{-1}(\sqrt{2}\sin\rho \sin\eta_1) \tag{6.11}$$

Following the similar derivation in [53], the plowing forces in the cutting and thrust directions are [54]

$$dF_{pc} = \tau\, da\, [(\cos(2\eta_1)\cos\psi + a_1 \sin\psi) l_b] \tag{6.12}$$

$$dF_{pt} = \tau\, da\, [(a_1 \cos\psi - \cos(2\eta_1)\sin\psi) l_b] \tag{6.13}$$

$$a_1 = (1 + 2\theta + 2\delta + 2\gamma + \sin(2\eta_1)) \tag{6.14}$$

For further details on the derivation of the presented force equations refer to reference [54]. Assuming that the plowing and shearing forces are both present during shearing-dominated cutting, and neglecting the additional slip-line which was added in [54], the different cases for the forces acting on the tool are given. This includes a third case which accounts for the tool jumping out of the cut during low feed rates and large tool vibrations.

Case I: $tc(t) > tc_{min} \rightarrow \begin{cases} dF_t = dF_{st} + dF_{pt} \\ dF_c = dF_{sc} + dF_{pc} \end{cases}$

Case II: $0 < tc(t) < tc_{min} \rightarrow \begin{cases} dF_t = dF_{pt} \\ dF_c = dF_{pc} \end{cases}$

Case III: $tc(t) < 0 \rightarrow \begin{cases} dF_t = 0 \\ dF_c = 0 \end{cases}$

6.2 Rake and Shearing Angles

The third assumption for the slip-line theory suggests that an effective rake angle, $\alpha_{r,e}$, needs to be utilized for oblique cutting and to account for the rake angle becoming highly negative at low feed rates. This is more prominent in micro-milling because the chip thickness is closer to the tool nose radius [47, 50]. A method in which the average rake angle is determined by drawing a line between the lowest point and a point on the rake face that is a multiple of chip thickness is used in [47] to calculate the effective rake angle. A method similar to the one used in [50] is used in this thesis to calculate the effective rake angle. The nominal rake angle,$\alpha_{r,n}$, shown in Fig. 6.1, can be used to determine a critical point, h_t, that defines the tangent point between the rake surface and the arc of the cutters edge as

$$\alpha_{r,e} = \begin{cases} [\sin^{-1}((tc(t)/r_e) - 1)], & tc(t) \le h_t \\ \alpha_{r,n}, & tc(t) > h_t \end{cases} \quad (6.15)$$

$$h_t = r_e(1 + \cos(\pi/2 - \alpha_{r,n})) \quad (6.16)$$

Note that when the chip thickness is below h_t, then the effective rake angle changes.

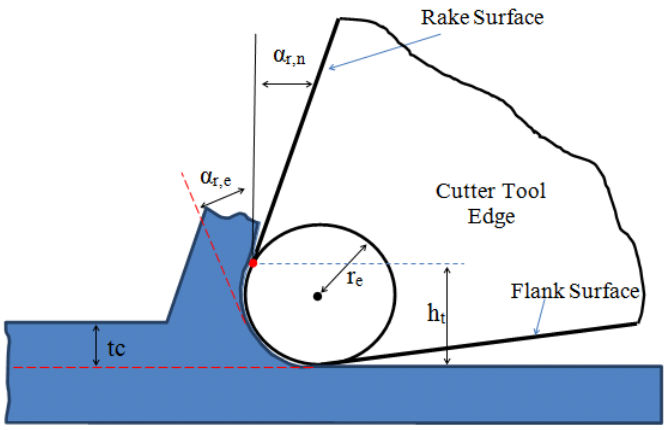

Fig. 6.1 Effective rake angle shown to be highly negative when chip thickness becomes small

To estimate the shearing angle, φ_s, many different methods have been utilized. A shearing angle associated with pearlite and ferrite materials researched in [47] is used in [60]. The shearing angle is calculated based off of the force and coefficient of friction values reported in [46]. The actual chip thickness and cutting forces are utilized in [53] and [52] to determine the shearing angle. The method in [60] provides a shearing angle

equation which is a function of chip thickness, allowing the angle to be changed dynamically with cutting conditions. This method is chosen for the presented model.

6.3 Chip Thickness

The slip-line force model, effective rake angle, and shear angle are all dependent upon the instantaneous chip thickness. Thus, accurately determining the instantaneous chip thickness, $tc_j(t)$, for each tooth, j, is critical to simulating the dynamics of the process. The instantaneous chip thickness calculation for each tooth that considers tool vibration [37-40] is given as:

$$tc_j(t) = fc * sin\varphi_j(t) + \Delta x sin\varphi_j(t) + \Delta y cos\varphi_j(t) \tag{6.17}$$

$$\Delta x = x(t) - x(t-\delta) \tag{6.18}$$

$$\Delta y = y(t) - y(t-\delta) \tag{6.19}$$

where φ_j is the immersion angle of tooth j (Fig. 6.4), fc is the feed rate per tooth, and $\delta = 60/(J * \Omega)$ is the time delay for a tool with J number of teeth rotating at a spindle speed of Ω revolutions per minute.

Traditional macro-milling has two different cases which need to be considered when simulating the milling process. The first case is when the tooth is immersed in the workpiece and the second case is when the tooth jumps out of the cut during larger vibrations or low feed rates. The second case is important because it limits the vibration amplitude that can be achieved by the tool [39]. The second case is shown in Fig. 6.2 where the actual tooth path at different moments in time is represented by the wavy lines oscillating about a smooth black curve which represents the tooth path under zero vibration. The highlighted area shows the tooth path at the next moment in time (blue

line) jumping out of the surface profile created by the previous tooth path (red line). There is an air gap between the tooth and the workpiece which is represented by a negative chip thickness. This negative chip thickness needs to be added to the chip thickness the next moment in time to account for the tooth jumping out of the cut as seen in Eq. (22) where the previous chip thickness is added to the current chip thickness.

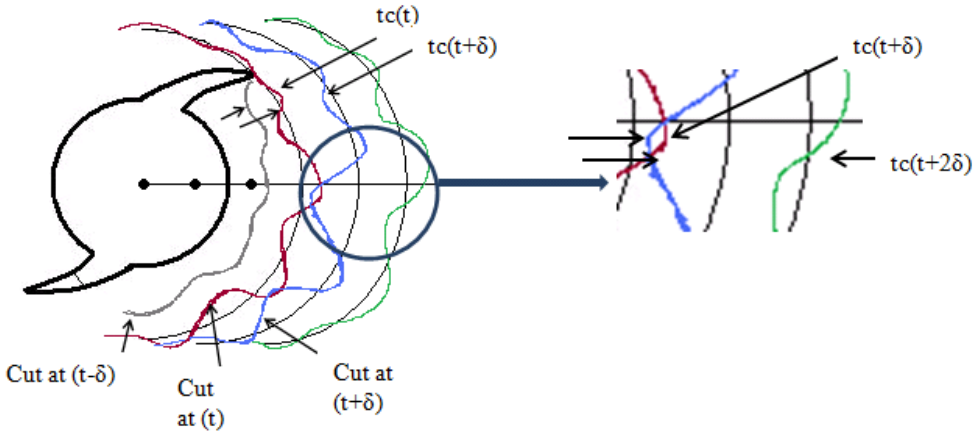

Fig. 6.2 Vibrating tooth path of the tool shown at different moments in time

For micro-milling there are two additional cases. These cases are due to the plowing phenomenon which occurs during micro-milling [54]. When the chip thickness is less than, tc_{min}, only the plowing forces are present. When this occurs, the material elastically recovers by a certain amount depending upon the elastic recovery rate,p_e, of the workpiece. When the chip thickness is less than tc_e, the chip thickness associated with full elastic recovery, the workpiece will elastically recover to its initial position.

When the chip thickness is between tc_e and tc_{min} the workpiece will elastically recover by elastic recovery rate of the material. This critical chip thickness value is important for modeling the micro-milling process because the plowing phenomenon is one of the prominent forcing mechanisms acting on the system. This has motivated the effort to accurately predict this value for different materials. In [43] the tc_{min} value for aluminum is determined to be $0.3*r_e$ and [44] provides the critical contact angle for the tc_{min} value. This angle is found to range from 28°-33° for different materials. Using a neutral point angle of approximately 30° for mild steel, the corresponding tc_{min} value was found to be approximately $0.15*r_e$. A method for predicting the critical contact angle given in [44] and [61] provides an analytical method for calculating this minimum chip thickness. In [60] tc_{min} values for ferrite and pearlite materials are given based on studies that focused on the micro-structure of machining ductile iron such as the study in [47] where damage exponents for pearlite and ferrite are determined. The elastic recovery rate is related to workpiece hardness and modulus of elasticity determined by performing scratch tests on various materials in [62]. The elastic recovery rates for pearlite and ferrite given in [60] are adopted. Since tc_e is very small and feedrates larger than the tool nose radius are used, the case of full elastic recovery is neglected, and only elastic recovery by the material elastic recovery rate is considered. The equations for calculating the three chip thickness cases are given in Eqs. (6.20) – (6.22), where $tc_j(t-\delta)$ is the chip thickness at that point for the previous revolution.

$$tc_j(t-\delta) > tc_{min} : \; tc_j(t) = fc * sin\varphi_j(t) + \Delta x sin\varphi_j(t) + \Delta y cos\varphi_j(t) \tag{6.20}$$

$$0 < tc_j(t-\delta) < tc_{min} : \; tc_j(t) = fc * sin\varphi_j(t) + \Delta x sin\varphi_j(t) + \Delta y cos\varphi_j(t) + p_e * tc_j(t-\delta) \tag{6.21}$$

$$tc_j(t-\delta) < 0 : \; tc_j(t) = fc * sin\varphi_j(t) + \Delta x sin\varphi_j(t) + \Delta y cos\varphi_j(t) + tc_j(t-\delta) \tag{6.22}$$

6.4 Helical Angle and Equations of Motion

When accounting for the helical angle (θ_h in Fig. 6.3), models in [40, 50] take into account the rake angle and chip flow angle. The slip-line field force model already accounts for these angles when determining the cutting and thrust forces. To account for the helical angle, the tool is decomposed into axial elements and for each axial element, the forces are projected into the global X-, Y-, and Z-direction and the vector sum of the force components on each axial element make up the total force acting on the tool. Figure 6.3 shows a small element of the cutting tooth face similar to what is used in [40, 50] to obtain the force components along the X-, Y-, and Z-direction.

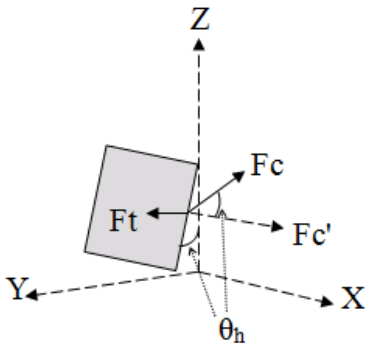

Fig. 6.3 Small element on the cutting tooth face of the micro-tool

$$F_x = -F_t \sin \varphi_j(t) + F_c' \cos \varphi_j(t) \tag{6.23}$$

$$F_y = -F_t \cos \varphi_j(t) - F_c' \sin \varphi_j(t) \tag{6.24}$$

$$F_z = F_c \sin \theta_h \tag{6.25}$$

where

$$F_c' = F_c \cos \theta_h \tag{6.26}$$

To simulate the micro-milling system, the angle φ seen in Fig. 6.4 for each tooth and axial element has to be determined so that it is known if that tooth and axial element is engaging in the workpiece and thus contributing to the overall force of the system. As one goes up axially on the tool, each tooth's axial element lags behind the axial element below. To determine the angle φ for each axial element, k, the angle $\Delta\varphi$ that each one element lags behind the other needs to be determined (Fig. 6.5).

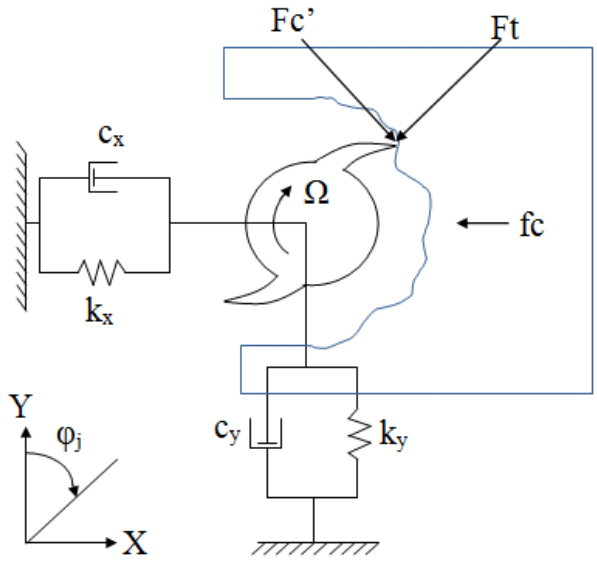

Fig. 6.4 The 2D lumped mass-spring-damper model of the micro-tool

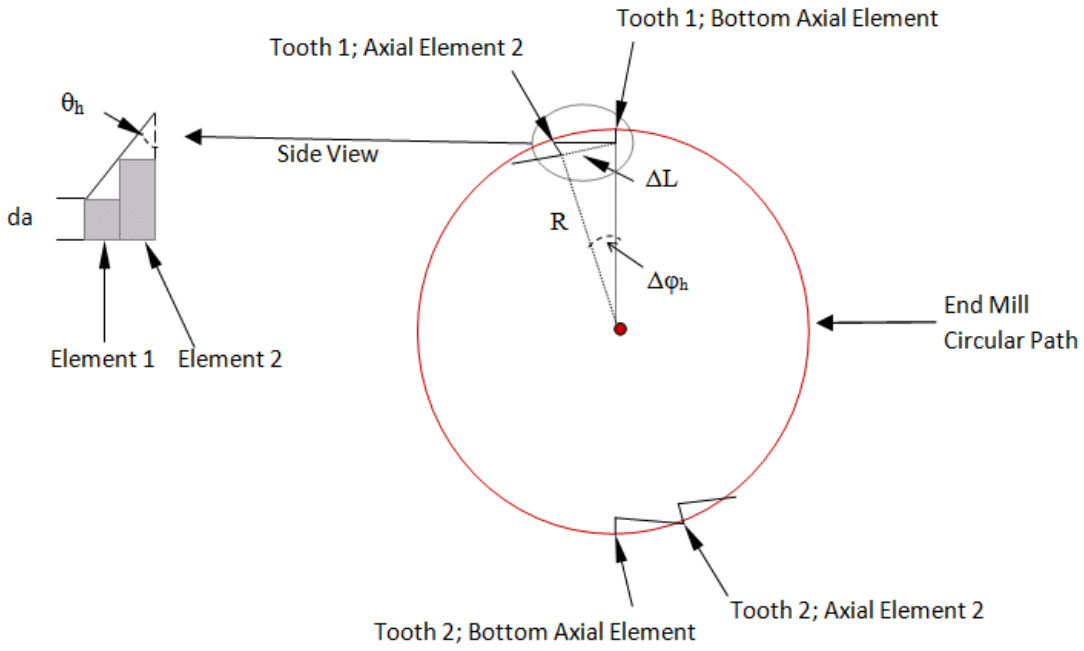

Fig. 6.5 Top view of the tool that shows the two bottom axial elements and the angle between them

To derive the angle of each axial element, Fig. 6.5 is utilized and the derivation is as follows:

$$\tan\theta_h = \Delta L/da \tag{6.27}$$

$$\alpha_k = ((\Delta\varphi_h/2) + k\Delta\varphi_h) \tag{6.28}$$

where ΔL is given in Fig. 6.5, R is the tool radius, and by using small angle assumptions ($\sin(\Delta\varphi_h/2) \approx (\Delta\varphi_h/2) = (\Delta L/2R)$), one has

$$\Delta\varphi_h = da\tan(\theta_h)/R \tag{6.29}$$

The angle φ_{jk} for each tooth (j = 1, 2 for two tooth micro-mill) and axial element (k = 1–n, where n is the number of axial elements) is given in Eq. (6.30), where φ_{ij} is the

initial angular position of tooth, *j*, for the bottom axial element. By setting an initial condition for the bottom axial element, Eq. (6.30) allows for the angular position of each tooth and axial element to be known and thus when it engages in the workpiece.

$$\varphi_{jk} = \left[\varphi_{ij} - (da/2 + kda)\tan\theta_h/R + (2\pi\Omega/60)\,t\right] \tag{6.30}$$

It is assumed that the tool can be modeled as the lumped mass-spring-damper system seen in Fig. 6.4. It is also assumed that because of the very high stiffness in the Z-direction, tool vibrations along the spindle direction can be neglected. This results in two coupled equations of motion for the X and Y displacements of the tool.

$$m\ddot{x} + c_x\dot{x} + k_x x = F_x(t, \Delta x, \Delta y) \tag{6.31}$$

$$m\ddot{y} + c_y\dot{y} + k_y y = F_y(t, \Delta x, \Delta y) \tag{6.32}$$

7. MICRO-MILLING MODEL VALIDATION

7.1 Comparison to Experimental Results in Literature

To investigate the ability of the presented model to simulate the dynamic signature of the micro-milling process, the model is subject to the same conditions used in [60] to compare with the experimental results. The model is run at 75,000 rpm with a feed rate of 2.0μm/tooth and utilizes the pearlite material parameters. The natural frequency of the tool is given as 13,990Hz and the damping ratio of 0.016 from [43] is adopted because a similar micro-milling tool was used and it has been presented in literature that damping values are approximately 1% for micro-mills [63, 64]. The effective mass of the tool is estimated which resulted in a stiffness value similar to that in [43], so this stiffness value of 2.1425MN/m is assumed adequate since a similar 500μm tungsten carbide tool was used for that study. Figures 7.1 and 7.2 are the simulation results, and the FFTs of both the force and vibration signals agree well with the experimental results reported in [60] including the high frequency components. It is observed that the tool vibration waveform and the FFTs (Fig. 7.2) agree better with the experimental force data than the simulated force waveform and FFTs (Fig. 7.1). A force sensor physically measures strain which is proportional to displacement and linearly related to force for linear systems. For a linear system the system will respond at the forcing frequency. However, for a nonlinear system the response may not have the same spectral characteristics as the forcing frequency. Thus, experimental force measurements capture the frequency response of the system vibrations and not

necessarily the spectral characteristics due to the underlying physics governed by the nonlinear force mechanism equations in Eqs. (6.31-6.32). The simulation produces the higher frequency components near the tool natural frequency and clearly shows the tooth passing frequency at 2500Hz. The experimental data also has a lower dominant frequency near the spindle speed (1250Hz) in its FFT which corresponds to tool run-out. Tool run-out is neglected in the presented model and the tool is assumed to be perfectly aligned so this frequency does not have enough energy to keep from being averaged out in the FFT but it is observed in the instantaneous frequency of the Y-direction component of the force. Neglected tool run-out also causes the predicted force magnitude values to not match exactly with the experimental values presented in [60]. With the focus of the research on the dynamics of the system, the presented model is able to adequately simulate the frequency signature including the higher frequencies and nonlinear characteristics.

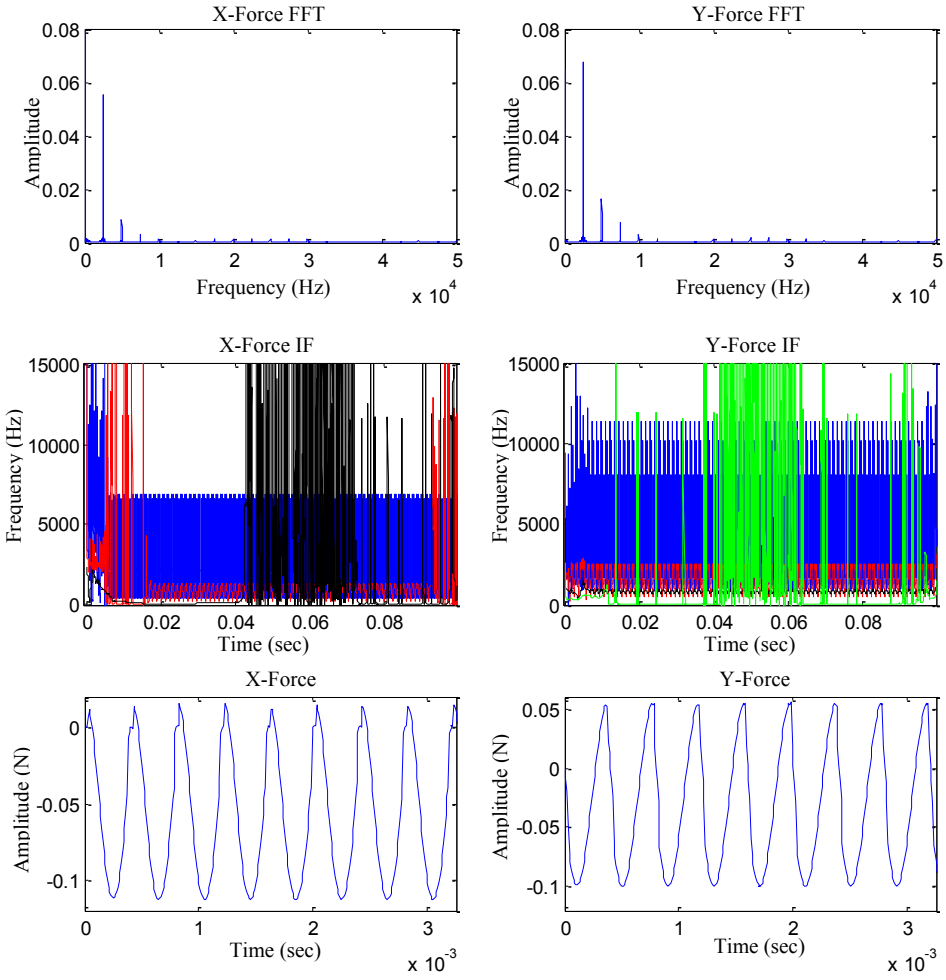

Fig. 7.1 Simulated force signal for pearlite material parameters at 75,000 rpm and 2μm/tooth feedrate

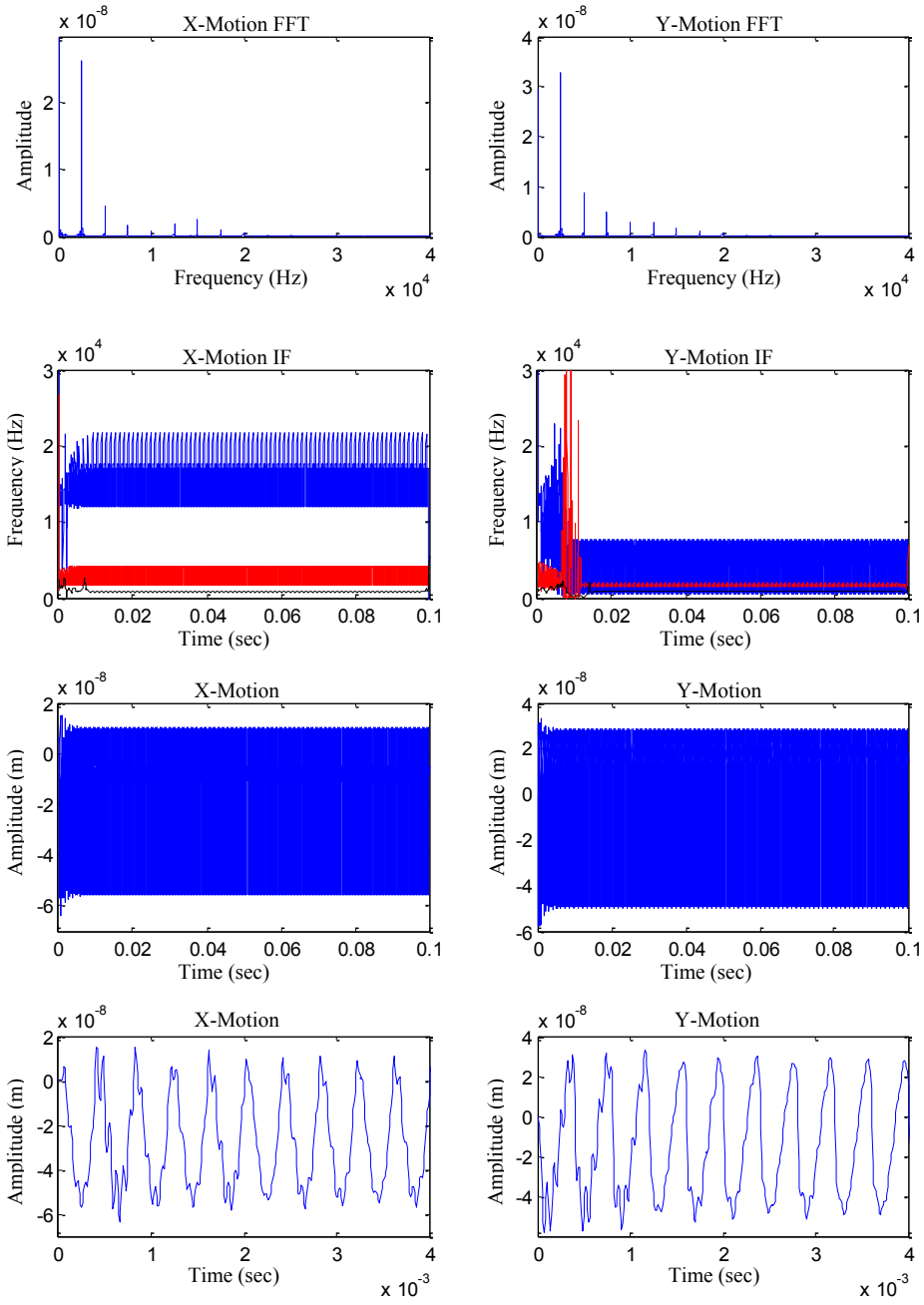

Fig. 7.2 Simulated vibration signal for pearlite material parameters at 75,000 rpm and 2μm/tooth feedrate

7.2 Advantages of Slip-Line Force Model

To study micro-milling dynamics an adequate dynamic model has to be utilized to simulate the process. To demonstrate the advantage of using the presented slip-line method for dynamic analysis over the common empirical cutting force coefficient method, the model is simulated under the conditions presented in [43] because the modal parameters of the tool are known. Aluminum is the material used in this study and the slip-line method requires many material properties. The Oxley method for calculating the effective shear flow stress is used for carbon steels in [61] and requires material properties that are not readily available. Due to the lack of these properties being readily available for aluminum, it is assumed that the ferrite properties from [60] can be used since ferrite is more ductile than pearlite [47]. The lack of accurate material properties can provide an explanation for discrepancies in the amplitude of the forces and slight discrepancies in the frequency values. By looking at the FFTs in Figs. 7.3 and 7.4 of the simulation at 60,000 rpm, 9μm/tooth feedrate, and 100μm DOC, it is seen that the presented model was able to produce the higher frequencies near the tool natural frequency of 4,035 Hz seen in the experimental data in [43] where the constant coefficient model did not always produce these high frequencies. This is because the presented slip-line model is highly dynamic with many changing variables. However, the force coefficient model will more accurately predict the magnitude of the cutting force and the slip-line method requires accurate or calibrated shear flow stress values to precisely predict the magnitude of the cutting force. With the focus of the research on

the dynamics of the system, the presented model is able to adequately simulate the frequency signature including the higher frequencies and nonlinear characteristics.

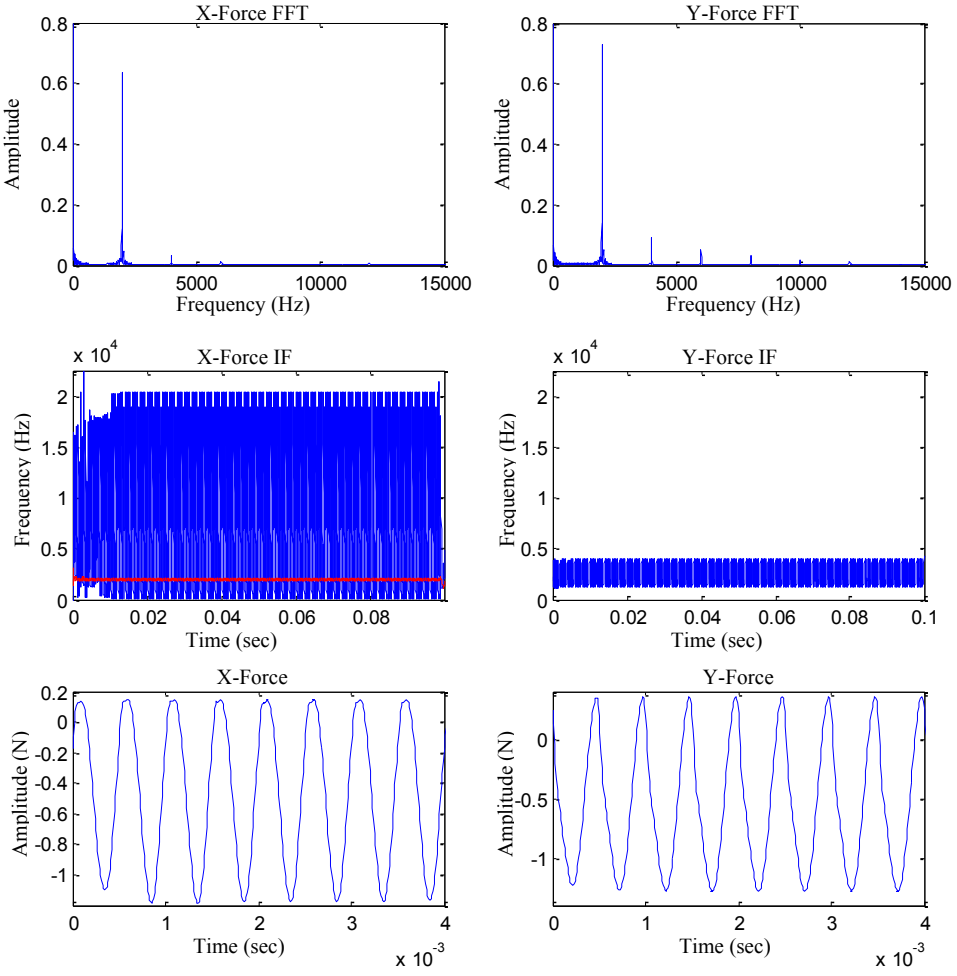

Fig. 7.3 Force simulation results for the conditions in [43] at 60,000 rpm and 9μm/tooth feedrate

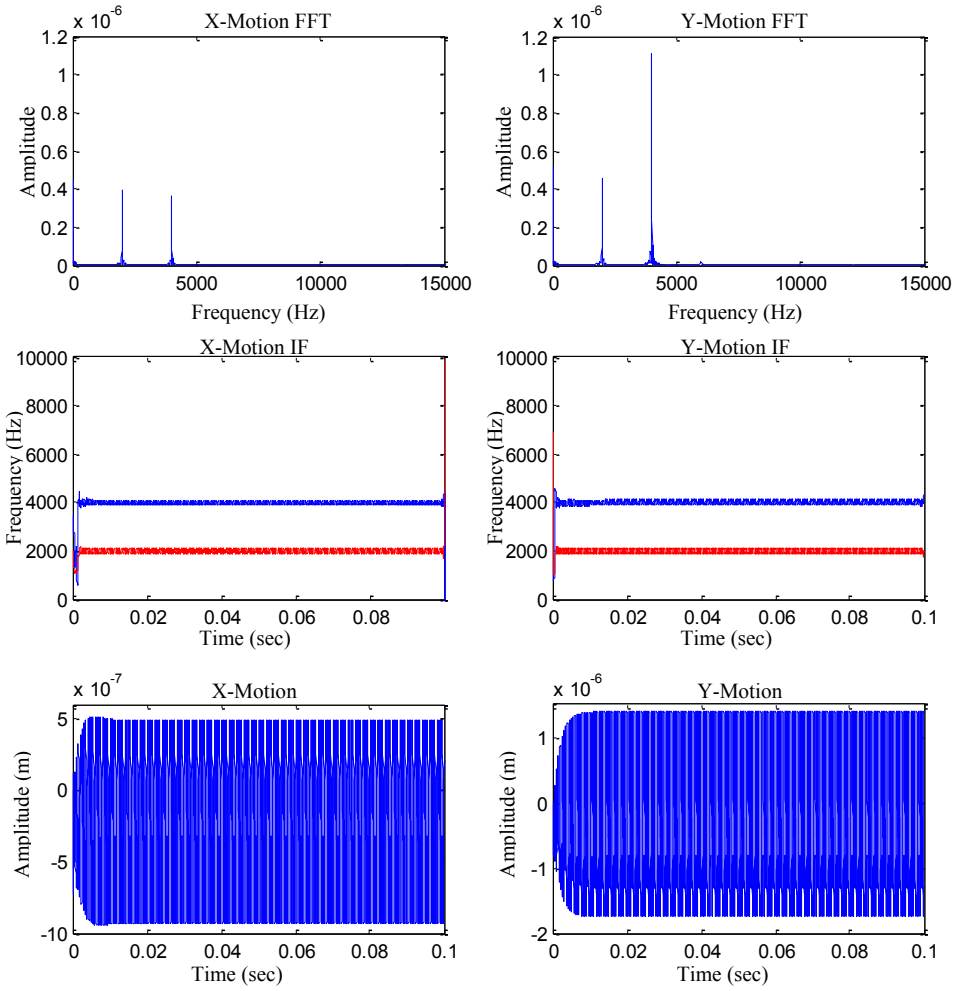

Fig. 7.4 Simulation vibration results for the conditions in [43] at 60,000 rpm and 9μm/tooth feedrate

7.3 Observations

By looking at the IFs (2nd row) and vibration signals (3rd row) for the X- and Y-direction motion of both simulations (Figs. 7.2 and 7.4), it is concluded that these are both stable cutting conditions. This agrees well with the experimental data which was obtained under stable cutting in [43] and [60]. The IF shows that the vibration signals have a stable and bounded spectrum. In Fig. 7.2 the IF shows three frequencies that correspond, respectively, to the natural frequency of the tool, tooth passing frequency, and the spindle frequency in the X-direction. However, for the Y-motion the high frequency is only half of the tool natural frequency which suggests the X and Y vibrations of the tool are quite different. For the conditions in Fig. 7.4, the IF shows two very stable and narrow bounded frequencies which correspond to stable cutting. The FFT shows the Y-motion has much more energy in the tool natural frequency while the X-motion has more energy in the tooth passing frequency which further supports that the tool vibrates differently in the X and Y directions. This suggests that both the X and Y vibrations need to be monitored simultaneously when investigating stability of micro-milling. More insight into the dynamics is gained by comparing the IF of the force signals to the FFT of the force signals. The IF in Figs. 7.1 and 7.3 shows that under stable cutting there are only one to three forcing frequencies present at any moment in time along with a few discontinuities. The FFT of the force signal suggests that there are many more force frequencies acting at any moment in time on the tool. However, the highest force frequency covers a wide range of frequencies which corresponds to the sudden nonlinear changes in the force values and is represented as many high

frequencies in the FFT. The broadband force frequencies and discontinuities are expected due to the sudden and extreme changes in the force values that occur because of the plowing, minimum chip thickness, and tool jumping out of the cut phenomenon. This also tells us that the dynamic signature of the forcing frequency and the cutting tool act very differently suggesting that the workpiece and the tool could have uncoupled vibrations.

8. INVESTIGATION OF CUTTING PARAMETERS ON CUTTING FORCES

Preventing tool failure is a primary goal in micro-milling research as a major issue for micro-mills is unpredictable tool life and premature tool failure [65]. Tool failure is commonly associated with increasing cutting forces exceeding the strength of the tool. Tooling is expensive, and inspection and resetting of the machine is time consuming [66] making improving the life of the tool important. As the spindle speed varies, unless the system is dynamically unstable, theoretically the force magnitude will not vary as long as the chip load (feed rate) and axial DOC are held constant. In micro-milling, efficient cutting requires high spindle speeds so that a low feed can be maintained while achieving reasonable material removal [66]. Higher spindle speeds increase the milling forcing frequency which greatly affects the dynamic response resulting in speeds where sudden tool failure or increased wear rates may be observed. The micro-milling model developed in Section 6 is used to investigate the effect that tool parameters have on the force magnitude, and how the spindle speed affects the response. The helical angle, rake angle, and natural frequency values for the micro-milling system will be varied along with the spindle speed. A constant feed of 5μm/tooth and a constant axial DOC of 50μm are used. The values for the slip-line variables and pearlite material properties as given in [60] are adopted and tool geometry for the two tooth micro-mill with a 500μm diameter and a nose radius of 2μm from [60] are used. For the helical and rake angle studies, the modal parameters from [43] including the natural frequency ω_n = 4035Hz, damping ratio ζ = 0.016, and stiffness k = 2.1425MN/m are utilized.

8.1 Effect of Helical Angle

In this study helical angles of 10°, 20°, 30°, 40°, and 45° are simulated at spindle speeds of 60,000, 75,000, 100,000, and 150,000 rpm along with a constant rake angle of 8°. Figures 8.1 and 8.2 are the force RMS values for the different helical angles and spindle speeds. These figures show that an increase in the helical angle results in a decrease of the cutting forces and that the Y-direction forces are slightly larger than the X-direction forces. As the helical angle is decreased, the mill acts more like a straight tooth tool in which most of the forces are distributed in the X- and Y-direction. The increased helical angle distributes higher forces into the Z-direction decreasing the forces seen in the X- and Y-direction. It also demonstrates that the RMS values for the different spindle speeds are identical except for the 75,000 rpm case.

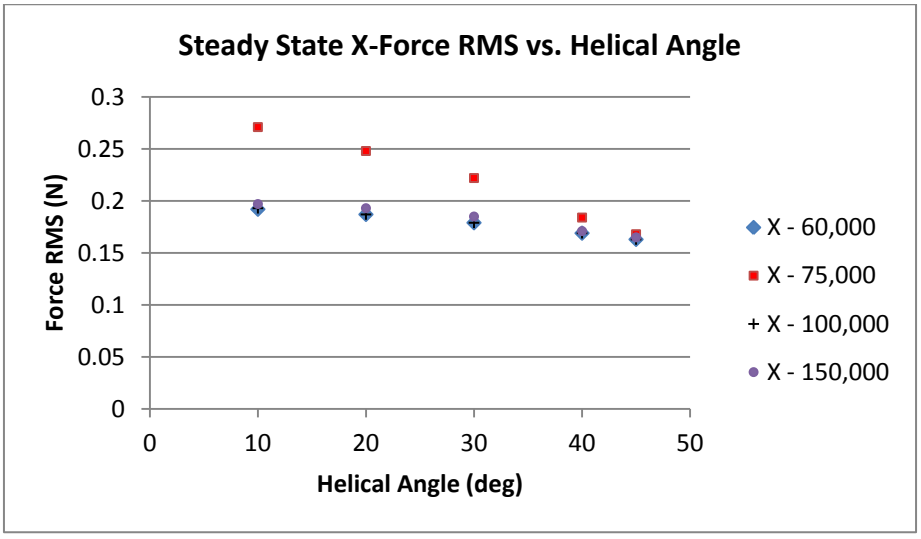

Fig. 8.1 X-direction force RMS values for varying helical angle

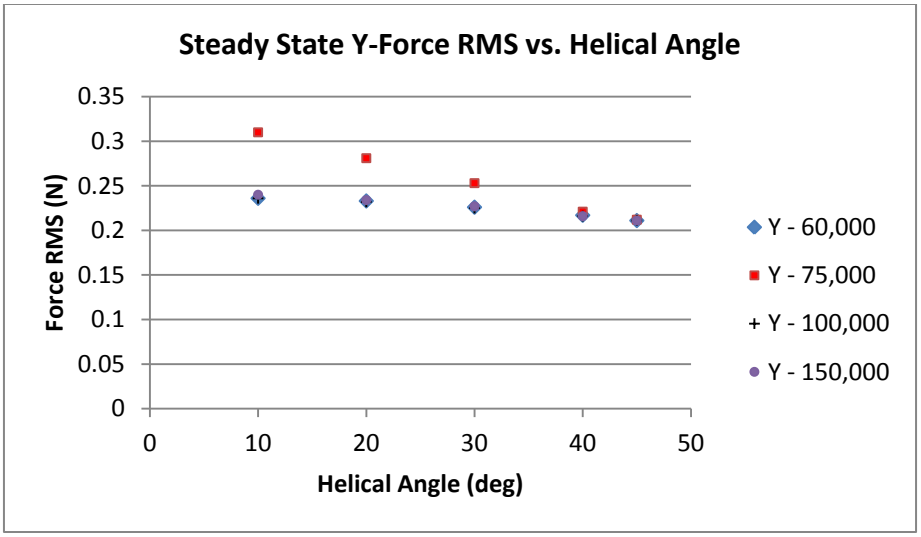

Fig. 8.2 Y-direction force RMS values for varying helical angle

The 75,000 rpm case is a spindle speed in which the forcing frequency of the system results in dynamically unstable cutting causing the force and vibration to oscillate at larger amplitudes. At a helical angle of 45°, the force RMS values for each spindle speed are coincident. However, the 75,000 rpm case still exhibits dynamic instability which results in increased vibrations and multiple frequencies in its dynamic response (Fig. 8.3). In Fig. 8.3, the 60,000 rpm and 75,000 rpm cases with a helical angle of 45° are shown. The 60,000 rpm cutting results in very stable cutting with low vibration magnitudes and a stable IF plot with two frequencies corresponding to the 2,000 Hz tooth passing frequency and 4,035 Hz tool natural frequency. It is observed that the Y-direction motion exceeds the X-direction motion for the 60,000 rpm case. As

the spindle speed is increased to 75,000 rpm, the X-direction vibrations increase but the steady state Y-direction vibration magnitude is similar to the 60,000 rpm case. The IF plots for the 75,000 rpm case show a highly bifurcated system with the tool responding at the 4,035 Hz tool natural frequency and a ~2,500 Hz tooth passing frequency which has multiple bifurcations. In Fig. 8.4 the corresponding X and Y force components and force IF plots are shown. The force plots for the two spindle speeds demonstrate similar magnitudes which correspond to the coincident RMS values for these spindle speeds. However, the force IF plot for the 75,000 rpm case demonstrates a forcing mechanism which has multiple frequencies acting on the system and these frequencies cover a broad range of values where the 60,000 rpm case only has one forcing frequency acting on the system at any moment in time. These two cases demonstrate cutting in which the force magnitudes are similar (Fig. 8.4) but the resulting dynamic response (Fig. 8.3) is much different with increased vibrations and frequencies in the 75,000 rpm case which would result in an increased rate of tool wear and decreased product quality.

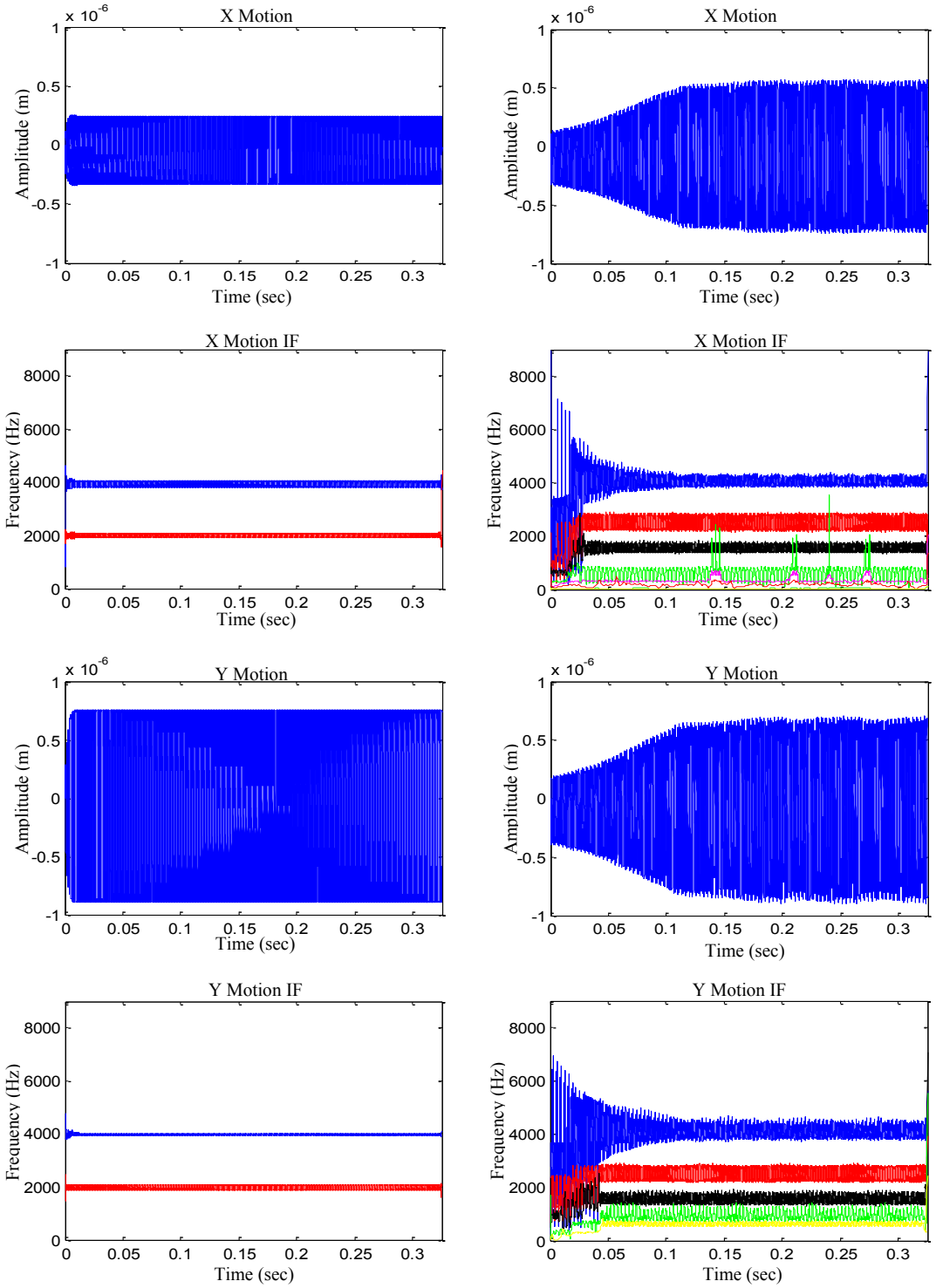

Fig. 8.3 X- and Y-direction motion and motion IF plots for 60,000 rpm (left) and 75,000 rpm (right) spindle speed for a 45° helical angle

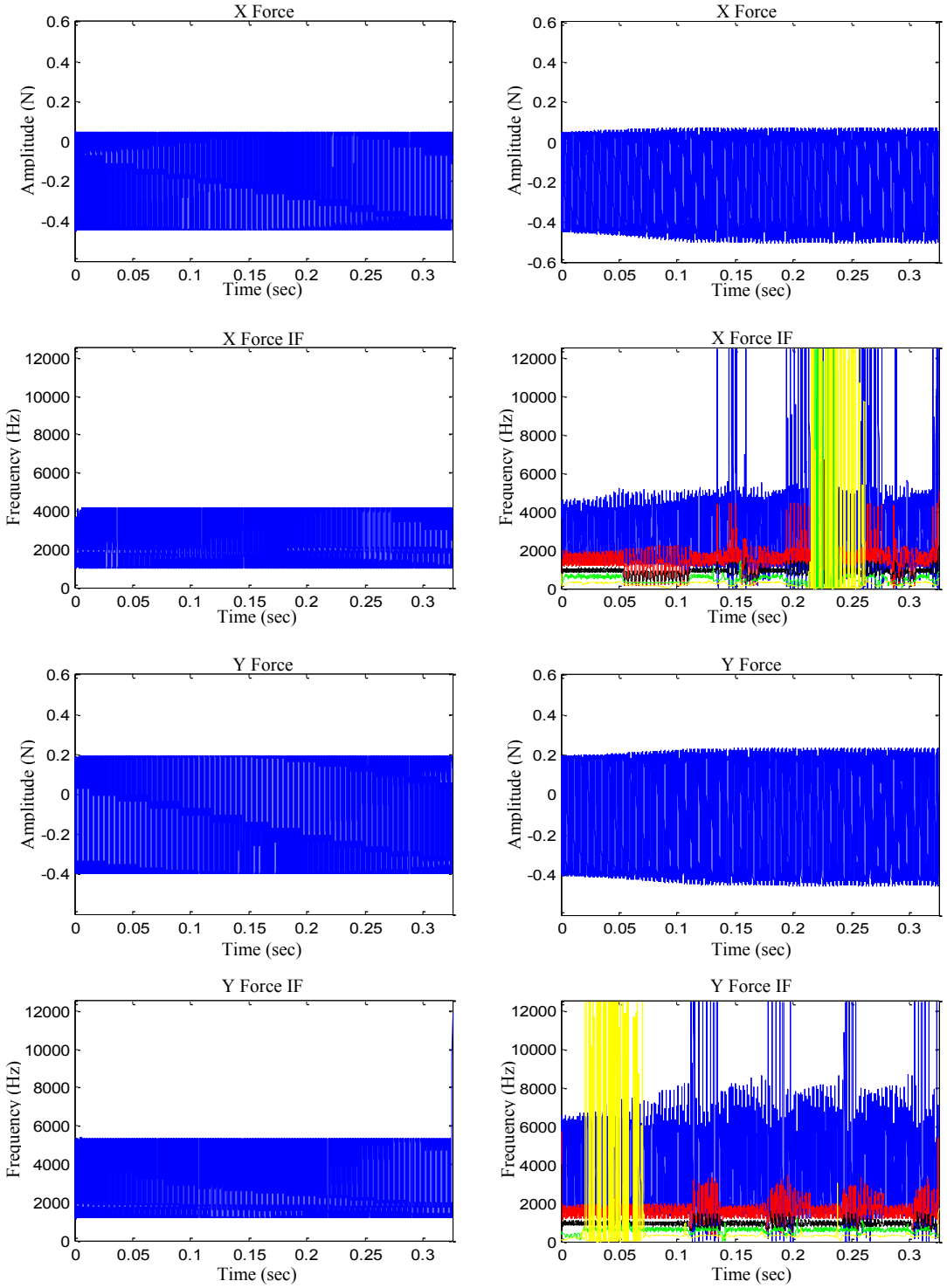

Fig. 8.4 X- and Y-direction forces and force IF plots for 60,000 rpm (left) and 75,000 rpm (right) spindle speed for a 45° helical angle

It is also observed that the 10°, 20°, 30°, and 45° helical angles result in similar frequency responses while the 40° helical angle excites additional frequencies in the response for each spindle speed. This is shown for the 100,000 rpm spindle speed in Figs. 8.5 and 8.6 where the motion and force plots for helical angles of 45° and 40° are shown. In Fig. 8.5 the X and Y motions for the 45^0 and 40^0 helical angles are similar in vibration amplitudes. The IF plots for each case show two different dynamic states of motion. The 45° case has one frequency at the tooth passing frequency of ~3,333Hz while the 40° case has a bifurcated tooth passing frequency with three additional lower frequency modes. Similar observations are made by analyzing the resulting forces in Fig. 8.6. The two helical angles result in similar force magnitudes. However, the frequency response of the forcing mechanism is quite different. The 45° case has one forcing frequency acting on the system at all time, but the 40° case has additional lower forcing frequencies acting on the system.

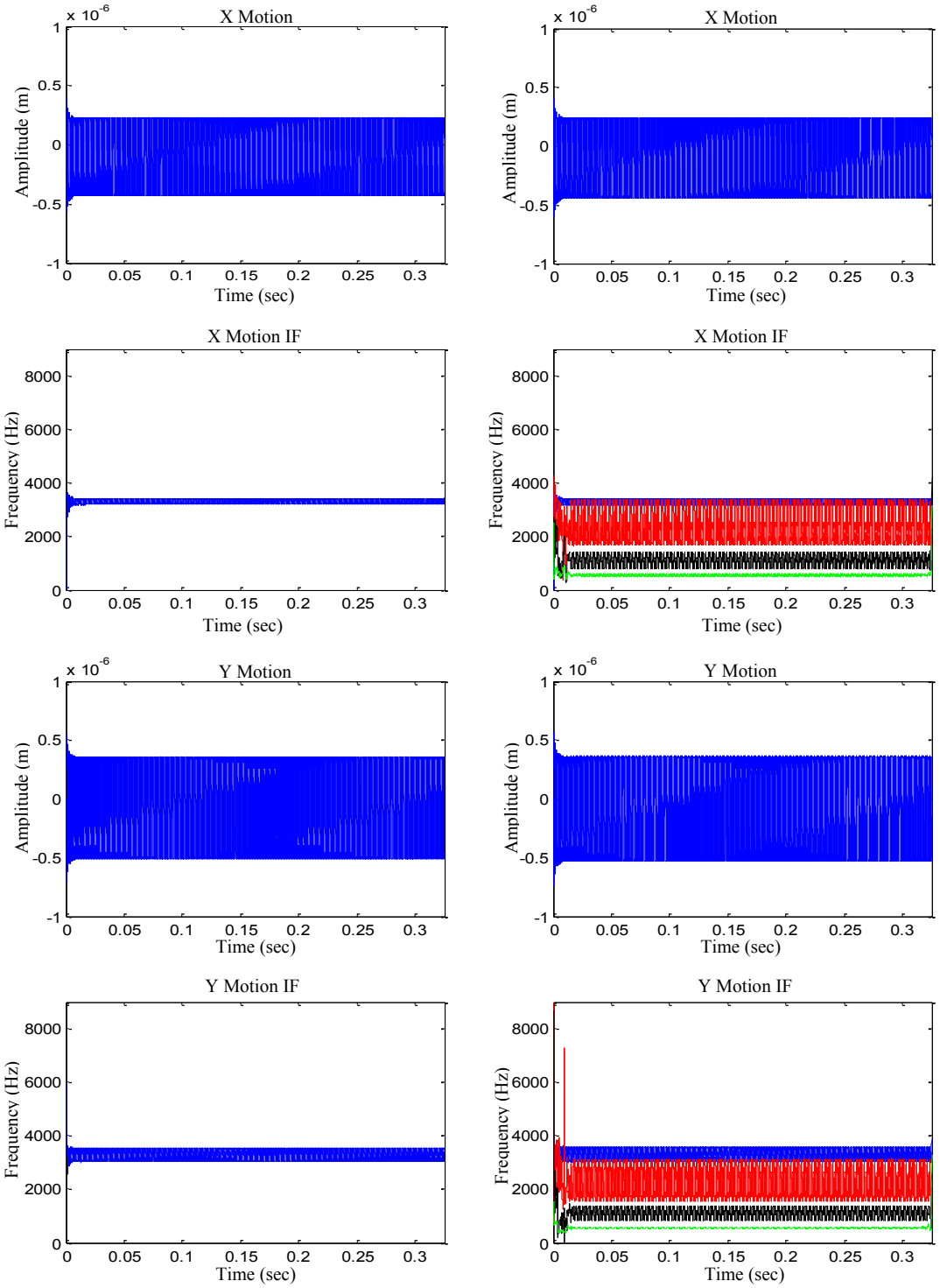

Fig. 8.5 X- and Y-direction motion and motion IF plots for 100,000 rpm spindle speed and 45° (left) and 40° (right) helical angles

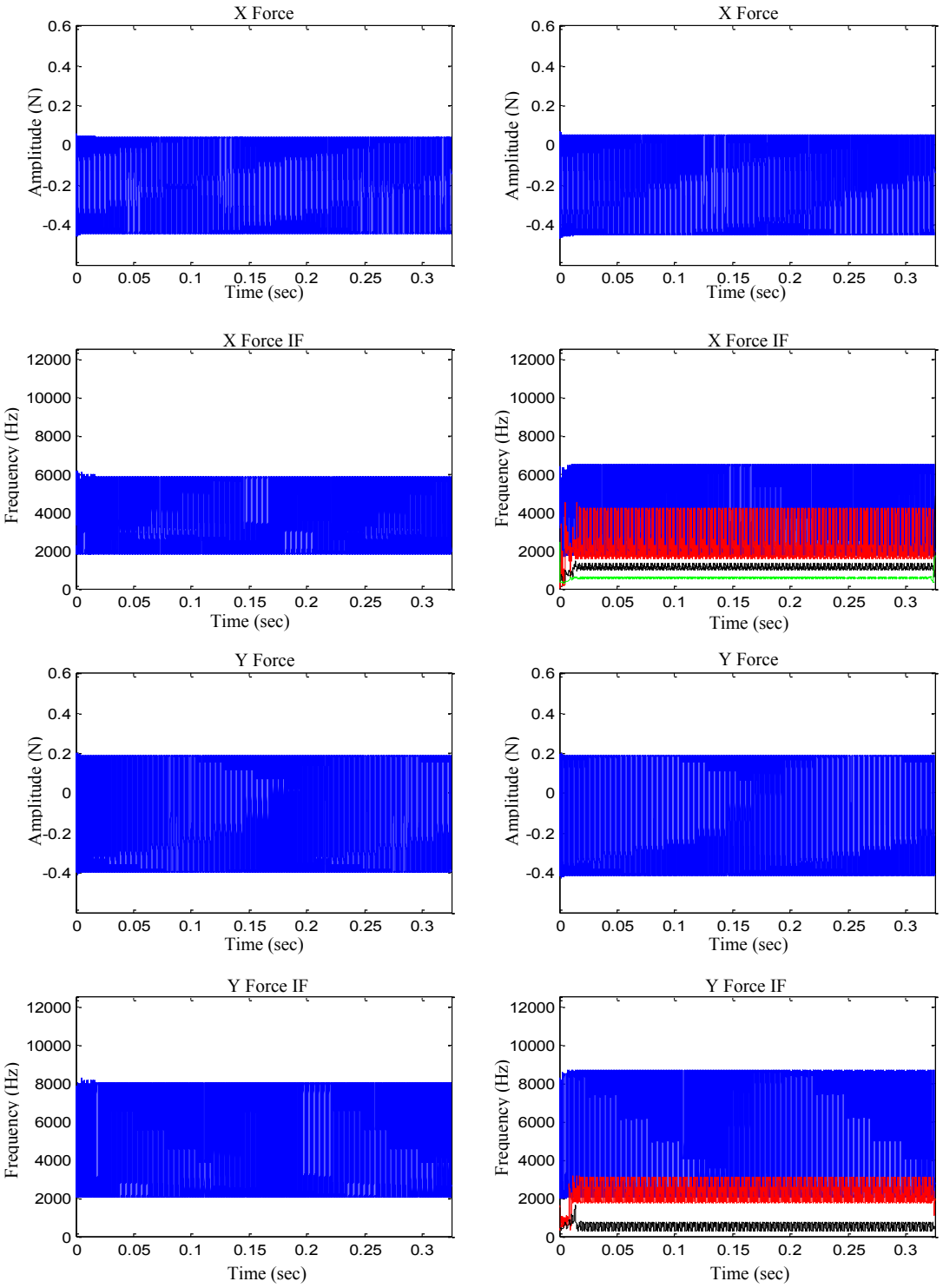

Fig. 8.6 X- and Y-direction forces and force IF plots for 100,000 rpm spindle speed and 45° (left) and 40° (right) helical angles

The effect that the 40° helical angle has on the resulting dynamics of the system is further shown in Figs. 8.7 and 8.8 where the X and Y motion and force responses are plotted for a spindle speed of 150,000 rpm. At the 0.17 second mark in Fig. 8.7 there is a sharp increase in the vibration amplitude, but the steady state vibration amplitude for both helical angles is similar. The IF plots for the two cases shown have similar features with frequency modes at the 4,035 Hz tool natural frequency, a mode oscillating around 3,000 Hz, and two lower frequency modes around 2,000 and 1,000 Hz. The force plots in Fig. 8.8 show that the force magnitudes and force IF plots for the two cases are very similar except for the sudden increase in the force value around the 0.17 second mark. This is due to a sudden discontinuity which occurs in the system and physically could result in a damaged tool. Overall an increase in the helical angle results in a decrease in the X- and Y-direction cutting forces, thus improving the vibration response and also the accuracy of the milling process. However, the dynamic instability of certain spindle speeds results in undesirable cutting parameters, and the 40^0 helical angle results in a poor dynamic response.

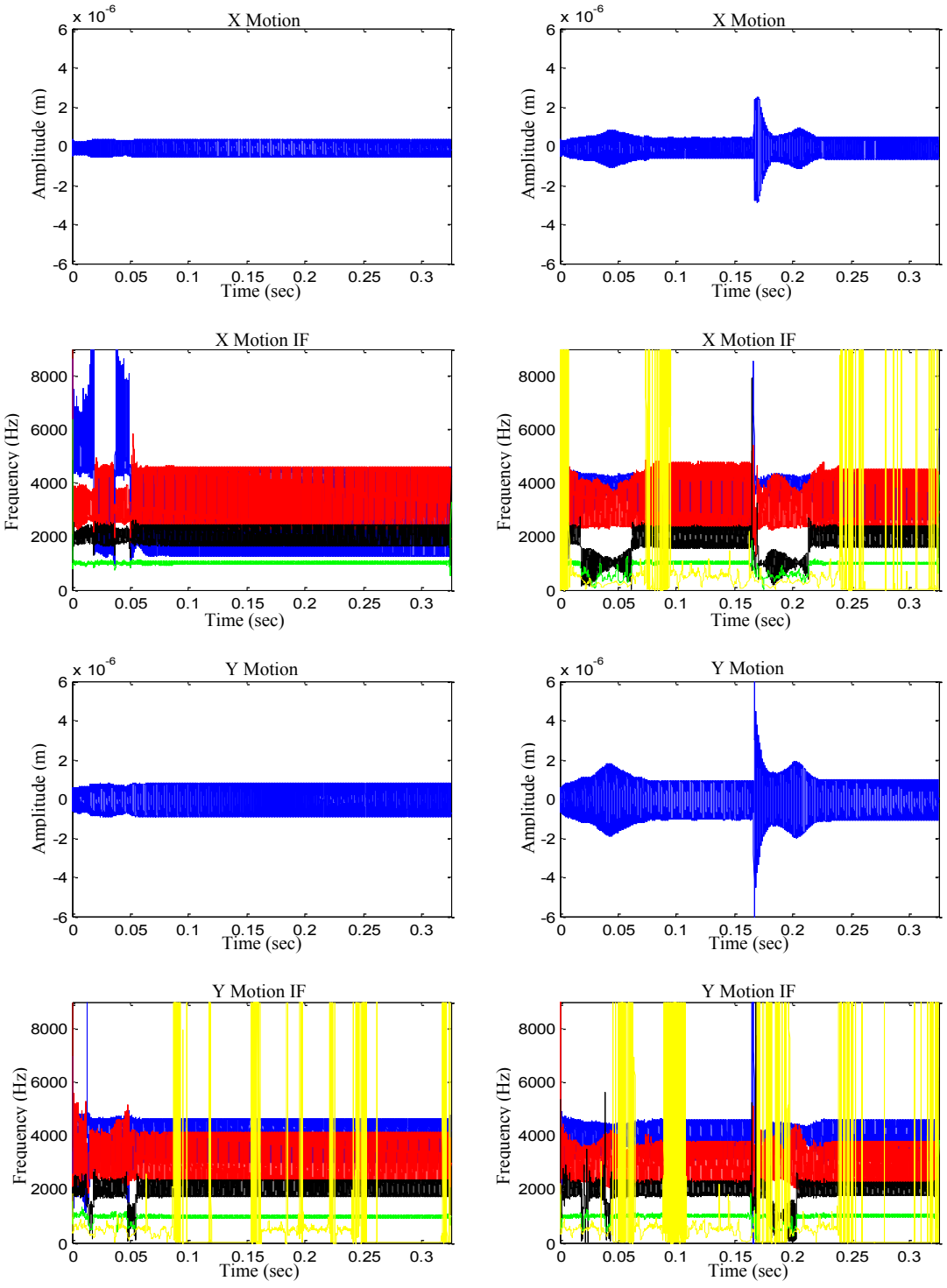

Fig. 8.7 X- and Y-direction motion and motion IF plots for 150,000 rpm spindle speed and 45° (left) and 40° (right) helical angles

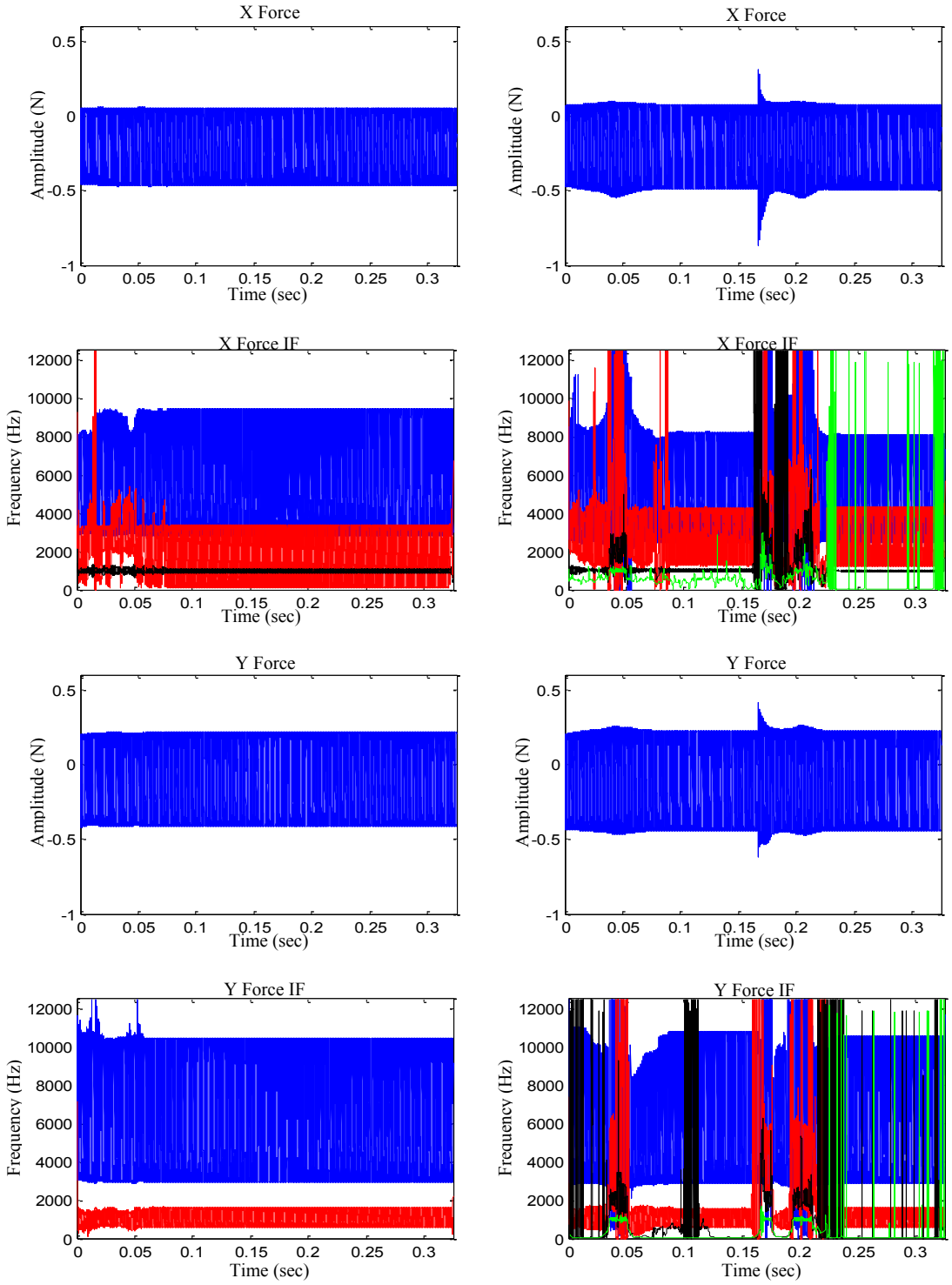

Fig. 8.8 X- and Y-direction forces and force IF plots for 150,000 rpm spindle speed and 45° (left) and 40° (right) helical angles

8.2 Effect of Rake Angle

The rake angles used for this study are 6°, 8°, 10°, and 12°, and a constant helical angle of 30° is used. The X- and Y-direction force RMS values are plotted for each rake angle and spindle speed in Figs. 8.9 and 8.10. From these figures it is apparent that for the range of rake angles considered there is a minimal effect on the resulting force RMS values. The 75,000 rpm case has force RMS values which are distinctively larger than the force RMS values for the other spindle speeds. This is again due to the dynamic instability of the system when excited at a spindle speed of 75,000 rpm. A rake angle of 12° results in similar force RMS values for each spindle speed suggesting that the force magnitude for dynamically unstable spindle speeds can be reduced by increasing the rake angle.

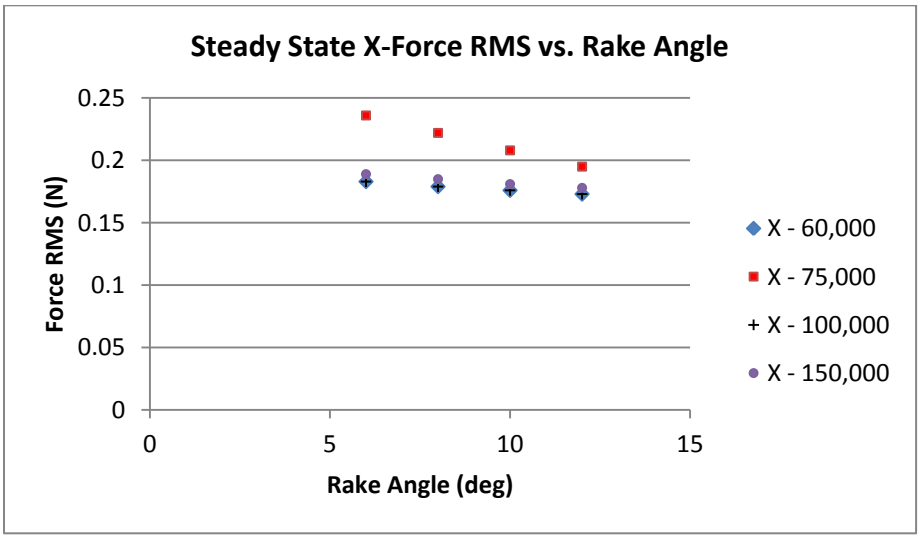

Fig. 8.9 X-direction force RMS values for varying rake angle

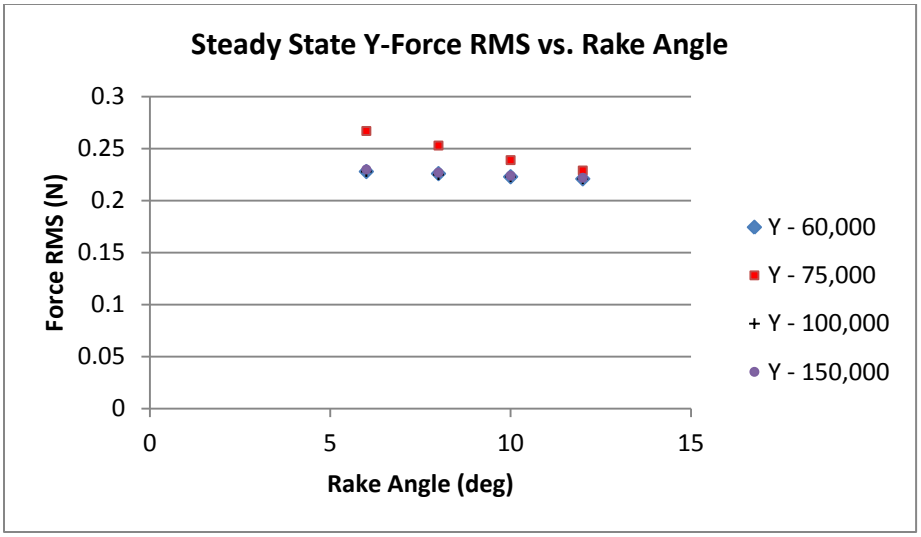

Fig. 8.10 Y-direction force RMS values for varying rake angle

The dynamic instability at 75,000 rpm and a rake angle of 10° is shown in Figs. 8.11 and 8.12. Here the 75,000 rpm case is plotted alongside the 100,000 rpm case which has a stable dynamic response. The 100,000 rpm case in Fig. 8.11 has stable motions and a stable IF plot in which the tool responds at the ~3,333 Hz tooth passing frequency. The increased force RMS values at the 75,000 rpm case results in increased unstable tool motions as presented in Fig. 8.11. Here the X- and Y-direction motions for the tool are much larger at 75,000 rpm than at 100,000 rpm, and the IF plots show a dynamic response in which there is a 4,035 Hz tool natural frequency mode and a 2,500 Hz highly bifurcated tooth passing frequency. The force response for the two cases in Fig. 8.12 shows that the forces for the 75,000 rpm case are much larger than the 100,000 rpm case. At 100,000 rpm the system is excited by one forcing frequency at any

moment in time as shown in the IF plots. For the 75,000 rpm case, the system is excited by multiple broadband forcing frequencies at all time.

The 150,000 rpm case in Fig. 8.13 has vibration amplitudes much larger than the vibration amplitudes for the 100,000 rpm case in Fig. 8.11. However, the force amplitudes remain the same suggesting that the increased spindle speed results in deteriorated dynamic stability producing increased vibrations. This is supported by the IF plots for both the motion and the force response in Fig. 8.13. The IF for both the X- and Y-direction motions consists of three frequencies at the 4,035 Hz tool natural frequency, a bounded mode oscillating around a 3,000 Hz frequency, and a low frequency mode oscillating around 1,000 Hz. When comparing the force IF plots in Figs. 8.11 and 8.13, it is observed that the 150,000 rpm case in Fig. 8.13 has an additional lower forcing frequency acting on the system and a wider range of forcing frequencies. At 150,000 rpm there is not increased force but there are increased vibrations and a bifurcated frequency spectrum which reduces product tolerances and increases the probability of tool damage.

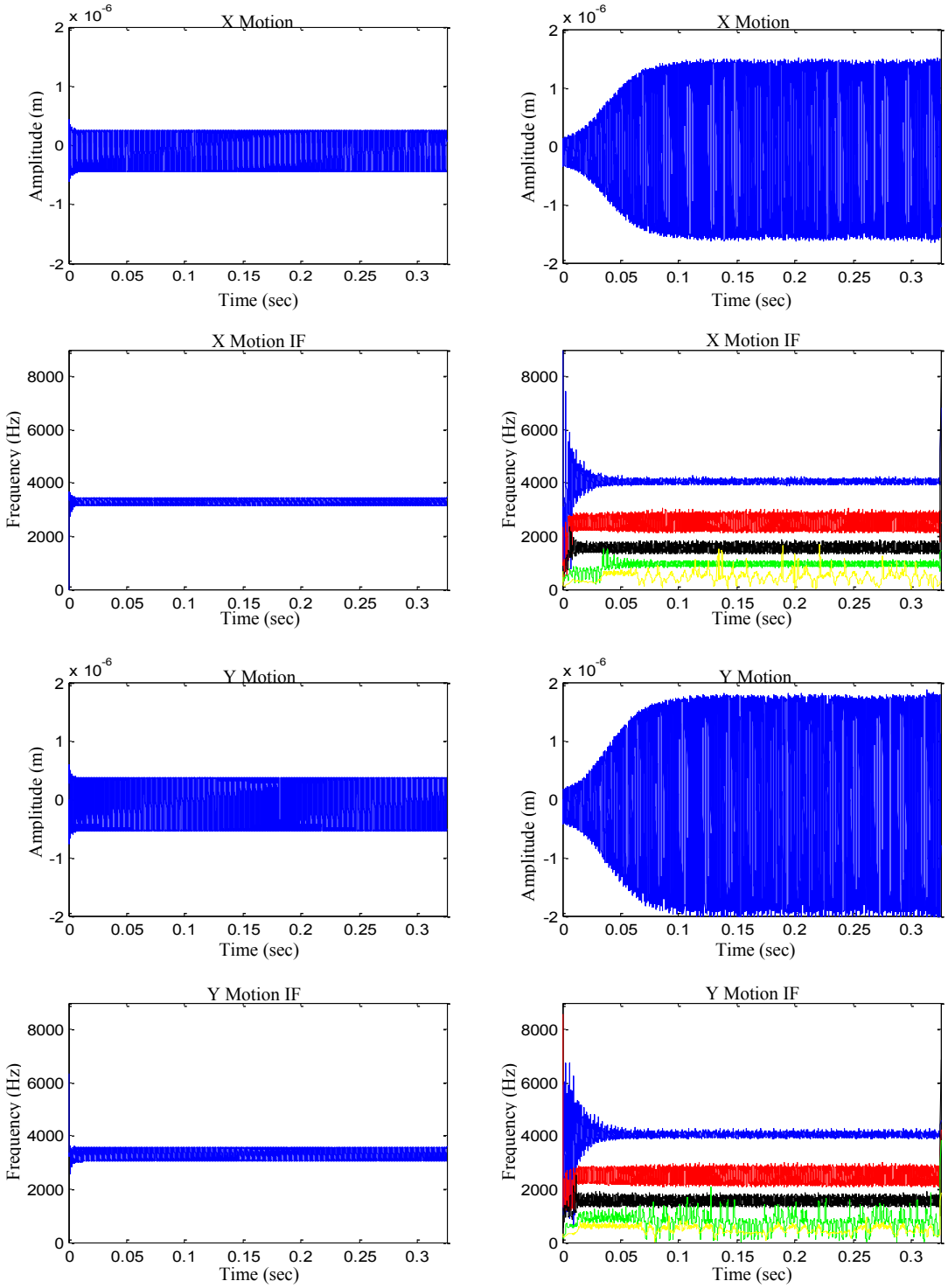

Fig. 8.11 X- and Y-direction motion and motion IF plots for 100,000 rpm (left) and 75,000 rpm (right) spindle speeds for a 10° rake angle

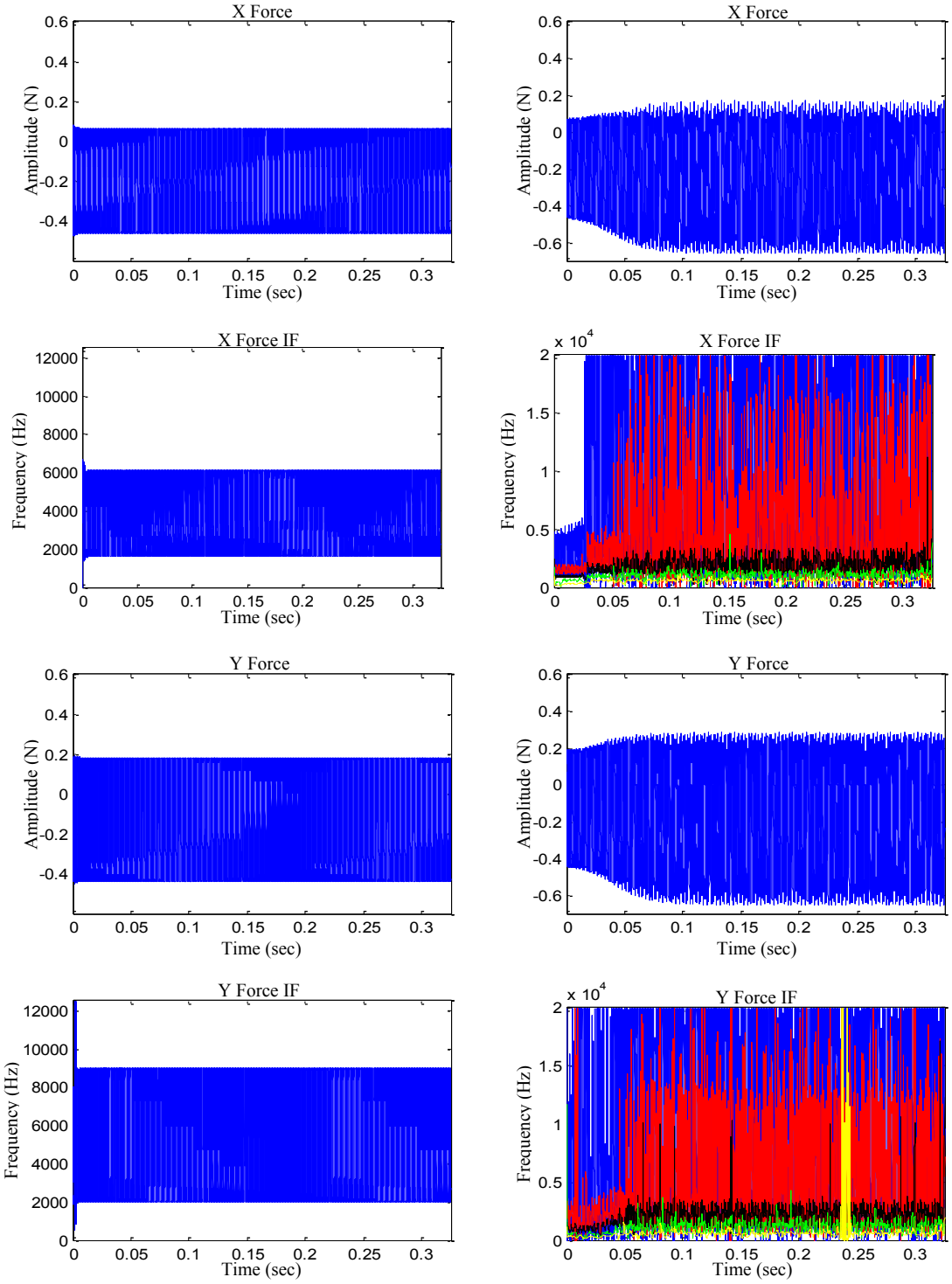

Fig. 8.12 X- and Y-direction forces and force IF plots for 100,000 rpm (left) and 75,000 rpm (right) spindle speeds for a 10° rake angle

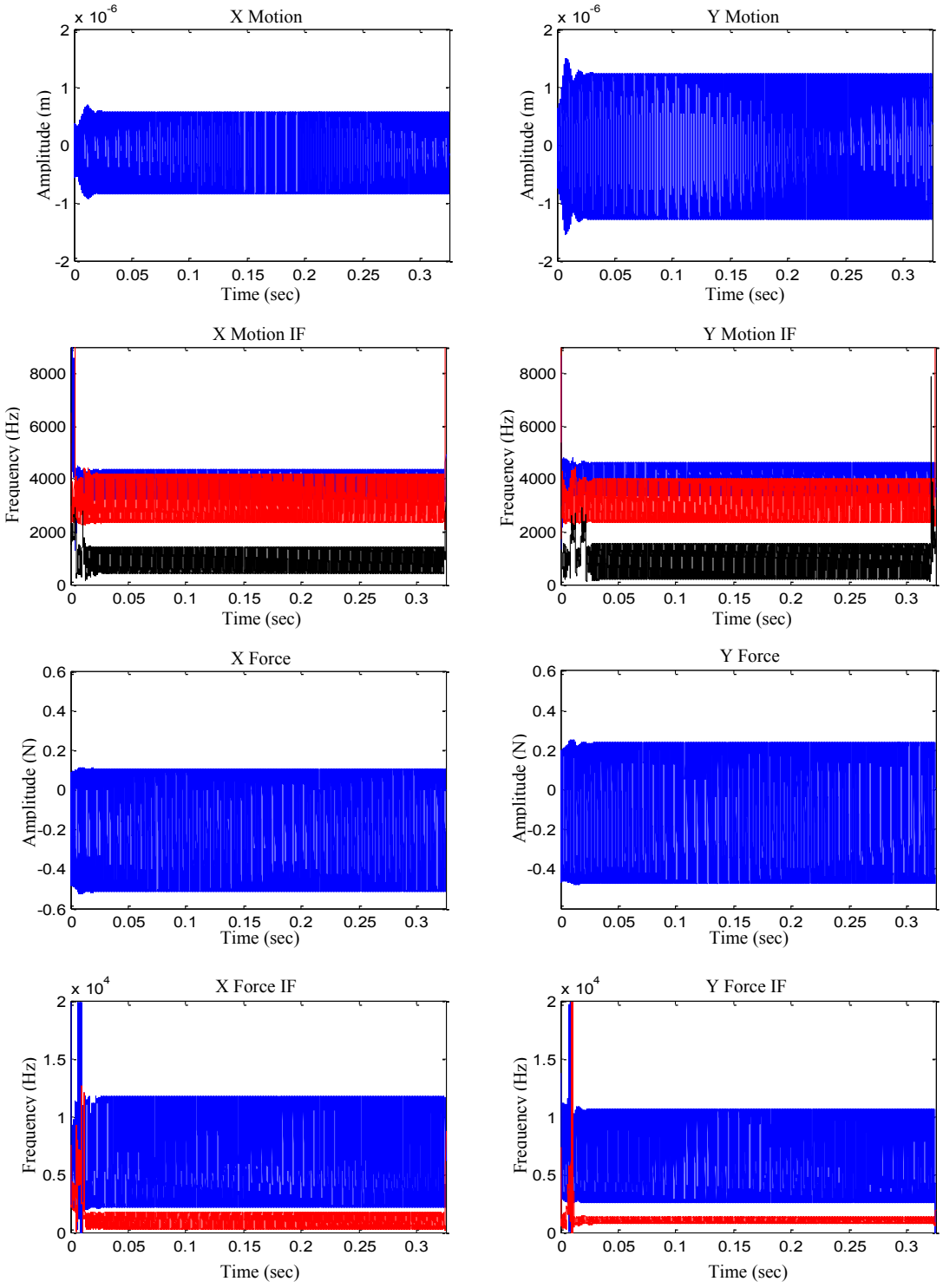

Fig. 8.13 X (left) and Y (right) direction motion (top) and force (bottom) plots for 150,000 rpm spindle speed and a 10° rake angle

8.3 Effect of System Stiffness

In this section the stiffness of the micro-milling system is varied to investigate how this affects the resulting forces and the dynamic response. An increase in tool stiffness represents varying the shank length or material properties of the tool. The modal parameters followed from [43] including the natural frequency ω_n = 4035Hz, damping ratio ζ = 0.016, and stiffness k = 2.1425MN/m result in a modal mass, $m = k/\omega_n^2 = 0.00333$ kg. This modal mass and damping ratio is held constant while the natural frequency is varied from 2,000, 4,035, and 6,000 Hz, and constant helical and rake angles of 30° and 8°, respectively, is used. This study shows that changing the system stiffness does not directly affect the resultant force but does affect the dynamic stability.

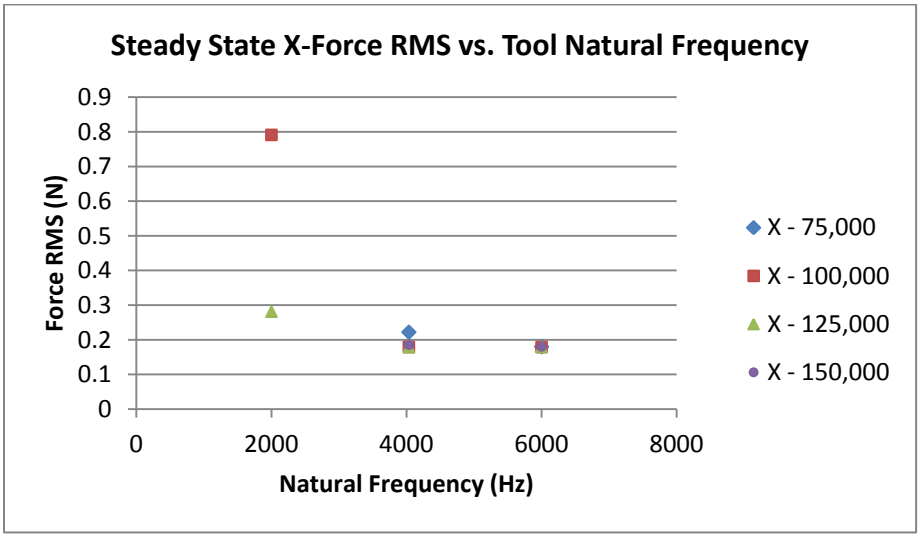

Fig. 8.14 X-direction force RMS values for varying system stiffness

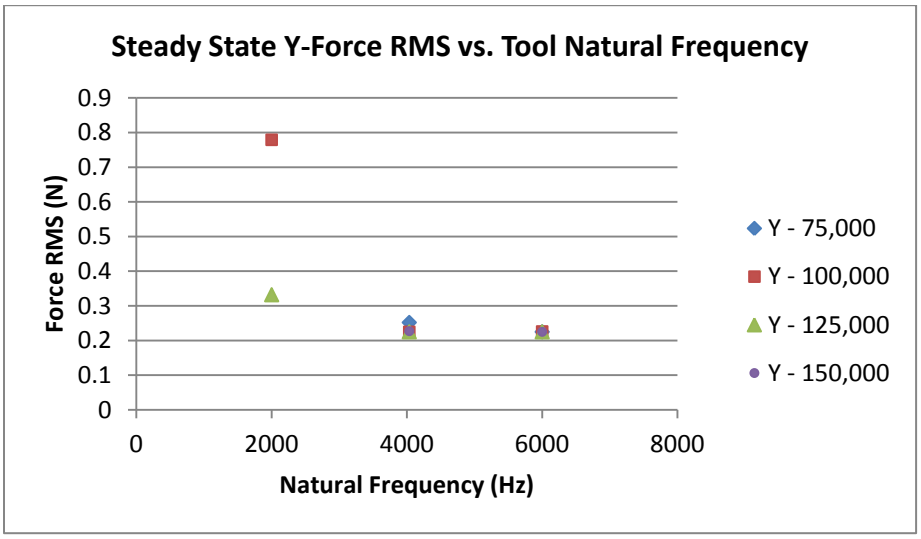

Fig. 8.15 Y-direction force RMS values for varying system stiffness

The 2,000 Hz natural frequency case results in large force vibrations for all spindle speeds as seen in Figs. 8.14 and 8.15. The 75,000 and 150,000 rpm spindle speeds at 2,000 Hz natural frequency results in very large forces (not shown). It is found that as the system stiffness is increased, the dynamic stability of the system improves and higher cutting speeds can be realized. In Sections 8.1 and 8.2 it was found that the 75,000 rpm case was dynamically unstable. This is observed in Figs. 8.14 and 8.15 where the force RMS at 75,000 rpm is larger than the other spindle speeds. When the stiffness is increased to 6,000 Hz, the force RMS value is coincident with the other speeds considered suggesting that the dynamic stability of the system has improved.

The motion and force response for the 75,000 rpm case with natural frequencies of 4,035 and 6,000 Hz are shown in Figs. 8.16 and 8.17. The vibration and IF plots for the 4,035 Hz case in Fig. 8.16 show a dynamic response with excessive vibrations and a highly bifurcated frequency spectrum. The 6,000 Hz case in Fig. 8.16 shows that when the system stiffness is increased the vibration magnitude decreases and the frequency domain is improved with only one frequency oscillating around the 2,500 Hz tooth passing frequency in the X-direction and two frequencies in the Y-direction. In the Y-direction, the IF plot has a very broad higher frequency mode closer to the tool natural frequency oscillating around 4,000 Hz and a narrow bounded 2,500 Hz tooth passing frequency. Interestingly, the increased stiffness reduced the number of frequencies in the IF plot, but the reduced number of modes in the IF plot cover a broader range of frequency values. The force and force IF plots for the 6,000 Hz case in Fig. 8.17 show that the frequency spectrum is of narrow bandwidth. Conversely, there are multiple broadband frequencies in the force IF plot for the 4,035 Hz case in Fig. 8.17. The reduced vibration magnitude observed as a result of increased system stiffness (Fig. 8.16) would improve the tolerances which are physically achievable.

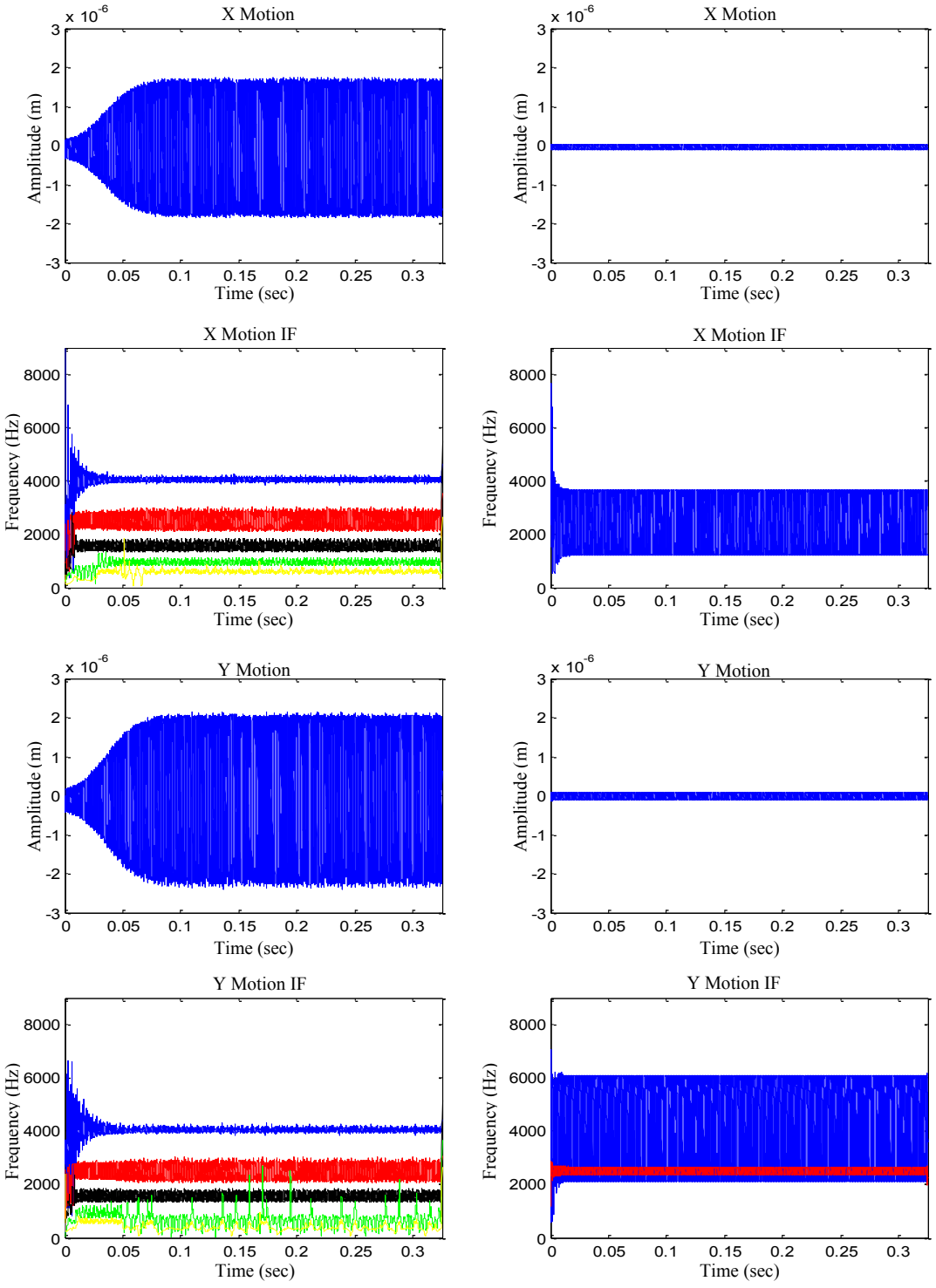

Fig. 8.16 X- and Y-direction motion and motion IF plots for 75,000 rpm spindle speed and natural frequencies of 4,035 Hz (left) and 6,000 Hz (right)

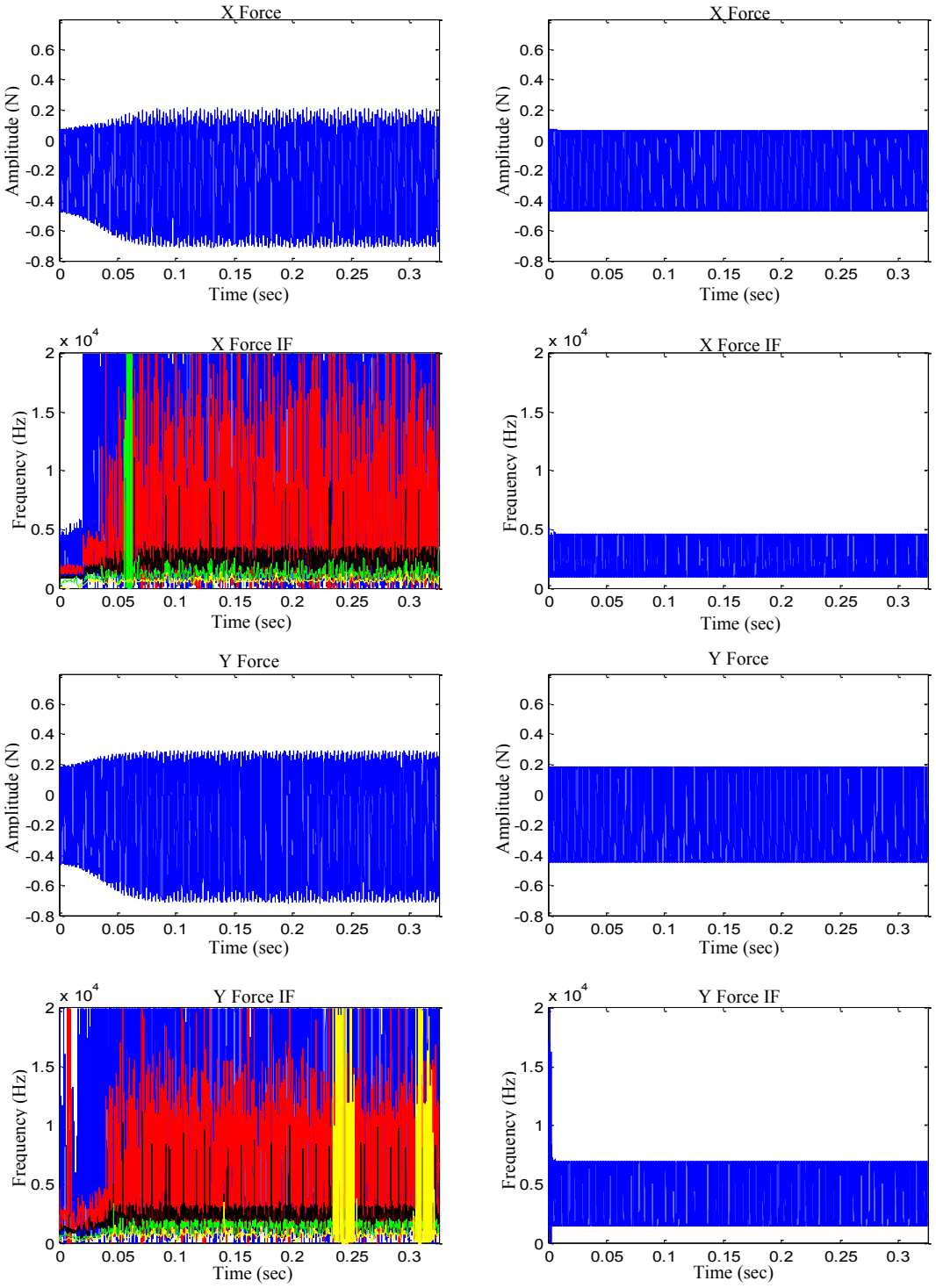

Fig. 8.17 X- and Y-direction forces and force IF plots for 75,000 rpm spindle speed and natural frequencies of 4,035 Hz (left) and 6,000 Hz (right)

It is observed that as the system stiffness increases there are decreased vibration magnitudes, but the frequency response does not always improve. The 100,000 rpm motion and force plots at 4,035 and 6,000 Hz are presented in Figs. 8.18 and 8.19. In this case, the increased stiffness does not affect the force magnitude as shown in Fig. 8.19 but it does reduce the vibration magnitude as seen in Fig. 8.18. The decreased vibrations due to a natural frequency of 6,000 Hz are also accompanied by additional lower frequencies as seen in the IF plot. These additional frequencies are not seen in the 4,035 Hz case in Fig. 8.18. The X and Y direction motions in Fig. 8.18 have similar magnitudes but the frequency response shows different states of motion. The Y direction motion has the higher tool natural frequency mode which oscillates between 6,000-8,000Hz as well as additional lower frequencies which cover a broad range of values. The X direction motion does not have a mode related to the tool natural frequency but rather has a broader 2,000-4,000 Hz tooth passing frequency and additional lower frequencies. The force IF plots in Fig. 8.19 show that there are additional forcing frequencies acting on the system for the 6,000 Hz case. The increased system stiffness decreases vibration magnitudes but results in additionally excited frequencies that could have a negative impact on the life of the tool.

The higher spindle speed of 150,000 rpm has an improved dynamic response when the system stiffness is increased to 6,000 Hz. The motion and force plots for the 4,035 and 6,000 Hz natural frequency cases at a spindle speed of 150,000 rpm are provided in Figs. 8.20 and 8.21. Figure 8.20 shows that when the natural frequency of the system is 4,035 Hz the vibration response is not excessive but the IF plots have four

frequency modes in the response which cover a wide range of values and consists of the 4,035 Hz tool natural frequency, a frequency oscillating about 3,000 Hz, and two lower modes oscillating at 500-1,000 Hz. When the natural frequency is increased to 6,000 Hz, it results in a reduced number of frequencies in the response to three modes of narrow bandwidth. These modes are a 5,000 Hz tooth passing frequency, a mode oscillating around 3,000 Hz, and a lower 1,500 Hz frequency. The force plots in Fig. 8.21 similarly demonstrate a system with improved dynamics when the natural frequency of the system is increased to 6,000Hz. The force magnitudes are slightly improved when compared to the 4,035 Hz case and the force IF plot for 6,000 Hz has more frequencies of narrow bandwidth. Thus, increasing system stiffness generally improves the dynamic response of the system, thus improving tool performance which agrees with the study in [67] where the tools with the highest rigidity provided the best experimental cutting tool life and performance.

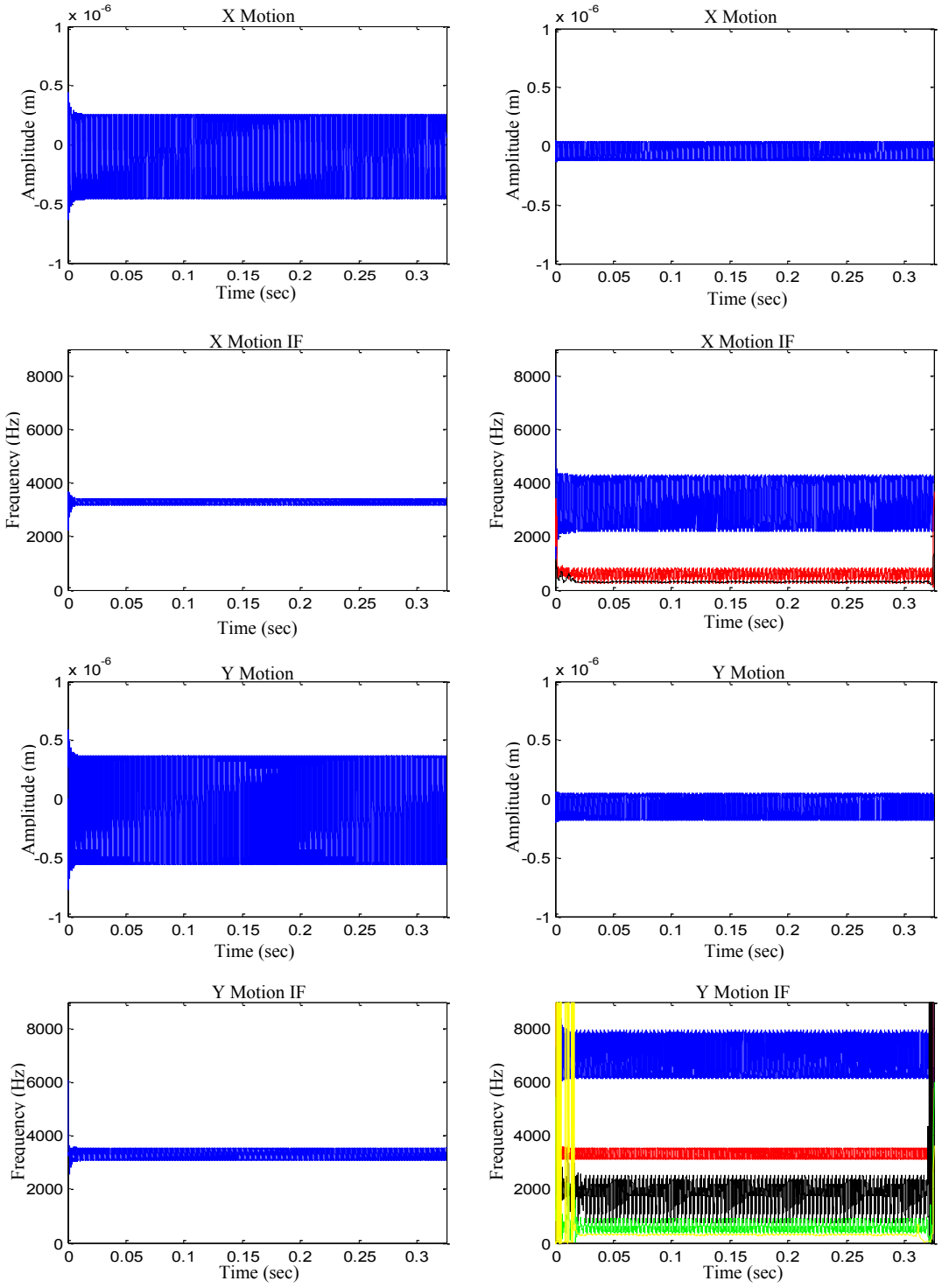

Fig. 8.18 X- and Y-direction motion and motion IF plots for 100,000 rpm spindle speed and natural frequencies of 4,035 Hz (left) and 6,000 Hz (right)

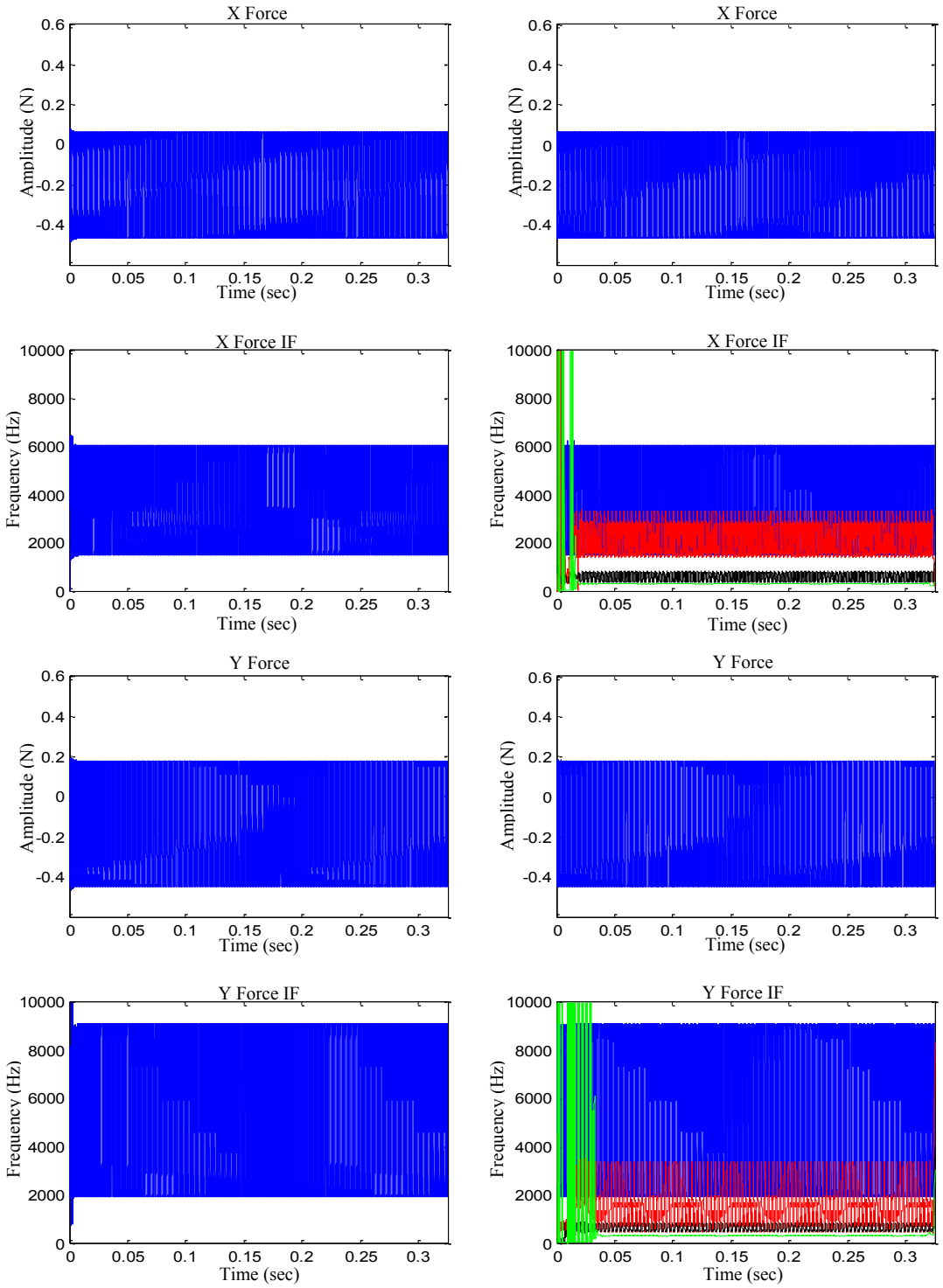

Fig. 8.19 X- and Y-direction forces and force IF plots for 100,000 rpm spindle speed and natural frequencies of 4,035 Hz (left) and 6,000 Hz (right)

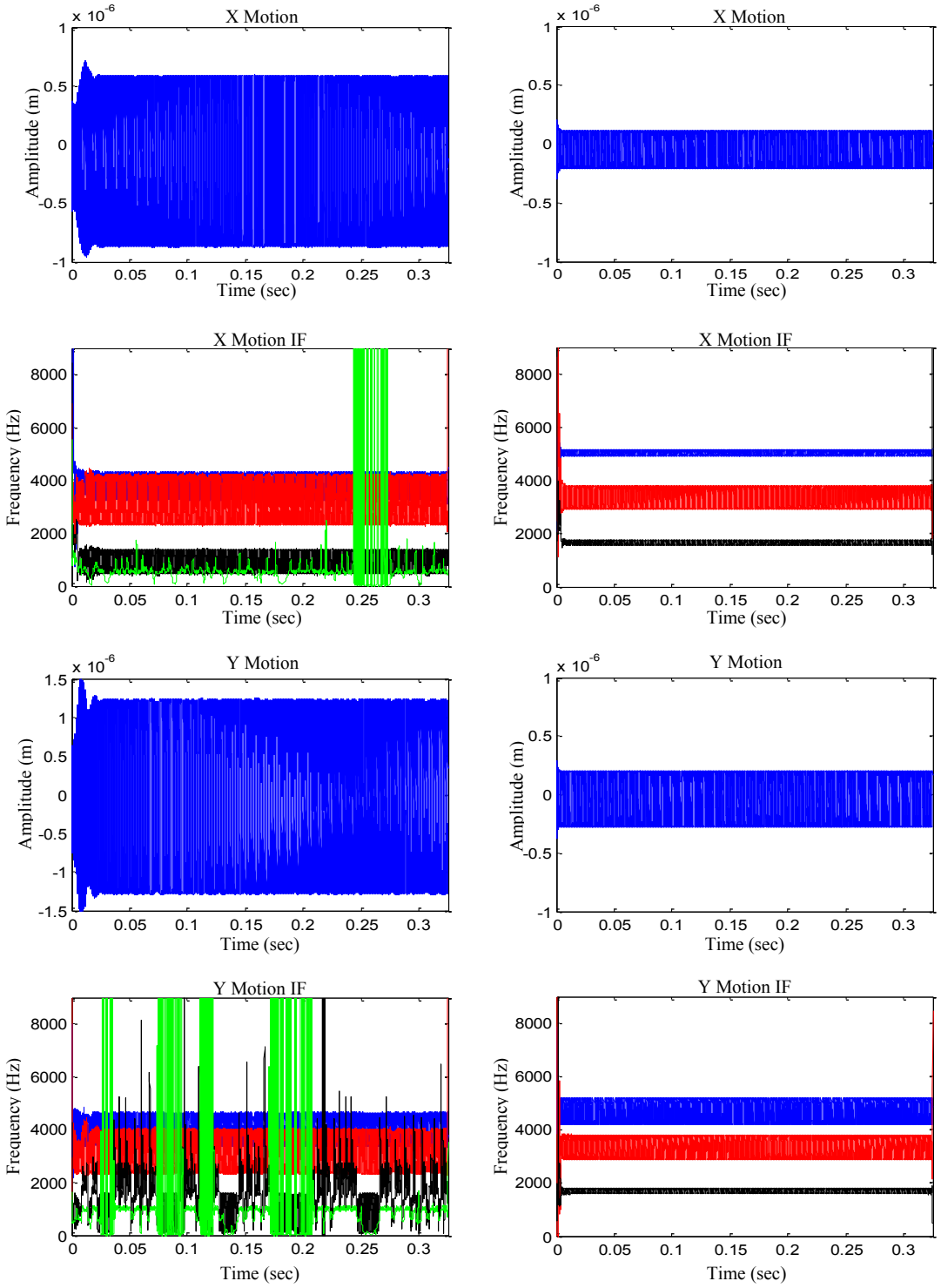

Fig. 8.20 X- and Y-direction motion and motion IF plots for 150,000 rpm spindle speed and natural frequencies of 4,035 Hz (left) and 6,000 Hz (right)

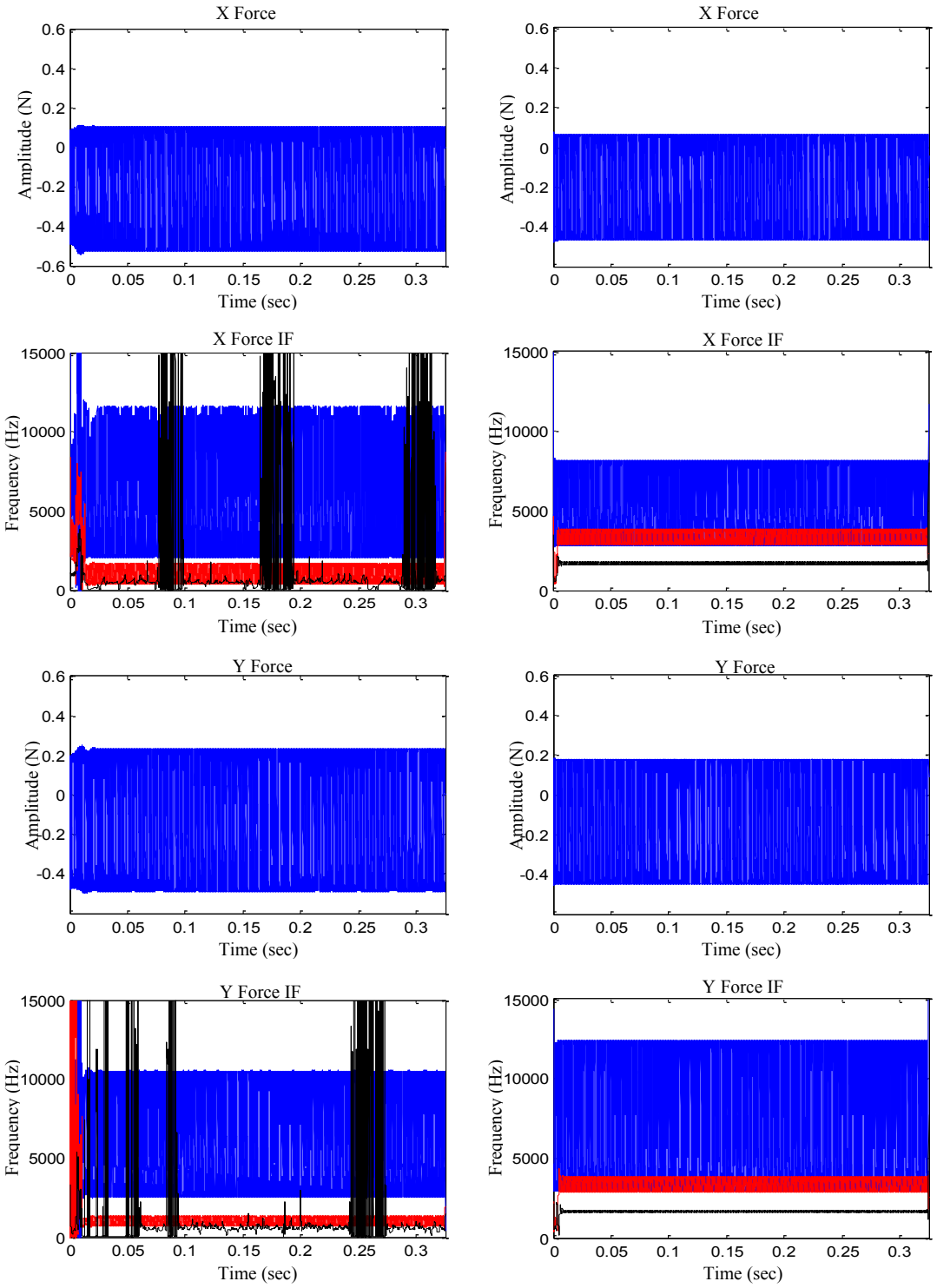

Fig. 8.21 X- and Y-direction forces and force IF plots for 150,000 rpm spindle speed and natural frequencies of 4,035 Hz (left) and 6,000 Hz (right)

9. SUMMARY AND RECOMMENDATIONS

9.1 Summary

The overall objective of the research was to expand the realm of knowledge about the underlying dynamics of the turning and micro-milling processes. To acquire further insight into the dynamics of turning, the 3D turning model in [24] was experimentally validated so that the model can be confidently used to investigate the cutting process. To validate the model, an experimental set-up was developed to acquire tool and workpiece vibration data for chatter-free and chatter cutting using a laser displacement sensor that ran on a sampling rate of 48 kHz. Since the machining process is by nature highly nonlinear with time varying amplitude and frequency, a tool capable of handling nonlinear and non-stationary signals is required to accurately analyze the signal and provide insight into the underlying dynamics. Instantaneous Frequency achieves this and was used throughout the research to investigate the response of the system. In Section 4 a method was developed to apply IF to experimental vibrations.

It was found that the experimental investigation of the turning process using IF was highly effective in characterizing cutting dynamics and identifying machining instability. It was identified that workpiece vibration was a function of the workpiece natural frequency, tool coupling, a lathe related frequency, and the spindle speed; while the tool dynamics was related to the tool natural frequency, a lathe related frequency, a varying low frequency cutting mode, and the spindle speed. The commencement of tool chatter was clearly identified using IF. For the case of the workpiece, IF identified

impending chatter before it was realized in the vibration amplitude. This demonstrated that time-frequency techniques with adequate resolution had the ability to identify and aid in controlling cutting instability. The in-depth analysis of the vibration signals demonstrated that the chatter observed in this study was characterized as follows:

Workpiece Chatter:

- Disappearance of workpiece natural frequency period-doubling mode and tool coupling mode
- Appearance of "chatter" frequency and bifurcations
- Increase in vibration magnitude

Tool Chatter:

- Shifting of tool vibrations modes to a "chatter" frequency and period-doubling bifurcation
- Increase in vibration magnitude

Operator observed excessive noise and poor surface finish cutting is commonly subjectively defined as chatter in the machine shop. The analysis method developed using IF provided a technique which was able to quantitatively identify and define unstable cutting. In addition, it was found that the tool and workpiece exhibited decoupled, nonlinear vibrations under chatter-free conditions. The workpiece was seen to retain its natural frequency when the tool and workpiece vibrations were dynamically coupled in chatter conditions. Thus, the workpiece exerted a non-negligible impact on

the turning process - one that greatly affected the cutting stability especially at higher speeds. This supports the need for including the effect of the workpiece in modeling to accurately characterize machining. Instantaneous Frequency provided significant insight into the underlying cutting dynamics that was not experimentally observed or available before, allowing additional knowledge about the deterioration to cutting instability and chatter to be gained.

The thorough characterization of the cutting process using IF provided the knowledge needed to effectively investigate the ability of the turning model in [24] to capture the underlying dynamics of the process. It was found that the underlying dynamics of the model in [24] accurately compared to the available physical data. The main components of the dynamics in the workpiece natural frequency, tool natural frequency, nonlinear tool stiffness, and spindle speed of the lathe cutting system were captured. The underlying mechanism of chatter as increased vibration amplitude and coupled vibrations at a chatter frequency for the simultaneous tool and workpiece motions was observed. With the ability of the model to capture the underlying dynamics and the chatter mechanism, the model was then used to investigate high-speed cutting dynamics. The model was run at various spindle speeds and DOCs to develop a stability diagram which showed that the chatter-free DOC limit generally increased with spindle speed and as the spindle speed surpassed 1,500 rpm the stability limit began to exponentially level out. It was observed for this workpiece configuration that the dynamics of the process was dominated by the workpiece at high spindle speeds. This increased influence of the workpiece motion on the dynamics of the process resulted in

excessive workpiece vibration amplitudes and highly nonlinear frequencies which were harmful to the workpiece tolerances and the life of the tool. The excessive workpiece vibrations created another cutting limit which was essentially a straight line near 2.75mm DOC. Thus, workpiece motions cannot be neglected when characterizing the dynamics of the system in experimental or numerical analysis and when developing control algorithms.

The miniature nature of the micro-milling process along with high spindle speeds causes prominent nonlinearities in the system. Thus, dynamic analysis of the micro-milling process is important for gaining insight into the underlying dynamics and the transition from stable to unstable cutting. This insight will help improve the process efficiency, tool longevity, and provide the knowledge needed to control the quality of the machining process by shedding light on the critical cutting parameters. Because micro-milling is inherently nonlinear, it is imperative that modeling and analysis retain the nonlinear characteristics of the process. This was achieved by using a novel approach for calculating the chip thickness and adopting a slip-line force model that was highly dynamic with constantly changing variables. It was demonstrated that the model was capable of accurately simulating the dynamic signature of the milling process and predicting the stable cutting. Analysis of the simulated signals with IF concluded that the X- and Y-direction vibrations needed to be monitored simultaneously when investigating the instability of the system since they exhibited different vibration signatures. It was also observed that the forcing frequency was quite different from the vibration frequency suggesting that the tool and workpiece could have uncoupled

vibrations. The slip-line model exhibited one drawback in the precise prediction of force amplitudes which suggested an experimental calibration and including tool run-out could aid in improving this accuracy. However, the focus of the research was on the dynamics of the system and the presented model demonstrates the ability to simulate the dynamics of the system, thus an adequate tool for further investigation into the underlying dynamics and instability of micro-milling.

The model was used to investigate the effect that the tool helical and rake angles, and stiffness have on the resulting X- and Y-direction forces, and the dynamic stability. It was found that an increase in the helical angle resulted in decreased X- and Y-direction forces because more of the force components were distributed in the Z-direction. This improved vibration response in the X- and Y-directions in turn would help to achieve tighter tolerances. However, it was observed that a helical angle of 40° excited additional frequencies in the system which was undesirable. The rake angle study showed that changing the rake angle of the tool had a minimal effect on the force RMS values. The 150,000 rpm case in the rake angle study showed that for certain spindle speeds additional frequencies were excited in the system resulting in increased vibration magnitudes while the force values were not increased. The helical and rake angle studies also showed that spindle speeds resulting in unstable dynamics had excessive cutting forces and vibrations which were detrimental to the cutting process. Thus, the main culprit for increased forces and thus tool failure was the dynamic response of the process. The stiffness of the system was varied to observe the resulting dynamic response, and an increase in stiffness generally resulted in improved stability.

For all spindle speeds, an increase in stiffness reduced the vibration magnitude which helps to improve workpiece quality. However, for spindle speeds of 100,000 and 125,000, the increased stiffness excited additional frequencies in the system that could increase the rate of tool wear. Also, the X- and Y-direction IF plots at 100,000 rpm spindle speed and 6,000Hz natural frequency had different dynamics further supporting the need to monitor both the X- and Y-direction motions when investigating the state of motion of the cutting process.

The micro-mill tool design studies showed that the dynamic response of the system had the largest impact on cutting forces and tool performance suggesting that cutting instability is a dynamics issue. Improving the dynamic response of the tool would have the greatest impact for achieving robust ultra-stable cutting. The dynamic response was dictated by the forcing frequency (spindle speed), modal parameters, workpiece, and chip load. When chip load was kept low enough to produce acceptable forces for a certain workpiece, the modal parameters and the spindle speed had the greatest effect on dynamic stability. Increasing the spindle speed will increase the material removal rate but may result in highly unstable cutting depending on the stiffness of the system. Improved stability due to increased system stiffness had the largest impact on cutting forces and the ability to realize increased cutting speeds and improved tolerances.

9.2 Contributions

The presented research contributes to the area of manufacturing in the following ways:

1. Provides the following guidelines for accurate experimental characterization of the underlying dynamics governing material removal.
    a. Monitor the workpiece and tool motions for the turning process
    b. Monitor the X- and Y-direction motions for the micro-milling process
    c. Use broadband sensors capable of acquiring the high frequency components with laser sensors being the recommended sensor technology
    d. Sample at the highest sampling rate possible but at a minimum sample fast enough to reproduce the high frequency components observed in theoretical research
    e. Use Instantaneous Frequency to analyze the unfiltered data in the time-frequency domain and to separate the modes related to the process of interest from the modes related to noise
    f. Monitor the signal for different states of cutting to identify the underlying dynamics and quantitatively define and identify instability of the process
2. Provides insight into cutting instability and the transition to instability which has not been observed before experimentally
3. Verified that the tool – workpiece interaction is prominent and non-negligible

4. Validation of a comprehensive turning model which can be used to further investigate turning instability as well as develop methods for preventing machining instability and developing control algorithms
5. Developed a comprehensive stability diagram that accounts for chatter and nonlinear dynamic instability, and workpiece and tool vibration magnitudes
6. For the workpiece configuration studied, workpiece dynamics dominates the system and must be considered to achieve high spindle speeds
7. Development of a nonlinear micro-milling model which accurately simulates the dynamic signature observed experimentally in literature that can be used to develop methods to improve micro-milling process as well as apply control techniques
8. Provided the following insight into micro-mill design
    a. Except for the 40° helical angle which decreases dynamic stability, an increase in helical angle decreases the magnitude of the in-plane (X- and Y-direction) force components, thus improving the dynamic stability
    b. Rake angle has minimal effect on the cutting forces and the dynamics
    c. An increase in system stiffness improves the dynamic response making high spindle speeds achievable
9. Spindle speed has the greatest influence on micro-milling performance

9.3 Recommendations for Future Work

The research also provides insight into future work which can be pursued to further investigate turning and micro-milling dynamics. The turning experiment set-up can be improved by using additional sensors so that the three-dimensional simultaneous tool – workpiece motions are captured and analyzed. Experiments can be performed for a wide range of cutting parameters and analyzed using IF in order to thoroughly investigate experimental cutting. The turning model can also be improved to better handle a wider range of cutting conditions. Revising the cutting force equations to account for the tool nose radius will allow the model to be applied to low DOC cutting. High spindle speeds generate excessive cutting temperatures which have a negative impact on the cutting process. Accounting for heat generation and the effect of applying coolant to the process would allow the model to investigate the effect of high spindle speeds on heat generation, and how different cooling techniques may improve the process. In the turning model the tool is simply modeled with a linear and nonlinear stiffness term and only the Z-direction motion is accounted for. The tool motions in the X-direction could be included in the model since the forces are the largest in the X-direction. To improve the accuracy of the turning model, experimental modal analysis of the tool should be performed to obtain accurate tool modal parameters. Also, the effect that the tailstock and chuck have on the workpiece stiffness could be included.

The literature review performed on micro-milling revealed limited research into micro-milling dynamics. The model developed requires modal parameters about a micro-milling system. However, there is limited information about the modal

parameters for different micro-mill configurations and it is demonstrated in this research that system stiffness greatly influences the dynamic response. The small size of the micro-mill makes it difficult to excite the system with a known force and capture its response using contact sensors. A laser displacement sensor and a miniature impact hammer could be employed to obtain the modal parameters for a micro-milling tool-spindle system needed for numerical study. Performing this experimental modal analysis for different tool designs, shank lengths, and spindles would provide important information regarding the dynamic characteristics of a micro-mill design. In addition, experimental vibrations should be acquired using broadband optical sensors and analyzed with IF to provide additional insight into the underlying dynamics of the process which will help to improve the modeling and design of micro-mill machine tools.

REFERENCES

1. Byrne, G., Dornfeld, D., and Denkena, B., 2003, "Advancing Cutting Technology", STC "C" Keynote, CIRP Annals, **52**(2), pp. 483-507
2. Arnold, R.N., 1945, “The Mechanism of Tool Vibration in the Cutting of Steel,” Cutting Tools Research: Report of Subcommittee on Carbide Tool I. Mech. E. pp. 261-284
3. Ota, H., and Kono, K., 1974, “On Chatter Vibrations of Machine Tool or Work Due to Regenerative Effect and Time Lag,” Journal of Engineering for Industry, **96**(4), pp. 1337-1346
4. Hanna, N.H., and Tobias, S.A., 1974, “A Theory of Nonlinear Regenerative Chatter,” Journal of Engineering for Industry, **96**, pp. 247-255
5. Shi, H.M., and Tobias, S.A., 1984, “Theory of Finite Amplitude Machine Tool Instability,” International Journal of Machine Tool Design and Research, **24**(1), pp. 45-69
6. Wu, D.W., and Liu, C.R., 1985, “An Analytical Model of Cutting Dynamics Part 1: Model Building,” Journal of Engineering for Industry, **107**(2), pp. 107-111
7. Wu, D.W., and Liu, C.R., 1985, “An Analytical Model of Cutting Dynamics Part 2: Verification,” Journal of Engineering for Industry, **107**(2), pp. 112-118
8. Tlusty, J., and Ismail, F., 1981, “Basic Non-Linearity in Machining Chatter,” CIRP Annals - Manufacturing Technology, **30** (1), pp. 299-304

9. Altintas, Y., and Budak, E., 1995, "Analytical Prediction of Stability Lobes in Milling," CIRP Annals – Manufacturing Technology, **44**(1), pp. 357-362
10. Ozlu, E., and Budak, E., 2007, "Analytical Modeling of Chatter Stability in Turning and Boring Operations – Part I: Model Development," Journal of Manufacturing Science and Engineering, **129**(4), pp. 727-732
11. Ozlu, E., and Budak, E., 2007, "Analytical Modeling of Chatter Stability in Turning and Boring Operations – Part II: Experimental Verification," Journal of Manufacturing Science and Engineering, **129**(4), pp. 733-739
12. Eynian, M., and Altintas, Y., 2009, "Chatter Stability of General Turning Operations with Process Damping," Journal of Manufacturing Science and Engineering, **131**(4), pp. 1-10
13. Clancy, B., and Shin, Y., 2002, "A Comprehensive Chatter Prediction Model for Face Turning Operation Including Tool Wear Effect," International Journal of Machine Tools and Manufacture, **42**(9), pp. 1035-1044
14. Tlusty, J. and Smith, S., 1990, "Update on High-Speed Milling Dynamics," Journal of Engineering for Industry, **112**, pp. 142-149
15. Wiercigroch, M., and Budak, E., 2001, "Sources of Nonlinearities, Chatter Generation and Suppression in Metal Cutting," Phil. Trans. R. Soc. Lond. A., **359**, pp. 663-693
16. Desphande, N., and Fofana, M.S., 2001, "Nonlinear Regenerative Chatter in Turning," Robotics and Computer Integrated Manufacturing, **17**(1), pp. 107-112

17. Gegg, B., Suh, C.S., and Luo, A., 2010, "Modeling and Theory of Intermittent Motions in a Machine Tool with a Friction Boundary," Journal of Manufacturing Science and Engineering, **132**(4), pp. 1-9
18. Wang, X.S., Hu, J., and Gao, J.B., 2006, "Nonlinear Dynamics of Regenerative Cutting Processes – Comparison of Two Models," Chaos, Solitons, and Fractals, **29**(5), pp. 1219-1228
19. Chandiramani, N.K., and Pothala, T., 2006, "Dynamics of 2-dof Regenerative Chatter During Turning," Journal of Sound and Vibration, **290**(1), pp. 448-464
20. Moon, F.C., and Kalmar-Nagy, T., 2001, "Nonlinear Models for Complex Dynamics in Cutting Materials," Phil. Trans. R. Soc. Lond. A., **359**, pp. 695-711
21. Ozlu, E., and Budak, E., 2007, "Comparison of One-Dimensional And The Multi-Dimensional Models in Stability Analysis of Turning Operations," International Journal of Machine Tools and Manufacture, **47**(1), pp. 1875-1883
22. Luo, X., Cheng, K., Luo, X., and Liu, X., 2005, "A Simulated Investigation on The Machining Instability and Dynamic Surface Generation," International Journal of Advanced Manufacturing Technology, **26**(7), pp. 718-725
23. Rao, B.C., and Shin, Y.C., 1999, "A Comprehensive Dynamic Cutting Force Model for Chatter Prediction in Turning," International Journal of Machine Tools & Manufacture, **39**(10), pp. 1631-1654
24. Dassanayake, A.V., and Suh, C.S., 2007, "Machining Dynamics Involving Whirling Part I: Model Development and Validation," Journal of Vibration and Control, **13**(5), pp. 475-506

25. Dassanayake, A.V., and Suh, C.S., 2007, "Machining Dynamics Involving Whirling Part II: Machining Motions Described by Nonlinear and Linearized Models," Journal of Vibration and Control, **13**(5), pp. 507-526

26. Rahman, M., and Ito, Y., 1986, "Detection of The Onset of Chatter Vibration," Journal of Sound and Vibration, **109**(2), pp. 193-205

27. Kunpeng, Z., San, W., and Soon, H., 2009, "Wavelet Analysis of Sensor Signals for Tool Condition Monitoring: A Review and Some New Results," International Journal of Machine Tools and Manufacture, **49**(7),pp. 537-553

28. Suh, C.S., Khurjekar, P.P., and Yang, B., 2002, "Characterisation and Identification of Dynamic Instability in Milling Operation," Mechanical Systems and Signal Processing, **16**(5), pp. 853-872

29. Teti, R., Jemielniak, K., O'Donell, G., and Dornfeld, D., 2010, "Advanced Monitoring of Machining Operations," CIRP Annals – Manufacturing Technology, **59**(2), pp. 717-739

30. Huang, N.E., Wu, Z., Long, S.R., Arnold, K.C., Chen, X., and Blank, K., 2009, "On Instantaneous Frequency," Advances in Adaptive Data Analysis, **1**, pp. 177-229

31. Loutridis, S.J., 2004, "Damage Detection in Gear Systems Using Empirical Mode Decomposition," Engineering Structures, **26**(12), pp. 1833-1841

32. Yang, B., and Suh, C.S., 2004, "Interpretation of Crack-Induced Rotor Non-Linear Response Using Instantaneous Frequency," Mechanical Systems and Signal Processing, **18**(3), pp. 491-513

33. Cardi, A., Firpi, H., Bement, M., and Liang, S., 2008, "Workpiece Dynamic Analysis And Prediction During Chatter of Turning Process," Mechanical Systems and Signal Processing, **22**(6), pp. 1481-1494

34. Ehrfeld, W., and Ehrfeld, U., 2001, "Progress and Profit Through Micro Technologies. Commercial Applications of MEMS / MOEMS," Proceedings of SPIE 4557, pp. 1-10

35. Dornfeld, D., Min S., and Takeuchi, Y., 2006, "Recent Advances in Mechanical Micromachining," CIRP Annals-Manufacturing Technology, **55**(2), pp. 745-768

36. Chae, J., Park, S.S., and Freiheit, T., 2006, "Investigation of Micro-cutting Operations," International Journal of Machine Tools & Manufacture, **46**(3), pp. 313-332

37. Altintas, Y., 2001, "Analytical Prediction of Three Dimensional Chatter Stability in Milling," JSME International Journal Series C, **44**(3), pp. 717-723

38. Altintas, Y., Stepan, G., Merdol, D., and Dombovari, Z., 2008, "Chatter Stability of Milling in Frequency and Discrete Time Domain," CIRP Journal of Manufacturing Science and Technology, **1**, pp. 35-44

39. Weingaertner, W.L., Schroeter, R.B., Polli, M.L., and Gomes, J.O., 2006, "Evaluation of High-speed Milling Dynamic Stability through Audio Signals," Journal of Materials and Processing Technology, **179**(1), pp. 133-138

40. Yun, W.S., and Cho, D.W., 2000, "An Improved Method for the Determination of 3D Cutting Force Coefficients and Runout Parameters in End Milling," International Journal Advanced Manufacturing Technology, **16**(12), pp. 851-858

41. Moradi, H., Vossoughi, G., Movahhedy, M., and Salarieh, H., 2011, "Optimal Control of the Regenerative Chatter in Nonlinear Milling Process", DETC2011-47527, Proceedings of ASME IDETC/CIE, pp. 1-9
42. Chittipolu, S., 2009, "Failure Prediction and Stress Analysis of Microcutting Tools," Master Thesis, Texas A&M University, College Station, TX
43. Malekian, M., Park, S., and Jun, M., 2009, "Modeling of Dynamic Micro-milling Cutting Forces," International Journal Machine Tools & Manufacture, **49**(7), pp. 586-598
44. Basuray, P.K., Misra, B.K., and Lal, G.K., 1977, "Transition from Ploughing To Cutting during Machining with Blunt Tools," Wear, **43**(3), pp. 341-349
45. Bao, W.Y., and Tansel, I.N., 2000, "Modeling Micro-end-milling Operations Part I: Analytical Cutting Force Model," International Journal of Machine Tools & Manufacture, **40**(15), pp. 2155-2173
46. Kang, I.S., Kim, J.S., Kim, J.H., Kang, M.C., and Seo, Y.W., 2007, "A Mechanistic Model of Cutting Force in the Micro end Milling Process," Journal of Materials Processing Technology, **187**, pp. 250-255
47. Vogler, M.P., Kapoor, S.G., and DeVor, R.E., 2004, "On the Modeling and Analysis of Machining Performance in Micro-Endmilling, Part II: Cutting Force Prediction," Journal of Manufacturing Science and Engineering, **126**(4), pp. 695-705

48. Vogler, M.P., DeVor, R.E., and Kapoor, S.G., 2003, "Microstructure-Level Force Prediction Model for Micro-milling of Multi-Phase Materials," Journal of Manufacturing Science and Engineering, **125**(2), pp. 202-209

49. Arcona, C., and Dow, T.A., 1998, "An Empirical Tool Force Model for Precision Machining," Journal of Manufacturing Science and Engineering, **120**(4), pp. 700-707

50. Lee, H.U., Cho, D.W., and Ehmann, K.F., 2008, "A Mechanistic Model of Cutting Forces in Micro-End-Milling with Cutting-Condition-Independent Cutting Force Coefficients," Journal of Manufacturing Science and Engineering, **130**(3), pp. 1-9

51. Fang, N., 2003, "Slip-line Modeling of Machining with a Rounded Edge Tool – Part I: New Model and Theory," Journal of the Mechanics and Physics of Solids, **51**(4), pp. 715-742

52. Kim, J.D., and Kim, D.S., 1995, "Theoretical Analysis of Micro-Cutting Characteristics in Ultra-Precision Machining," Journal of Materials Processing Technology, **49**(3), pp. 387-398

53. Waldorf, D.J., DeVor, R.E., and Kapoor, S.G., 1998 "A Slip-Line Field for Ploughing During Orthogonal Cutting," Journal of Manufacturing Science and Engineering, **120**, pp. 693-699

54. Jun, M.B., Liu, X., DeVor, R.E., and Kapoor, S.G., 2006, "Investigation of the Dynamics of Microend Milling – Part I: Model Development," Journal of Manufacturing Science and Engineering, **128**(4), pp. 893-900

55. D.J. Inman, 2008, *Engineering Vibration 3rd Edition,* Pearson Education, Inc.

56. J.C. Goswami and A.K. Chan, 2011, *Fundamentals of Wavelets: Theory, Algorithms, and Applications*, John Wiley and Sons, Inc.

57. Jauregui, J.C., 2001, "Chapter 2: Phase Diagram Analysis for Predicting Nonlinearities and Transient Responses," Recent Advances in Vibrations Analysis, InTech, pp. 27-46

58. Lauterborn, W., and Parlitz, U., 1988, "Methods of Chaos Physics and Their Application to Acoustics," Journal of Acoustic Society of America, **84**(6), pp. 1975-1993

59. Kim, J.S., and Lee, B.H., 1991, "An Analytical Model of Dynamic Cutting Forces in Chatter Vibrations," International Journal of Machine Tools and Manufacture, **31**(3), pp. 371-381

60. Jun, M.B., DeVor, R.E., and Kapoor, S.G., 2006, "Investigation of the Dynamics of Microend Milling – Part II: Model Validation and Interpretation," Journal of Manufacturing Science and Engineering, **128**(4), pp. 901-912

61. Liu, X., DeVor R.E., and Kapoor, S.G., 2006, "An Analytical Model for the Prediction of Minimum Chip Thickness in Micromachining," Journal of Manufacturing Science and Engineering, **128**(2), 474-481

62. Jardret, V., Zahouani, H., Loubet, J.L., and Mathia, T.G., 1998, "Understanding and Quantification of Elastic and Plastic Deformation During a Scratch Test," Wear, **218**(1), pp. 8-14

63. Matsumura, T., Miyahara, Y., and Ono, T., 2008, "Dynamic Characteristics in the Cutting Operations with Small Diameter End Mills," Journal of Advanced Mechanical Design, Systems, and Manufacture, **2**(4), pp. 609-618

64. Rahnama, R., Sajjadi, M., and Park, S.S., 2009, "Chatter Suppression in Micro End Milling with Process Damping," Journal of Material Processing Technology, **209**(17), pp. 5766-5776

65. Gandarias, S., Dimov, S., Pham, D.T., Ivanov, A., Popov, K., Lizarralde, R., and Arrazola, P.J., 2006, "New Methods for Tool Failure Detection in Micromilling," Proc. IMechE Part B: Journal Engineering Manufacture, **220**(2), pp. 137-144

66. Tansel, I., Rodriguez, M., Trujillo, E., and Li. W., 1998, "Micro-end-milling – I. Wear and Breakage," International Journal of Machine Tools & Manufacture, **38**(12), pp. 1419-1436

67. Fang, F.Z., Wu, H., Liu, X.D., Liu, Y.C., and Ng, S.T., 2003, "Tool Geometry Study in Micromachining," Journal of Micromechanics and Microengineering, **13**(5), pp. 726-731

68. "High-speed, High-accuracy CCD Laser Displacement Sensor LK-G Series User's Manual" Keyence Cooperation 2010, www.keyence.com

APPENDIX A

LABVIEW DATA ACQUISITION PROGRAM

The LabView VI shown in Fig. A.1 is constructed for saving and gathering the analog signal from the laser. The DAQ Assistant block is setup to communicate with the DAQ board. The while loop is used to ensure the DAQ Assistant block continuously takes data until the loop is stopped by the STOP button. The Write To Measurement File block is used to save the data to a text file on the desktop. The real-time data is not plotted to a chart because this affected the sampling performance of the VI. To accurately obtain data at the desired sampling rate, it is important to properly configure the DAQ Assistant block (Fig. A.2). Set the DAQ Assistant block to read data continuously by selecting Continuous Samples and then correctly adjust the Samples to Read and Rate blocks. Perform some basic data collection tests and analysis to ensure the VI is performing as desired.

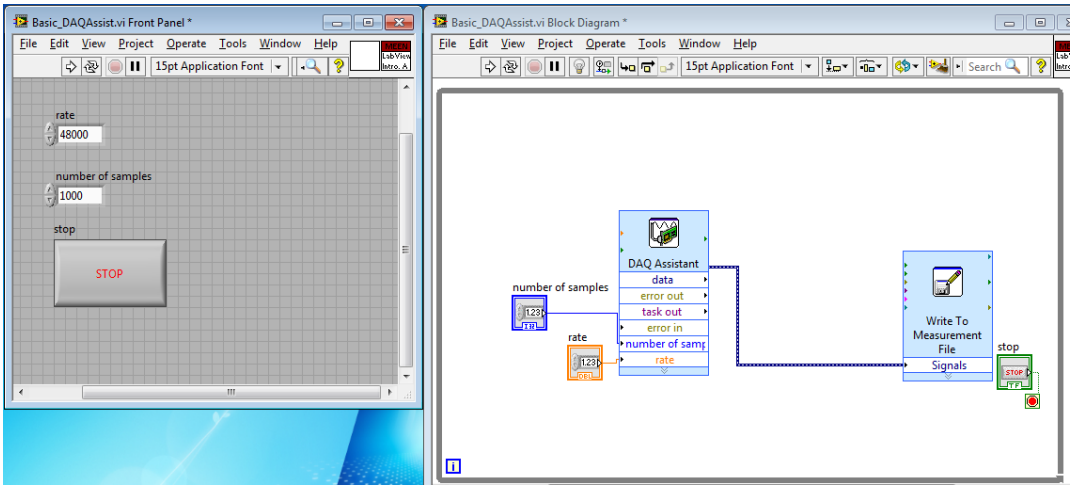

Fig. A.1 LabView VI constructed for data collection

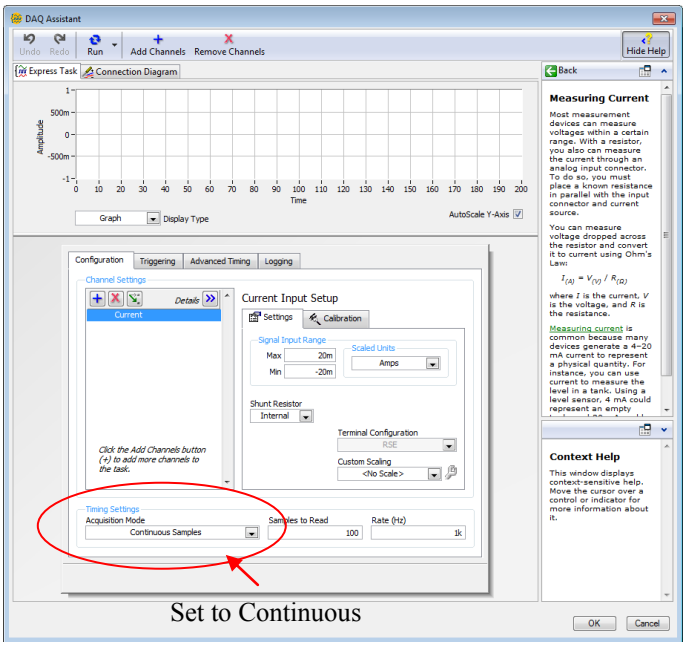

Fig. A.2 Proper configuration of the DAQ Assistant block by setting the acquisition mode and sampling rate

APPENDIX B

LASER CONFIGURATION

The information in this appendix is a step-by-step guide to properly setting up the laser for data collection. It is important to pay attention to the settings of the laser, especially the filter settings, as these will affect the quality of the data acquired. The Keyence LK-G Series user manual [68] should be consulted for more detailed information about the steps provided below.

1. The laser must be positioned at the correct distance away from the measurement target and set at the desired sampling rate. It is important to note that for a high sampling rate of 50 kHz the measurement range narrows to a range of 125.5 mm to 108.5 mm with a reference distance of 117 mm. Reference Pages 1-12 of the user manual in [68] for more details
2. Lasers capture the changing of the laser wave phase by capturing the reflection of the laser. Different target materials will reflect the laser differently, so the laser must be calibrated for the particular target material. The Keyence laser has a built in calibration function called ABLE calibration. The different ABLE settings for the head are provided on Page 3-3 of the manual and the steps for setting and performing the ABLE calibration are also provided in the manual. The default setting of the laser is found to be a setting of Manual and 42 High and 35 Low. For this research the ABLE calibration was set to automatic and the

calibration procedure provided in the manual was followed for the workpiece and the tool materials.

3. The offset of the laser is left at zero as the offset of the signal can be accounted for during data analysis.
4. The minimum display unit for the laser is set to 0.0001 by following the procedure provided in the manual in [68].
5. The method for adjusting the conversion factors of the measurement data is provided in [68] and the setting of 0.1 display to 0.1 output is used for this research.
6. The sampling rate of the laser is set to 50 kHz following the procedure described in [68].
7. The laser controller provides multiple filtering options which can negatively impact the recorded data if not correctly set. The controller doesn't provide a "No Filter" setting so an average filter of 1 point is used for this research since this setting will result in unfiltered data.

VITA

Name:	Eric Ben Halfmann
Address:	Department of Mechanical Engineering, 3123 TAMU, College Station, TX, 77843, USA
Email Address:	eric.b.halfmann@gmail.com
Education:	B.S., Mechanical Engineering, Lamar University, USA, 2010 M.S., Mechanical Engineering, Texas A&M University, USA, 2012